FUNCTIONAL AND BIOCHEMICAL STUDIES OF THE VPS4 ATPASE IN *SACCHAROMYCES CEREVISIAE*

by

Anna Shestakova

A dissertation submitted to the faculty of
The University of Utah
in partial fulfillment of the requirements for the degree of

Doctor of Philosophy

Department of Biology

The University of Utah

December 2011

The University of Utah Graduate School

STATEMENT OF DISSERTATION APPROVAL

The dissertation of **Anna Shestakova**

has been approved by the following supervisory committee members:

Markus Babst	, Chair	**10-28-2011** Date Approved
Leslie Sieburth	, Member	**10-28-2011** Date Approved
Villu Maricq	, Member	**10-28-2011** Date Approved
Dennis Winge	, Member	**10-28-2011** Date Approved
Janet Shaw	, Member	**10-28-2011** Date Approved

and by **Neil Vickers** , Chair of the Department of **Biology**

and by Charles A. Wight, Dean of The Graduate School.

ABSTRACT

The multivesicular body (MVB) is a late endosomal compartment containing intralumenal vesicles enriched with a subset of transmembrane cargoes that form as a result of the inward budding of the endosomal limiting membrane. In *Sacchoromyces cerevisiae* ESCRT (endosomal sorting complexes required for transport) machinery, consisting of distinct protein complexes ESCRT-0, I, II and III, together with the AAA+ (ATPases associate with the variety of cellular activities) Vps4 (vacuolar protein sorting 4) ATPase are responsible for the MVB sorting. Solubilization of ESCRTs by the active Vps4 oligomer is thought to be the final step in the biogenesis of MVB.

Vps4 consists of N-terminal ESCRT-III-interacting MIT (microtubule interaction and trafficking) domain, C-terminal nucleotide ATPase domain and the linker region that connects them. Function of the Vps4 is regulated through its recruitment from the cytoplasm through a complex network of interactions with ESCRT-III-associtaed proteins Did2, Ist1, Vta1 and Vps60 to the endosome-associated ESCRT-III consisting of Vps20, Snf7, Vps2 and Vps24 where Vps4 assembles into an active oligomer. ATPase domains of Vps4 subunits promote oligomerization into closed rings and two stacked rings form an active Vps4 oligomer that contains a functionally important central cavity. Position of the MIT domains in the oligomer varies, suggesting that function of the active Vps4

oligomer might require flexibility in movement of the MIT domains.

In Chapter 2, we have perfomed a detailed *in vivo* analysis of the interactions that mediate recruitment of Vps4 to ESCRT-III. Our data revealed a high degree of redundancy in the Vps4 interaction network. In our model, we propose that interactions with Did2 and Ist1 recruit Vps4 from cytoplasm to ESCRT-III and subsequent interaction with Vta1 promotes formation of an active Vps4 ATPase. We speculate that two rings that comprise active Vps4 oligomer have different functions - one ring is important for the ATP hydrolysis and substrate processing by Vps4, whereas the second ring is not directly involved in the ATP hydrolysis and serves a regulatory role.

In Chapter 3, we have investigated if MIT domains need to be tucked away from the central cavity of the active Vps4 oligomer to allow processing of a substrate. We performed detailed functional and biochemical analysis of the serial deletions within the linker region. In our model, we propose that MIT domains are positioned around the central cavity region and cooperate together in solubilization of a substrate.

This thesis is dedicated to my grandparents

Bondar Pavel Zakharovich,

Bondar Margarita Vartanovna and

my mother Shestakova Galina.

TABLE OF CONTENTS

ABSTRACT…….. iii

LIST OF TABLES……..... viii

LIST OF FIGURES……..... ix

ACKNOWLEDGMENTS……..... xi

1 INTRODUCTION…..……..... 1

General principles of the membrane trafficking..... 2
Overview of intracellular membrane trafficking pathways……. 4
Characterization of the *vps* mutants……. 13
ESCRT machinery promotes MVB biogenesis…… 17
ESCRT-III…….. 23
Vps4 AAA+ ATPase ……. 28
References..... 37

2 ASSEMBLY OF THE AAA ATPASE VPS4 ON ESCRT-III…..... 46

Abstract….. ……... 47
Introduction ……... 47
Materials and methods…… 48
Results……..…… 48
Discussion ……..…… 57
Acknowledgments…… 58
References..... 58

3 FUNCTIONAL AND BIOCHEMICAL STUDIES OF THE LINKER REGION OF THE VPS4 PROTEIN …… 60

Abstract….. ……... 61
Introduction ……... 62
Materials and methods…… 68
Results and discussion……..……. 75
Role of the Vps4 in the cytokinesis of budding yeast……. 96

References……. 106

4 CONCLUSIONS AND FUTURE DIRECTIONS…….. 111

Summary for Chapter 2: Functional importance of Vps4-ESCRT-III-mediated interactions *in vivo*…….. 112
Summary for Chapter 3: Functional and biochemical studies of the linker region of Vps4 ……... 114
Future directions …….…… 116
References ……...……...……. 118

LIST OF TABLES

Table	Page
1-1. VPS genes required for the transport to the vacuole……..	16
1-2. Proteins that regulate MVB sorting…….	18
2-1. Strains and plasmids used in this study……	49
2-2. Mutations used in this study……	51
2-3. CPY-invertase secretion…..……	53
3-1. Plasmids, yeast strains and E. coli used in this study……	70
3-2. Fluorescence microscopy of the GFP-CPS sorting in yeast expressing mutant Vps4 proteins……..	77
3-3. Fluorescence microscopy of the GFP-CPS sorting in yeast lacking Vps4-regulatory genes expressing different Vps4(linker mutations) …….	84
3-4. Fluorescence microscopy of the GFP-CPS sorting in yeast expressing Vps4(pore mutants)…….	96
3-5. Cell cycle progression of yeast cells synchronized with α-factor after release……..	103

LIST OF FIGURES

Figure	Page
1-1. Three steps of membrane trafficking ……	3
1-2. Intracellular membrane trafficking pathways…….....	5
1-3. ESCRT-dependent sorting into MVBs……. …….	11
1-4. Interactions of ESCRTs with ubiquitin, lipids and each other……	20
1-5. Structure of the Vps4 AAA+ ATPase…….	29
1-6. Network of interactions between Vps4 and ESCRT-III proteins……	35
2-1. Interactions between Vps4 and its substrate and regulators…….	51
2-2. MIM1 and MIM2 interactions contribute to the recruitment of Vps4 to ESCRT-III…….	52
2-3. Phenotypic analysis of mutations affecting Vps4 interactions……..	53
2-4. Localization of mutant Vps4 proteins ……..	55
2-5. Ist1 and Did2 form a stable complex ……	56
3-1. Linker region of Vps4 …….	64
3-2. Vps4(linker mutations) have defect in solubilization of ESCRT-III (Snf7)……..	81
3-3. Functional Vps4(linker deletions) are more sensitive to the canavanine in the background of *Δdid2* or *Δvps60*…….	87
3-4. Vps4(Δ79-118) has higher ATPase activity than wild-type Vps4…	90

3-5. Mutant Vps4(Δ85-115+GT) induces formation of larger intralumenal MVB vesicles…….. 92

3-6. Abnormal elongated cellular morphology of *Δelm1* is not exacerbated in *Δelm1Δvps4* grown at permissive room temperature (~21℃) …….. 100

3-7. Functional Vps4 rescues temperature-sensitive growth defect of *Δvps4Δelm1*……... 101

ACKNOWLEDGMENTS

This thesis is dedicated to all of my colleagues and family, who have made this work possible. I thank all members of the Babst laboratory, especially Shrawan for continuous help with my work. I thank all my committee members, Leslie Sieburth, Dennis Winge, Janet Shaw and Villu Maricq, for the advice they have given me to help my work progress. I am particularly thankful for the support and encouragement I have received from my mentor Markus Babst.

I want to thank my close family, especially my grand parents and my mother for their encouragement. I am grateful to my husband Anton Burtsev for his patience and help in everything including my graduate career. Thank you to my little daughter Sophia – joy and happiness of my life.

CHAPTER 1

INTRODUCTION

General principles of the membrane trafficking

Vesicular transport mediates exchange of material between subcellular organelles [1]. Vesicular traffic can be subdivided into three essential steps i) vesicle budding, ii) vesicle tethering and iii) vesicle fusion. Steps of the vesicular transport are regulated by the concerted function of intracellular trafficking machinery including coat proteins, small Rab GTPases, tethering molecules and SNARES (Soluble NSF (N-ethylmaleimide-sensitive factor) attachment protein (SNAP) receptors) (reviewed in [2 3 4 5 6]).

Formation of the vesicle (Figure 1-1) is promoted by the transient assembly of coat proteins (reviewed in [2]). In addition to physically sculpting vesicles, coat proteins actively sort cargo proteins and impact transport specificity through interacting with organelle-specific Rabs, tethers and SNAREs. The tethering step is mediated by the activated Rabs [3] that recruit tethering factors [4 7]. Tethering factors function through establishing initial loose contact between the vesicle and acceptor membrane and through interaction with SNAREs (Figure 1-1). SNAREs localize to opposite membranes, v-SNAREs localize to vesicles and t-SNAREs to target membranes, and promote membrane fusion by forming *trans*-SNARE-complexes [8 9 10 11] (Figure 1-1). Trans-SNARE complexes are disassembled by the function of the NSF ATPase and α-SNAP (Soluble NSF attachment protein) [12].

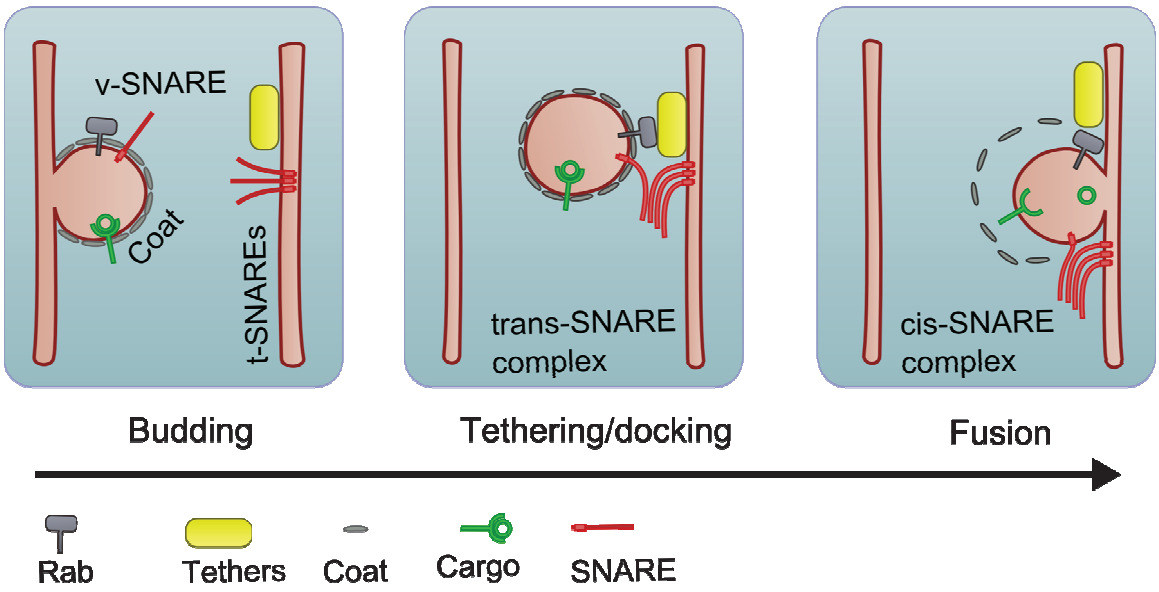

Figure 1-1. Three steps of membrane trafficking. Coat proteins promote budding of the vesicle from the donor membrane. Tethering is mediated by the interactions between tethers, Rabs and SNAREs. Trans-SNARE complex drives membrane fusion (modified from Brocker et al. 2010).

Overview of intracellular membrane trafficking pathways

Newly synthesized luminal and transmembrane proteins are transported between ER and Golgi in vesicles. At the trans-Golgi network (TGN), proteins are sorted to their destination compartments. For instance, cell surface proteins are packaged into exocytic vesicles that are delivered to the plasma membrane [13]. Vacuolar resident proteins, vacuolar hydrolases and SNAREs, are actively sorted at the TGN into the endosomal system *en route* to the vacuole.

A variety of cellular activities, including downregulation of the cell surface transmembrane proteins and uptake of essential nutrients, are based on endocytosis [14]. Endocytosis regulates expression of the transmembrane cell surface proteins by either recycling them to the plasma membrane or sorting into the endosomal system *en route* to the vacuole for degradation (Figure 1-2).

Secretory pathway. Proteins are synthesized by ribosomes that associate with pore complexes on the ER membrane, thereby releasing soluble proteins into the ER lumen or incorporating transmembrane proteins into the ER membrane. Proteins that are folded and posttranslationaly modified are transported to the Golgi in COPII (Coat Protein Complex II) vesicles [2]. The small GTPase Sar1 bound to GTP activates COPII components that directly sculpt vesicles and help sort cargo proteins [15] [16]. Tethering and fusion of the anterograde COPII vesicles are mediated by the small Rab GTPase Ypt1 and tethering factors Uso1 and TRAPPI (Transport protein particle I). Ypt1 and tethers function through establishing initial interactions between vesicles and the Golgi membrane and priming SNAREs Sed5, Bos1, Sec22 and Bet1 for the

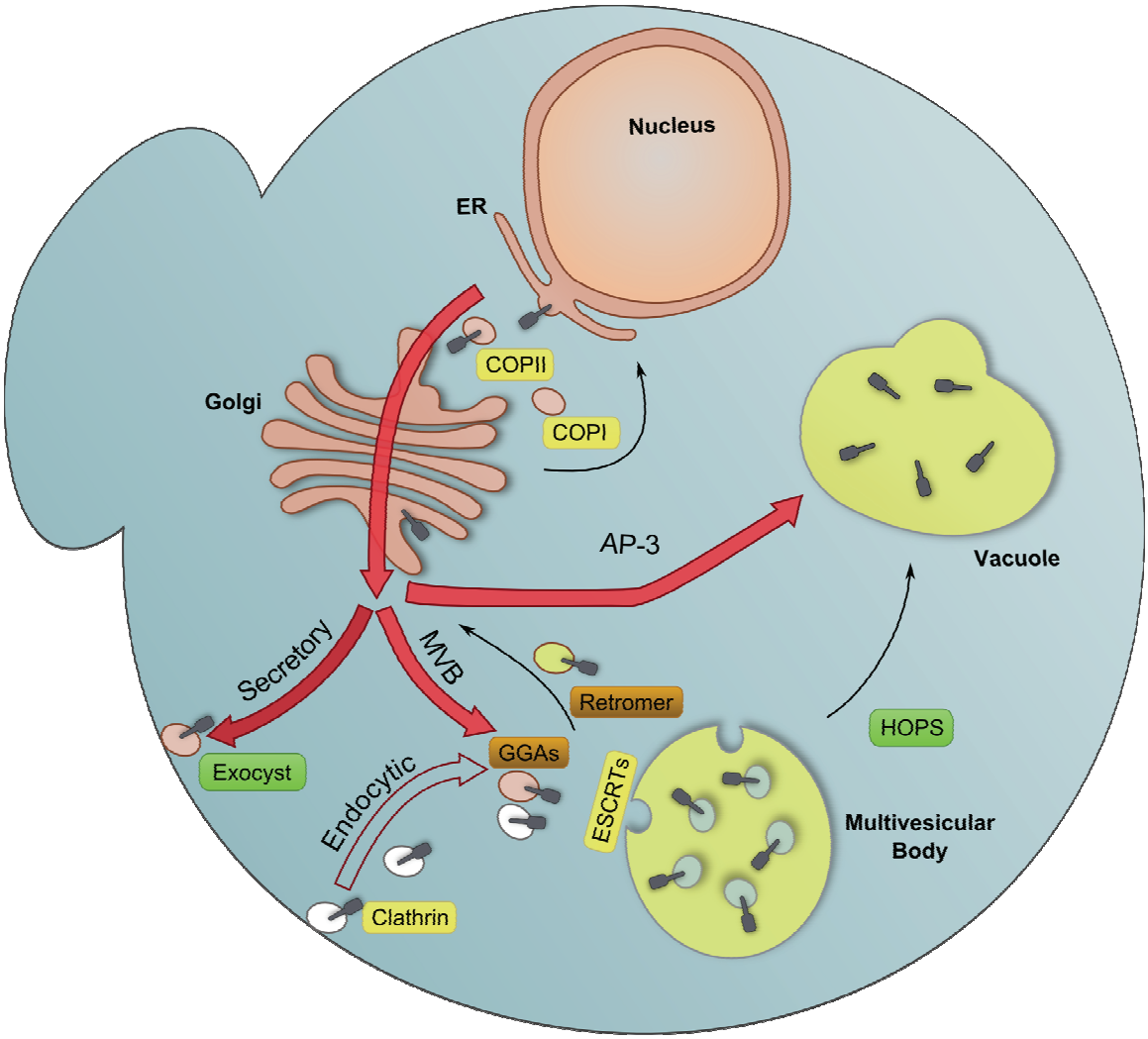

Figure 1-2. Intracellular membrane trafficking pathways. Secretory and biosynthetic cargoes are transported through ER to Golgi. At the *trans*-Golgi network (TGN), cargo destined to the cell surface is packaged into exocytic vesicles that traffic to the plasma membrane; vacuolar resident proteins that belong to the biosynthetic pathway are sorted into endosomal system. The endocytic pathway sorts transmembrane cell surface cargo into endosomal system *en route* to the vacuole.

membrane fusion.

Retrograde intra-Golgi and Golgi-to-ER traffic is important in maintaining compartment-specific distribution of proteins that continuously traffic in vesicle carriers [17]. COPI (Coatomer Complex I) vesicles mediate retrograde intra-Golgi and Golgi to ER traffic, which is important to retain ER- and Golgi-resident proteins. Activated Golgi-localized ARF (ADP-ribosylation factor) GTPase recruits pre-assembled COPI (Coatomer Complex I) [18]. COPI retrograde traffic depends on the ER-localized tethering complex Dsl1 [19] Ufe1, Sec22, Sec20 and Use1 SNAREs [20].

Proteins of the secretory pathway are sorted at TGN into exocytic vesicles that are transported to the plasma membrane. Exomer, a yeast coat protein complex (Chs5 and Chs6), mediates transport from TGN to the plasma membrane [21]. The Rab GTPase Sec4 together with tethering complex exocyst and SNAREs Sec9, Snc1, Snc2, Sso1 and Sso2 promote the fusion step of the exocytosis [22 23].

Endocytic pathway. Endocytosis is involved in a plethora of cellular functions including regulation of intracellular signaling cascades by downregulation of cell surface receptors, degradation of misfolded cell surface proteins, and degradation of plasma membrane proteins in response to the starvation [24]. Endocytosed transmembrane proteins can be either recycled back to the plasma membrane or sent for the degradation to the vacuole. Sorting of the endocytosed cargo into the late endosomal compartment termed the Multivesicular body (MVB) ensures delivery to the vacuole.

A highly organized network of proteins including endocytic adaptors, clathrin and actin cytoskeleton regulate endocytosis. AP-2 is a heteromeric complex composed of four subunits (α2, β2, μ2 and σ2) that recruits clathrin to the site of endocytosis through interaction with plasma membrane phosphoinositides and dileucine and tyrosine-based motifs in cytosolic tails of the cargo proteins [25]. Ent1 and Ent2 are monomeric adaptor proteins that regulate endocytosis through binding to clathrin, plasma membrane lipids and ubiquitinated cargoes [26] [27] [28].

Attachment of ubiquitin, a highly conserved 76 amino acid protein, marks proteins not only for internalization but also for the sorting of these proteins into the MVB sorting pathway [14] [29]. Rsp5 is an E3 ubiquitin ligase that is required for the efficient ubiquitination of endocytic cargo [30]. A single ubiquitin attached to the lysine residue of a plasma membrane protein appears to be sufficient to signal receptor internalization [31]. On the other hand, endocytic cargo can be deubiquitinated at the endosome which results in the recycling of the cargo back to the plasma membrane [32]. Cargo proteins that remain ubiquitinated are sorted into MVBs which mediates their delivery into the vacuolar lumen for degradation (mechanism of the MVB sorting is described below).

Biosynthetic pathway. The biosynthetic pathway delivers soluble (CPY – Carboxypeptidase Y) and transmembrane (CPS – Carboxypeptidase S) vacuolar hydrolases as well as vacuolar SNAREs to the vacuole. There are two major routes that transport cargo to the vacuole – i) AP-3-dependent; and ii) AP3-independent sorting including sorting into the MVB pathway.

AP-3-dependent pathway. AP-3-dependent transport delivers the transmembrane vacuolar proteins ALP (alkaline phosphatase) and Vam3 (vacuolar t-SNARE) to the vacuolar limiting membrane [33]. Membrane association of AP-3 heteromeric adaptor complex is regulated by the ARF GTPase [34]. The cytosolic N-terminus of ALP and Vam3 contains an acidic dileucine sorting signal (EQTRLV) that mediates interaction with AP-3, thereby redirecting sorting of this protein at the TGN into the AP-3 pathway, away from the delivery to the MVB pathway [33 35].

AP-3-independent sorting pathway. The GGA proteins (Golgi-localizing, gamma-adaptin ear homology domain, ARF-binding) are sorting adaptors that are major determinants of the transport from TGN to endosome [36]. GGAs are monomeric and they have a unique four-domain structure consisting of a VHS (Vps27, Hrs, STAM) domain, a GAT (GGA and TOM1) domain, a hinge-like domain and an ear domain. GGA proteins are recruited to late Golgi membranes by the action of ARF GTPase and bind to clathrin through a hinge-like region and to acidic dileucine cargo sequence through VHS domain [37]. In addition, GGAs were shown to bind ubiquitin through the GAT domain, indicating their role in ubiquitin-sorting at the TGN [38 36]. Defects in TGN to endosome trafficking in AP-1 mutant, heteromeric adaptor complex, are exacerbated by deleting *GGAs*, suggesting that AP-1 and GGAs functions might overlap [25].

Retrieval from endosomes to TGN. Resident TGN proteins that contain specific retention signals, for instance CPY receptor Vps10 and Kex2 protease that processes α-factor, are prevented from entering the vacuole by an active

retrieval mechanism from the endosomal system to the TGN. Cytosolic tails of the proteins Kex2 and Vp10 were demonstrated to contain aromatic sequences that serve as a retention signal for the retromer complex. This protein complex consists of five Snx proteins (sorting nexins), a Vps5-Vps17 dimer and Vps26-Vps29-Vps35 trimer. Snx proteins contain PX domains (phox homology) that allow binding to the endosome-specific lipid phosphatidylinositol 3-phosphate PI(3)P. Furthermore, the Snx proteins contain BAR domains that are predicted to induce membrane curvature [39] [40].

MVB-dependent sorting. The "multivesicular body" (MVB) was first described in the 1960s by George Palade [1] as a special organelle that consists of a single limiting membrane enclosing multiple vesicles. MVBs represent late endosomes that are packed with intralumenal vesicles enriched with cargo proteins. MVBs play a key role in delivering endocytic cargo and AP-3-independent biosynthetic cargo (for instance transmembrane CPS) to the vacuolar lumen by sorting cargo into intralumenal MVB vesicles. Upon fusion of the MVB with the vacuole, the MVB vesicles are delivered into the vacuolar lumen. However, cargo that was retained on the limiting membrane of the MVB will not reach the vacuolar lumen, but rather be delivered to the vacuolar limiting membrane.

ESCRTs form MVBs. MVB biogenesis, or formation of intralumenal vesicles, depends on the function of ESCRT (Endosomal Sorting Complex Required for Transport) machinery that directly sorts cargo into MVB vesicles and promotes formation of MVB vesicles [41]. Sequential recruitment of four

different ESCRTs (0-, I-, II-, III) to the endosomal membrane, assembly and their subsequent solubilization by the Vps4 ATPase are essential steps for cargo sorting and formation of intralumenal MVB vesicles. Specificity of ESCRT recruitment to the endosomal membrane is achieved through interactions with ubiquinated cargo and endosome-enriched lipids and by binding of ESCRTs to other ESCRT proteins. Although the mechanism by which ESCRTs promote vesicle formation remains not well understood, it is clear that ESCRTs do not physically sculpt vesicles similar to coat proteins such as COP-II and clathrin, but rather force vesicles to form away from the cytosol.

The current model (Figure 1-3) of ESCRT-mediated sorting of cargo into MVB vesicles suggests that ESCRT-0 is recruited to endosomes via interaction with lipids and ubiquitinated cargo and can potentially interact with clathrin and GGA proteins. ESCRT-0 recruits ESCRT-I that also interacts with ubiquitinated cargo and lipids. ESCRT-I induces endosomal localization of ESCRT-II that also bind ubiquitin and lipids. ESCRT-II mediates membrane recruitment of ESCRT-III subunits Vps20, Snf7, Vps2 and Vps24. Polymerization of ESCRT-III subunits is believed to drive cargo concentration and deformation of the endosomal membrane resulting in formation of vesicles. Vps4 ATPase is the only known enzyme that is involved in the MVB formation. Energy provided by the ATP hydrolysis by Vps4 is used to remove the ESCRT-III and possibly ESCRT-0, I and II from the endosomal membrane. Vps4-dependent solubilization of ESCRTs is believed to be the final step in the formation of intralumenal MVB vesicles.

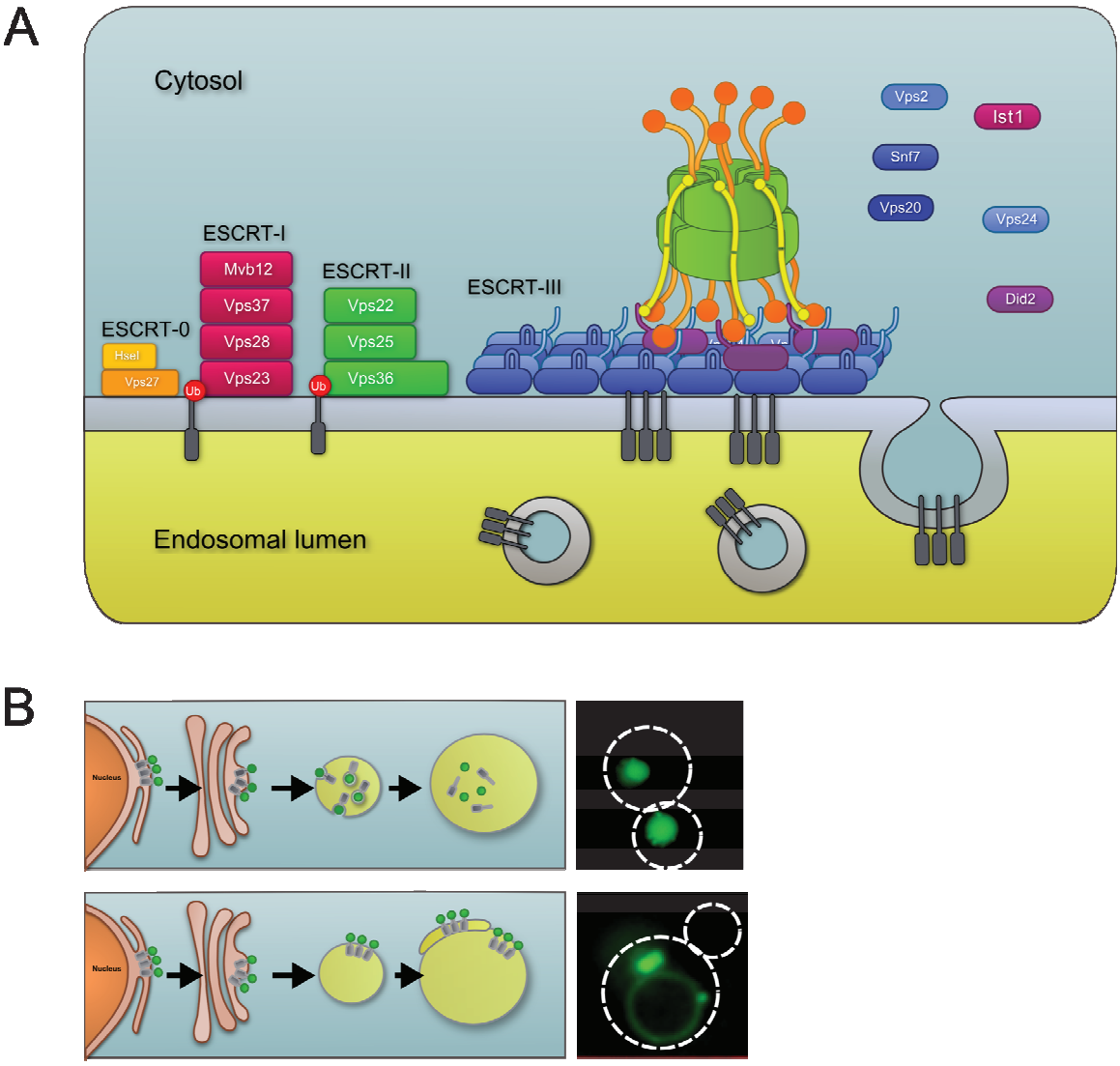

Figure 1-3. ESCRT-dependent sorting into MVBs. A. General model of the ESCRT-driven MVB biogenesis. ESCRT-0, I, II and III are recruited sequentially to the endosomal membrane where they promote cargo sorting into intralumenal vesicles. ESCRTs are solubilized by the Vps4 ATPase. B. Sorting of the GFP-CPS. Functional MVB pathway sorts GFP-CPS in MVB vesicles that delivers GFP-CPS into the vacuolar lumen (upper panel). Block in the MVB pathway results in the accumulation of GFP-CPS in the aberrant endosomal compartment (lower panel).

Activity of Vps4 is regulated by its recruitment to the ESCRT-III complex by ESCRT-III-associated proteins Did2, Ist1, Vta1 and Vps60.

Ubiquitin is a signal for sorting into MVBs. The major sorting signal that is recognized by the ESCRTs is ubiquitin. Interaction of ESCRTs with ubiquitinated cargo promotes sorting of that cargo into MVB vesicles [30]. Single ubiquitin was demonstrated to be sufficient for re-routing transmembrane cargo to the sorting into MVBs, indicating that monoubiqutination is a sufficient signal that sends cargo for sorting into MVBs [31]. Mutations that abolish ubiquitination of the CPS block sorting of the CPS into intralumenal MVB vesicles [29]. Intracellular ubiquitin levels are in part maintained by deubiquinating enzymes that recycle ubiquitin from cargo proteins before these proteins are sorted into the MVB vesicles [42]. Doa4, a member of a large family of ubiquitin-specific processing proteases (UBP), is the primary UBP that functions on MVBs to remove ubiquitin from ubiquitin-protein conjugates [43].

The sorting of the MVB cargo CPS fused to GFP is depicted in the Figure 1-3-B. GFP-CPS is sorted into MVB vesicles and is delivered into the vacuolar lumen, which is observed as homogeneous fluorescence in the vacuolar lumen (Figure1-3-B). When MVB formation is blocked, GFP-CPS is retained on the limiting membrane of the endosome and thus is delivered to the limiting membrane of the vacuole (Figure1-3-B). There is also accumulation of GFP-CPS in the aberrant late endosome, termed the class E compartment, which accumulates adjacent to the vacuole in MVB mutant strains.

Fusion of MVBs/endosomes with vacuole. Fusion of endosomes/MVBs with

the vacuole delivers cargo proteins into the vacuolar lumen. The yeast vacuole is an acidic compartment that is involved in a variety of functions including amino acid storage, inorganic ion storage and the degradation of macromolecules. Vacuolar resident proteins are hydrolases that function in the proteolytic cleavage of proteins. Amino acids that accumulate in the vacuolar lumen as a result of proteolysis are being pumped back to the cytosol where they can be reused for further rounds of protein translation. Yeast cells contain one to four vacuoles of ~0.5 μm in diameter that are seen under DIC imaging as round organelles [44]. Heterotypic fusion of endosomes with the vacuole is promoted by the activated Rab Ypt7, which interacts with the HOPS (homotypic fusion and vacuole protein sorting) tethering complex (Seals et al. 2000). The membrane-associated HOPS complex promotes the formation of a *trans*-SNARE complex containing Vam7, Vam3, Vti1 and Nyv1 [45].

Characterization of the *vps* mutants

The observation that the sorting of vacuolar proteins is an active process came from experiments which showed that mutations in the N-terminus of the soluble vacuolar hydrolase CPY or its overproduction resulted in the secretion of CPY [46]. Over thirty years ago, several genetic screens in *Saccharomyces cerevisiae* were performed in an attempt to identify the cellular protein machinery that mediates delivery of the proteins to the vacuole (summarized in [47]). As a result of combined efforts of Tom Stevens and Scott Emr working in Randy Schekman's group over 45 genes termed *VPS* (Vacuolar Protein Sorting) were

identified as involved in the transport of newly synthesized hydrolases to the vacuole.

A majority of the genetic screens identified mutants that secret CPY as an indication of the perturbed transport to the vacuole. For instance, a screen performed by the Tom Steven's group selected for the acquired auxotrophic growth as a result of CPY secretion in mutagenized yeast. Secreted CPY catalyzes peptide bond cleavage of the N-blocked dipeptide N-CBZ-L-phenylalanyl-L-leucine (CBZ-pheleu) and therefore allows leucine auxotrophs to grow on medium supplemented with CBZ-pheleu as a sole leucine source [48].

Scott Emr's group performed a genetic screen that selected for the spontaneous sucrose-fermenting mutants as a result of the secretion of CPY-invertase fusion protein. Invertase is a secretory enzyme that catalyzes sucrose hydrolysis allowing yeast to utilize sucrose as a carbon source. Fusion of CPY to Invertase targets the fusion protein to the vacuole and hence the cells are unable to utilize sucrose as carbon source. Therefore, mutations in genes that are required for transport to the vacuole allow growth on sucrose-rich medium [49].

Vacuolar morphology of *vps* mutants was characterized using fluorescent dyes that label vacuoles. These experiments identified three classes: class A containing large vacuoles, class B containing fragmented vacuoles and class C that lacked structured vacuoles [50]. Tom Stevens's group continued to classify *vps* mutants based on the vacuolar morphology using immunofluorescence microscopy and an antibody against transmembrane vacuolar hydrolase ALP. Assembly of the vacuolar H+-ATPase (v-ATPase) was assayed using antibody

against 60 kDa subunit of the v-ATPase. Vacuolar acidification was judged by quinacrine staining [51]. The result of this analysis was a classification of the ~45 *vps* mutants into six groups (Class A to F; see Table 1-1) [52].

Class A: Wild-type vacuoles, with properly assembled V-ATPase

Class B: Fragmented vacuole with properly assembled V-ATPase;

Class C: Absence of coherent vacuoles;

Class D: Defect in vacuole inheritance and acidification;

Class E: Aberrant prevacuolar compartment termed “class E” found adjacent to the vacuole;

Class F: Large central vacuole with one or two vacuoles adjacent.

The class E VPS group. Thirteen *VPS* genes comprise the class E group. Transmission electron microscopy (TEM) demonstrated that the defining feature, the class E compartment, consists of aberrant elongated endosomal membranes that accumulate adjacent to the vacuole [53]. The class E compartment is an aberrant late endosome that is devoid of intralumenal vesicles. As a result of the block in the intralumenal MVB vesicle formation, endocytic (for instance Ste3) [54] and biosynthetic (for instance CPS) [53] cargoes that normally undergo sorting into MVB vesicles accumulate on the limiting membrane of the class E compartment. Extensive biochemical and cell biological studies identified that most of the class E proteins comprise subunits of the ESCRT proteins that mediate the formation of MVB vesicles. The function of the ESCRTs, together with the Vps4 ATPase, is described in detail in the next sections.

Table 1-1. VPS genes required for the transport to the vacuole.

Class	Gene names	Vacuolar phenotype
A	*VPS*8 (CORVET), *VPS*10, *VPS*13, *VPS*29 and *VPS*35 (retromer), *VPS*30 (Atg6, Beclin), *VPS*38 (PtdIn3 kinase complex), *VPS*44 (N+/K=/H+ exchanger), *VPS*46 (Did2, Doa4-independent degradation)	Wild-type vacuoles, with properly assembled V-ATPase
B	*VPS*5 and *VPS*17 (retromer); *VPS*39 and *VPS*41 (HOPS), *VPS*43 (Vam7)	Fragmented vacuole with proper V-ATPase
C	*VPS*11, *VPS*16, *VPS*18, *VPS*33 (CORVET)/HOPS	Absence of coherent vacuoles
D	*VPS*3 (CORVET), *VPS*6 (SNARE), *VPS*9 (GEF for Rab5), *VPS*15, *VPS*19, *VPS*21 *VPS*34 (kinase, synthesizes PI(3)P), *VPS*45 (*SEC1* homolog)	Defect in vacuole inheritance and acidification
E	*VPS*2, *VPS*4, *VPS*20, *VPS*22, *VPS*23, *VPS*24, *VPS*25, *VPS*27, *VPS*28, *VPS*31 (Bro1), *VPS*32 (Snf7), *VPS*36, *VPS*37.	Aberrant prevacuolar compartment Class E found adjacent to the vacuole
F	*VPS*1 (Dynamin homolog), *VPS*26 (Pep8 - retromer)	Large central vacuole with one or two vacuoles adjacent

ESCRT machinery promotes MVB biogenesis

ESCRT-dependent cargo sorting into MVBs. Genetic screens in yeast identified 13 class E *vps* mutants that have defects in sorting of proteins into MVBs. Twelve of the class E Vps proteins comprise four ESCRT protein complexes (0-, I-, II- and III) and enzyme Vps4 ATPase [55] [29] [56] [57]. Each of these complexes has human orthologs that are required for trafficking into lysosome, the mammalian equivalent of the yeast vacuole (Table 1-2).

There is genetic and biochemical data to suggest that the ESCRT complexes are recruited sequentially to the endosomal membranes where they interact with endosomal lipids, ubiquitinated cargo and each other in promoting MVB sorting. Vps4 ATPase belongs to the class E *vps* proteins and is thought to function in the final step of the MVB formation by disassembling the ESCRT-III complex from endosomes. The function of Vps4 is regulated through its recruitment to ESCRT-III. Regulation of Vps4 recruitment to ESCRT-III is a focus of current research and is therefore described in detail in the following chapter. It is important to note that the ability of the ESCRTs to interact with cargo molecules and deform membranes placed them as key components in other cellular processes besides formation of MVBs. ESCRTs promote the abscission step of cytokinesis reviewed in [58], viral budding, including HIV-1 reviewed in [59], autophagy [60] and melanosome biogenesis [61]. ESCRTs function on the cytosolic side of the membrane and promote deformation and scission of membranes “away” from the cytosol and ESCRTs, therefore unifying seeming unrelated processes of MVB formation, HIV-1 budding and cytokinesis.

Table 1-2. Proteins that regulate MVB sorting

Complex name	Yeast	Mammalian
ESCRT-0	Vps27 Hse1	Hrs STAM1/2
ESCRT-I	Vps23 Vps28 Vps37 Mvb12	Tsg101 Vps28 Vps37 A, B, C Mvb12
ESCRT-II	Vps36 Vps22 Vps25	EAP45 EAP30 EAP22
ESCRT-III	Vps20 Snf7 Vps24 Vps2	CHMP6 CHMP4A, B, C CHMP3 CHMP2A,B
AAA+ ATPase	Vps4	VPS4A, B
Bro1	Bro1	Alix
Regulatory proteins		
Ist1	Ist1	Ist1
Did2	Did2	CHMP1A,B
Vta1	Vta1	Lip5
Vps60	Vps60	CHMP5

ESCRT-0. Vps27 and Hse1 comprise the ESCRT-0 complex required for the MVB sorting of endocytic and biosynthetic ubiquitinated cargo molecule [62]. ESCRT-0 functions in engaging ubiquitinated cargo from early endosomes to sorting into MVBs. ESCRT-0 functions through interaction with ubiquitinated cargo, endosome-enriched lipids, interaction with clathrin and GGAs proteins. Endocytic cargo that does not interact with ESCRT-0 recycles back to the plasma membrane [63] whereas biosynthetic cargo that does not associate with ESCRT-0 is missorted to the vacuolar membrane [64] [65].

Vps27 contains an amino-terminal VHS (Vps27, Hrs and STAM) domain, FYVE FYVE (*F*ab-1, *Y*GL023, *V*ps27 and *E*EA1) [66], two UIM (Ubiquitin Interaction Motifs) binding domains, GAT (GGA and TOM) and clathrin-binding domains (Figure 1-4). The domain structure of Hse1 includes an N-terminal VHS domain, an UIM domain, an SH3 domain (Src homology 3 domain) and a GAT domain. Vps27 and Hse1 interact with each other through the GAT domains [67].

The FYVE domain of Vps27 specifically interacts with endosome-enriched PI(3)P [65] [62]. Interaction of ESCRT-0 with the ubiquitin-tag of MVB cargo is essential for the vacuolar delivery of these cargo proteins, as exemplified by the endocytic cargo Ste3 and the biosynthetic cargo CPS [68]. Two UIM domains in Vps27 and one UIM domain in Hse1 are the major determinants that mediate ubiquitin binding [69].

ESCRT-I. Endosome-localized ESCRT-0 recruits ESCRT-I via interaction of the C-terminal PSDP motif of Vps27 with the N-terminal domain of Vps23 [65] [70]. ESCRT-I is recruited to endosomes by an interaction with the ESCRT-0 and this

Figure 1-4. Interactions of ESCRTs with ubiquitin, lipids and each other. ESCRT-0, I and II interact with ubiquitinated cargo and lipids. Structure of ESCRT-III and ESCRT-III-like proteins is similar – coiled-coil, N-terminus is positively charged, and C-terminus is negatively charged. C-terminus of ESCRT-III proteins mediates interaction with Vps4 ATPase.

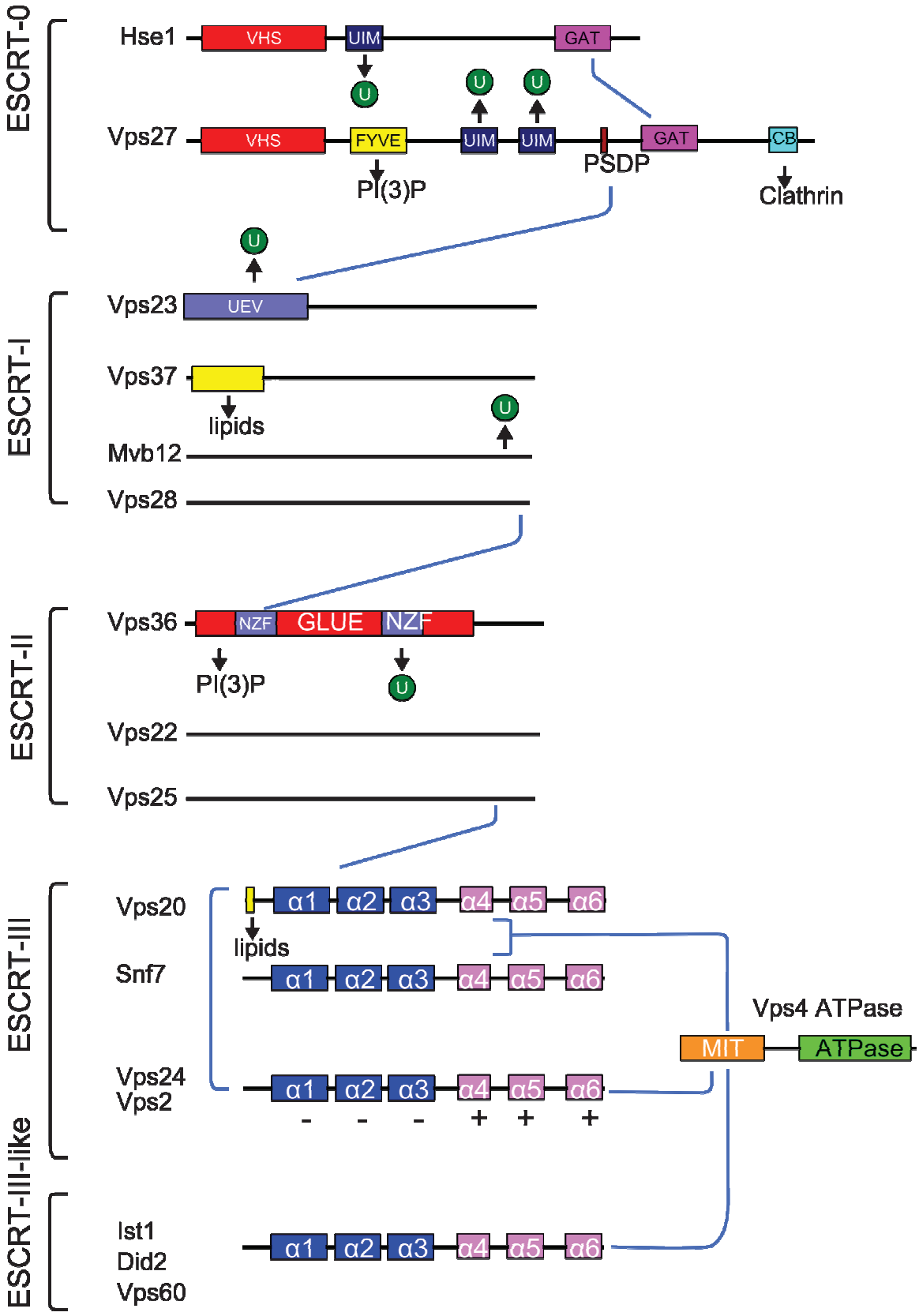
ESCRT-0
Hse1
VHS
UIM
GAT
U
Vps27
VHS
FYVE
UIM
UIM
GAT
CB
PSDP
PI(3)P
Clathrin
ESCRT-I
Vps23
UEV
Vps37
lipids
Mvb12
Vps28
ESCRT-II
Vps36
NZF
GLUE
NZF
PI(3)P
Vps22
Vps25
ESCRT-III
ESCRT-III-like
Vps20
lipids
Snf7
Vps24
Vps2
Ist1
Did2
Vps60
α1
α2
α3
α4
α5
α6
- - - + + +
Vps4 ATPase
MIT
ATPase

recruitment is required for downstream cargo sorting [29]. The main role of ESCRT-I is to recognize ubiquitinated cargo via the UEV (enzyme E2 variant) domain of the Vps23 [71] [64] and ESCRT-I exists as a preassembled complex that consists of four subunits in a 1:1:1:1 ratio - Vps23 Vps28, Vps37 and Mvb12 (Multivesicular body 12) [72].

The crystal structure of the yeast ESCRT-I complex revealed an elongated heterotetramer of ~20 nm in length consisting of stalk and headpiece [73]. The N-terminal UEV domain of Vps23, which projects from the ESCRT-I stalk, mediates interactions with ESCRT-0. The C-terminus of Vps28, which projects from the head piece, mediates interaction with the N-terminal GLUE (*G*RAM-*l*ike ubiquitin-binding in *E*AP45) domain of Vps36. The N-terminal UEV domain of Vps23 together with the C-terminal domain of Mvb12 [74] mediate binding to ubiquinated cargo (Figure 1-4).

Endosome localization of ESCRT-I is achieved in part by weak binding of lipids through the positively charged N-terminus of Vps37 [73]. Moreover, association with ESCRT-II results in the increased affinity of ESCRT-I to lipids, in particular PI(3)P, suggesting that ESCRT-II helps in recruiting ESCRT-I. ESCRT-I acts upstream of ESCRT-II as demonstrated by the rescue of MVB sorting defect by the overexpression of ESCRT-II in cells lacking ESCRT-I [56].

ESCRT-II. ESCRT-II is a stable cytosolic complex that contains Vps22, Vps36 and two subunits of Vps25. Dissection of the ESCRT-II assembly *in vivo* demonstrated that the “stem” of the “Y” shape of the ESCRT-II complex is contributed by Vps36 and Vps22, whereas “ears” are contributed by two subunits

of Vps25 [75].

ESCRT-II functions in binding to ESCRT-I, PI(3)P and ubiquitinated cargo through the GLUE domain of Vps36. Binding of the GLUE domain together with the FYVE domain of Vps27 provide specificity of interaction with PI(3)P that is enriched in endosomes. [72]. Two NZF (*N*pl4-type *z*inc *f*inger) domains are inserted into the GLUE domain of Vps36 - the first NZF (110-151 amino acids) binds to Vps28, and the second NZF (176-205) binds ubiquitin (Figure 1-4) [72]. Vps25 mediates recruitment of ESCRT-III through interaction with the N-terminus of Vps20 [76].

ESCRT-III

ESCRT-III is functionally the most downstream of the ESCRTs. The core of ESCRT-III consists of the four subunits Vps20, Snf7, Vps2 and Vps24. In contrast to ESCRT-0, -I and –II, ESCRT-III subunits do not interact with ubiquitin and do not exist as a preformed cytosolic complex [57]. Current models of ESCRT-III organization propose that the ESCRT-III subunits assemble into a large molecular weight complex. This oligomerization is initiated by the membrane-localization of Vps20 which nucleates polymerization of Snf7 into spiral-like structures. Recruitment of Vps24 and Vps2 regulates size of the Snf7 oligomer [77]. After ESCRT-III is assembled on the membrane, the Vps4 ATPase is recruited. Vps4 is essential for the disassembly of ESCRT-III which is believed to promote vesicle formation. ESCRT-III-associated proteins Did2, Ist1, Vta1 and Vps60 aid in the recruitment of Vps4 by direct binding to ESCRT-III core subunits

and Vps4.

ESCRT-III proteins are structurally similar. ESCRT-III proteins (Vps20, Snf7, Vps24, Vps2, Ist1, Did2 and Vps60) are soluble small ~200 amino acids proteins that have a similar secondary structure. They are composed of a common set of six predicted alpha-helices, of which the N-terminally localized α1-α3 are basic (positively-charged) and α4-α6 are acidic (negatively-charged) [78] (Figure 1-4). The N-terminal region of ESCRT-III proteins is required for the membrane association, as deletion of the part of alpha-1 shifted Snf7 to the soluble fraction [79]. ESCRT-III subunits interact with each other through their N-termini as demonstrated by the crystal structure of the N-terminal part of CHMP3, mammalian homolog of Vps24 that formed antiparallel dimers mediated by the helix 2 regions of two subunits [80]. C-terminal regions of ESCRT-III subunits mediate interaction with the N-terminus of the Vps4 ATPase MIT (Microtubule Interaction and Trafficking) domain [79] [81].

ESCRT-III core complex assembly in vivo. Core components of the ESCRT-III complex, Vps20, Snf7, Vps2 and Vps24, were first characterized by Markus Babst as one of the class E proteins that accumulated on the endosomal membranes in *vps4* mutant strains [82]. Initial biochemical analysis demonstrated that ESCRT-III subunits exist as monomers or dimers in the cytosol, as demonstrated by the size exclusion chromatography (SEC) [82]. In contrast, the endosome-associated ESCRT-III complex formed a large structure that was sedimentable at 100,000 X g [82]. The membrane-associated ESCRT-III complex was demonstrated to be partially resistant to the treatment with detergent [81]. The

core of ESCRT-III does not exist in a stoichiometric 1:1:1:1 ratio [77]. Snf7 is represented by ~7000 molecules/cell and is ten times more abundant than Vps20 and twice more abundant than Vps2 and Vps24. The proposed stoichiometry of ESCRT-III core complex is Vps20:Snf7:Vps24:Vps2 = 1:10:5:5 [77].

Membrane localization of ESCRT-III is achieved through interaction of Vp20 with Vps25 and through lipid interaction by the myristyl group attached to the N-terminus of Vps20 [82]. ESCRT-III subunits were demonstrated to be recruited in the sequential manner. Membrane-localization of Vps20 nucleates recruitment and polymerization of Snf7. Deletion of either *VPS20* or *SNF7* did not abolish formation of the ESCRT-III complex, but rather result in the formation of two ESCRT-III subcomplexes, Vps20/Vps2/Vps24 and Snf7/Vps2/Vps24. Those ESCRT-III subcomplexes accumulate on endosomes in a Vps4-dependent manner, suggesting that they are recycled by the Vps4 ATPase [82]. Deletion of both *VPS20* and *SNF7* abolished recruitment of Vps2 and Vps24 to membranes, suggesting that Vps20 and Snf7 are recruiting determinants for Vps2 and Vps24. Furthermore, Vps2 and Vps24 require each other for the proper recruitment to the ESCRT-III subunits and for the recruitment of Vps4.

In vivo recruitment of the ESCRT-III-associated proteins. Recruitment and assembly of the Vps4 ATPase is aided by ESCRT-III-associated proteins Did2, Ist1, Vta1 and Vps60.

Did2 binds Vps2 and Vps24 through its N-terminus, as deletion of either Vps2 or Vps24 caused Did2 to remain cytosolic [83]. The N-terminus of Did2 (similar to other ESCRT-III core proteins) is sufficient to interact with Vps2 and

Vps24 as demonstrated by endosomal localization of Did2(N)-GFP and *in vitro* binding of Did2(N-terminus) to Vps24 [83]. Furthermore, Did2 mediates solubilization of ESCRT-III through recruitment of the Vps4 ATPase as deletion of Did2 results in the enhanced membrane association of Snf7 and Vps2 [84].

Ist1 (Increased salt tolerance 1) is a 298- amino acid soluble protein containing a coiled-coil C-terminal region and a conserved N-terminal ELYC domain [85]. Full-length Ist1 and the C-terminus of Ist1 were identified through yeast two-hybrid assays as a potential interactor with Vps4 [85]. Although studies have shown that Ist1 is a regulator of Vps4, the deletion of *IST1* does not have an obvious defect in MVB sorting [85]. The current model proposes that Did2 and Ist1 function together in regulating the recruitment of Vps4 to ESCRT-III [86].

Vta1 (Vps20 associated 1) is a soluble 330 amino acid protein. Vta1 was identified as an interactor with Vps4 and by yeast two-hybrid and GST-pulldown assays [87]. Vta1 is composed of two N-terminal MIT (Microtubule Interacting and Trafficking) domains (MIT1 and MIT2) and a C-terminal conserved VSL (Vta1/BP1/Lip5) domain of 30 amino acids. Structural analysis revealed that Vta1 exists as an elongated homodimer with VSL regions in the middle and MIT domains pointing in opposite directions [88]. Vta1 binds to the Vps4 ATPase domain through its VSL region. Vta1 binds to the ß-domain of Vps4 in the ATP-dependent manner, in a 1:2 ratio (12 Vps4/ 3 dimers Vta1 per oligomer) [89] [86]. The second MIT domain of Vta1 binds to the C-terminus of Did2 and Vps60 [88]. Vta1 requires Vps4 and Did2 for endosomal localization, as demonstrated by cytosolic distribution of Vta1-GFP in *Δvps4Δdid2* cells [84].

Vps60 is a 229 amino acid protein homologous to Snf7 and other subunits of the ESCRT-III complex. The first three helices are basic (1-120) and α4-α5 (127-174) are acidic. α4-α5 (127-174) of Vps60 are sufficient for binding to MIT2 of Vta1 [88].

ESCRT-III subunits deform membranes and polymerize into tubular structures. ESCRT-III core subunits were demonstrated to have an intrinsic ability to polymerize into tubular structures *in vitro* [80 90 91 92 93]. ESCRT-III was demonstrated to polymerize into spiral-shape structures *in vivo* [94] that is believed to promote concentration of cargo and deform membranes. Overexpression of the mammalian homologs of Snf7, CHMP4A and CHMP4B, in mammalian cells results in their targeting to the plasma membrane where they self-associate into a circular array consisting of ~5 nm-long curved filaments, structures resembling spirals. Human Vps4B hydrolytic mutant, which is incapable of solubilizing CHMP4, promoted bending of membrane associated Snf7 spirals which resulted in the formation of membrane-covered tubes that protruded outwards from the cell. This observation suggested that Snf7 polymers are able to induce membrane deformation [94].

In vitro studies done by Dr. Hurley's group reconstituted ESCRT-driven formation of vesicles using Giant Unilamellar Vesicles (GUVs). ESCRT-0 was demonstrated to concentrate ubiquitinated cargo and ESCRT-I and II deformed the membrane into buds, in which cargo was confined. ESCRT-III localized to the bud neck and promoted membrane scission resulting in the formation of intralumenal vesicles devoid of ESCRT components [95 96].

Current model of ESCRT-III polymerization. The endosome-associated ESCRT-III core complex is thought to polymerize into a large spiral-shape structure [94] that is believed to promote concentration of cargo and promote membrane deformation and scission. Once assembled on the endosomal membrane, ESCRT-III requires energy provided by the Vps4 ATPase to be solubilized from the membranes. Solubilization of ESCRT-III by the Vps4 ATPase is believed to be the final step that results in vesicle formation [57]. Function of the Vps4 ATPase is regulated by its recruitment to ESCRT-III by the four ESCRT-III-associated proteins Did2, Ist1, Vta1 and Vps60.

Vps4 AAA+ ATPase

Vps4 belongs to a large family of AAA+ (ATPase associated with a variety of cellular activities) ATPases [97]. Vps4 is a soluble, nonessential protein that consists of 437 amino acids containing three functionally and structurally separate regions: the N-terminal substrate interacting or MIT (Microtubule Interacting and Trafficking) domain (amino acids 1-79) [98], the unstructured linker domain (79-123) and the C-terminal ATPase domain, which is composed of a large and a small subdomain (amino acids 123-437) (Figure 1-5-A) [99]).

The AAA+ family comprises functionally diverse group of enzymes that function in a variety of cellular processes by inducing conformational changes in substrate proteins [100]. The defining feature of AAA+ proteins is a structurally conserved ATPase domain containing ATP-binding pockets at the interface of neighboring subunits that promote assembly into oligomeric rings [101]. Various

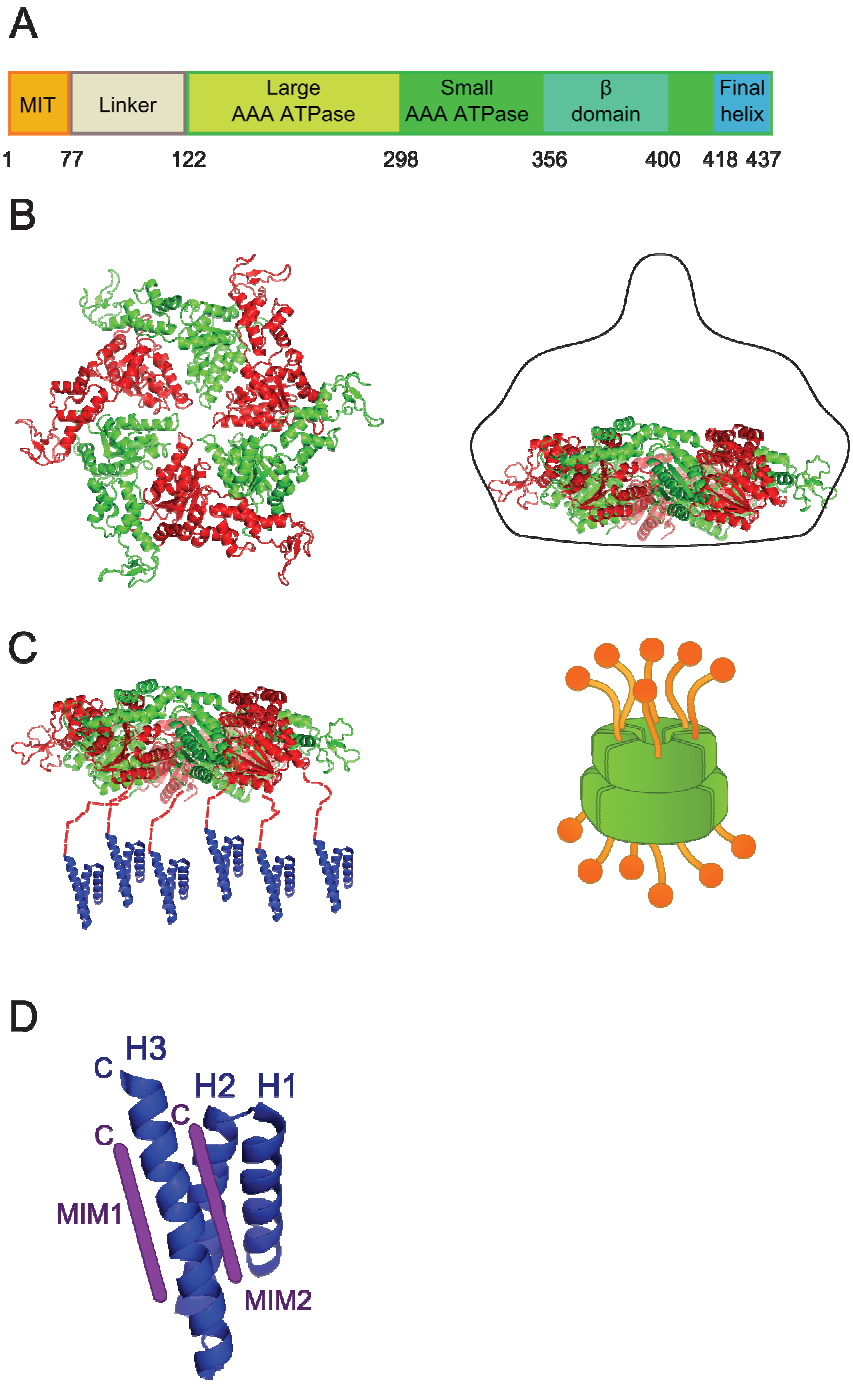

Figure 1-5. Structure of the Vps4 AAA+ ATPase. A. Schematic of the domain organization. B. Model of the hexameric ring composed of ATPase domains, top view and side view including linker region and MIT domains. C. Hexameric ring positioned in the oligomeric structure. D. MIM1 and MIM2 binding sites on the MIT domain.

domains that are attached to the ATPase domains provide functional specificity to AAA+ proteins by interacting with adaptor proteins or substrates [102]. For instance, the N-terminal MIT domain provides substrate specificity for Vps4 through interaction with ESCRT-III proteins.

Walker A and Walker B motifs are integral parts of the AAA+ ATP-binding pocket. A lysine residue within the Walker-A motif GXXGXGKT/S directly interacts with the phosphates of ATP. Therefore, mutation of this lysine residue of the Walker A domain eliminates nucleotide binding and inactivates the AAA+ protein [102]. A glutamate residue within the Walker-B D(D/E) motif promotes ATP hydrolysis by activating a water molecule. Therefore, mutation of this glutamate blocks nucleotide hydrolysis and produces a nonfunctional ATP-locked form of the AAA+ ATPase. Conserved arginine residue from the neighboring subunit functions together with Walker A and B motifs and completes the functional bi-partite nucleotide binding pocket. Therefore, binding of ATP to the bi-partite nucleotide-binding pocket promotes oligomerization of AAA+ ATPases that function as oligomeric rings [101].

Class I and Class II. Class I AAA ATPases contain a single ATPase cassette, for instance Katanin and Vps4. Class II AAA ATPases contain two ATPase cassettes termed D1 and D2, for instance mammalian ATPases p97 and NSF [101]. Class II ATPases assemble into ring structures where both ATPase domains stack in two separate rings on top of each other. In the case of the NSF, the D1 ATPase domain was demonstrated to be the major ATPase, responsible for the ATP-dependent activity of this enzyme. In contrast, the D2 domain has

only minor ATPase activity but seems to play an important structural role in stabilizing the oligomer. Unlike NSF, the D1 domain of p97 is important for oligomerization while the p97-D2 domain is the major ATPase domain [103]. Class I ATPases usually assemble into a single hexameric or heptameric ring. For instance, Katanin assembles into a single hexameric ring and this assembly is promoted by binding to microtubules, the substrate of katanin. ATP hydrolysis by katanin severs the bound microtubule [104]. In contrast to katanin, the Vps4 oligomer was reported to assemble into a double ring structure. Similar to Class II ATPases, one ring in the Vps4 oligomer is proposed to provide ATP hydrolysis whereas the second ring contributes to a stable assembly of the Vps4 oligomer.

Structure of the Vps4 oligomer. The crystal structures of human Vps4B and yeast Vps4 ATPase domains revealed small and large subdomains with a distinct beta-domain inserted within the small ATPase domain [105] [106] (Figure 1-5-B). Assembly of the Vps4 hexamer was modeled using the previously solved structure of related AAA+ ATPase p97 [107], predicting diameter of the Vps4 hexamer ring ~110 Å (145 including beta-domains) and height 35 Å [108].

Three different structures of the assembled Vps4 oligomer revealed a double-stacked assembly of hexameric rings [89] [109] or heptameric rings [108]. The dodecameric model of the Vps4 oligomer composed of two hexameric rings assembled back-to-back with MIT domains projected outside from both rings fits into the data obtained from modeling of the Vps4 assembly using p97 crystal structure [89]. Yu and colleges reported a double-stacked ring structure is ~ 9 nm tall. The bottom ring is ~10 nm in diameter and is similar to the p97 ring

conformation. The top ring contains a large cavity of ~ 5 nm in diameter. MIT domains of the top ring form a dense structure of ~ 3.5 nm long above the cavity. MIT domains in the bottom ring are found at the periphery (Figure 1-5-B and C).

Function of the Vps4 ATPase in the MVB sorting. Higher metazoans express two alleles, VPS4A and VPS4B, whereas fungi, including *S. cerevisiae*, express a single *VPS4* allele. Human Vps4A and Vps4B share 80% identity between each other and share ~60% identity with yeast Vps4 (for sequence alignment see [105]). Deletion of *VPS4* in *S. cerevisiae* by was rescued by murine Vps4B (and Vps4A to a lesser extent), indicating conserved function of Vps4 proteins [110].

The function of Vps4 in the formation of MVBs was first described by Markus Babst [97]. Deletion of *VPS4* displayed phenotypes similar to those of other class E *vps* mutants. Strains mutated for *VPS4* secreted CPY and stabilized the plasma membrane protein Ste6 [111]. Furthermore, ESCRT-III core proteins where observed to accumulate on endosomes in *Δvps4* cells, suggesting that ESCRT-III might be a substrate for the Vps4 ATPase [57]. Further proof that ESCRT-III proteins are a substrate for the Vps4 ATPase was obtained from studies that solved the crystal structure of the C-terminus of Vps2 in complex with the Vps4 MIT domain [112] and the C-terminus of CHMP1A, homolog of Did2, with the human Vps4A MIT domain [113].

In vitro biochemical characterization demonstrated that ATPase activity of Vps4 was dependent upon protein concentration. Titration experiments with increasing concentration of Vps4 measured an ATPase activity at 0.3 μM of ~10

ADP/min/Vps4 which increased to ~25 ADP/min/Vps4 at ~1 μM Vps4, suggesting that Vps4 oligomerizes in the concentration-dependent manner [82]. Introducing point mutations in the ATPase cassette (K179A or E233Q) abolished Vps4 ATPase activity. The K179A mutation in Vps4 renders the protein defective in ATP binding [82]. The E233Q mutation impairs hydrolysis of the bound ATP and thus interferes with the function of Vps4.

MIT domains interact with ESCRT-III C-terminal regions. The MIT domain of Vps4 was identified by homology to other MIT domain-containing proteins, including katanin and spastin [98]. The MIT domain of Vps4 directly interacts with ESCRT-III and therefore mediates recruitment of Vps4 to MVBs. The MIT domain binds similar motifs at the C-termini of ESCRT-III subunits that are termed MIMs (MIT Interaction Motifs). Two distinct MIMs have been identified in ESCRT-III subunits, called MIM1 and MIM2 [110]. The MIT domain of Vps4A forms an antiparallel three helix bundle [114]. Helices two and three form coiled-coil structure and interact through canonical “knob in holes” side chain interaction. The MIM1- and MIM2-binding sites are localized to different groves of the MIT domain, enabling simultaneous binding to both types of MIMs (Figure 1-5-D) [115].

The MIM1 consensus motif (- - - LXX+LAAL+) is found at the very C-terminus of Vps2, Vps24, Did2 and Ist1 [116]. Structural studies of the Vps4 MIT domain bound to the C-terminus of CHMP1A, human homolog of Did2, and Vps2 revealed that the MIM1 motif binds parallel to helix three in the groove between helix two and three of the Vps4 MIT domain.

The MIM2 consensus motif (ϕ - LP - VPS- x LP) lies in between helices four

and five of Vps20 and Snf7. The NMR structure of the Vps4A MIT domain with the mammalian homolog of Vps20, CHMP6, demonstrated that the MIM2 motif binds parallel to helix three of the MIT domain in the groove between helices one and three [115]. As a result of binding to different surface areas of the MIT domain, MIM1 and MIM2 motifs can bind simultaneously to the MIT domain.

Ist1 is the only ESCRT-III-type protein that has both MIM1 and MIM2 motifs. As a consequence, Ist1 binds the Vps4 MIT domain with a Kd of ~3 μM, lower than any Kd found for other MIM-Vps4 MIT interactions [91].

Interactions of the Vps4 ATPase with ESCRT-III proteins. Interactions with ESCRT-III proteins mediate recruitment of Vps4 to endosome-associated ESCRT-III (Figure 1-6) (detailed network of interactions is summarized in Chapter 2 [86]) In addition, interaction with ESCRT-III proteins regulates ATPase activity of Vps4 [117]. Ist1 negatively regulates Vps4 ATPase activity by disrupting oligomerization of Vps4 producing Ist1-Vps4 dimers [85]. The C-terminal domain of Ist1 binds to the MIT domain of Vps4 and the N-terminus of Ist1 binds the ATPase cassette Vps4 [85].

Binding to Vta1 promotes oligomerization of Vps4 and therefore stimulates Vps4 ATPase activity. Vta1 binds to the Vps4 ATPase domain through its C-terminal VSL region [83] that is sufficient to stimulation ATPase activity of Vps4. Vta1 binds to Vps4 in an ATP-dependent manner, forming a protein complex of 12 Vps4 subunits together with 3 Vta1 dimers [89].

Recent studies from Dr. Katzmann's group revealed that binding of Vps2, Did2 and ESCRT-III proteins to the MIT domain of Vps4 stimulates Vps4 ATPase

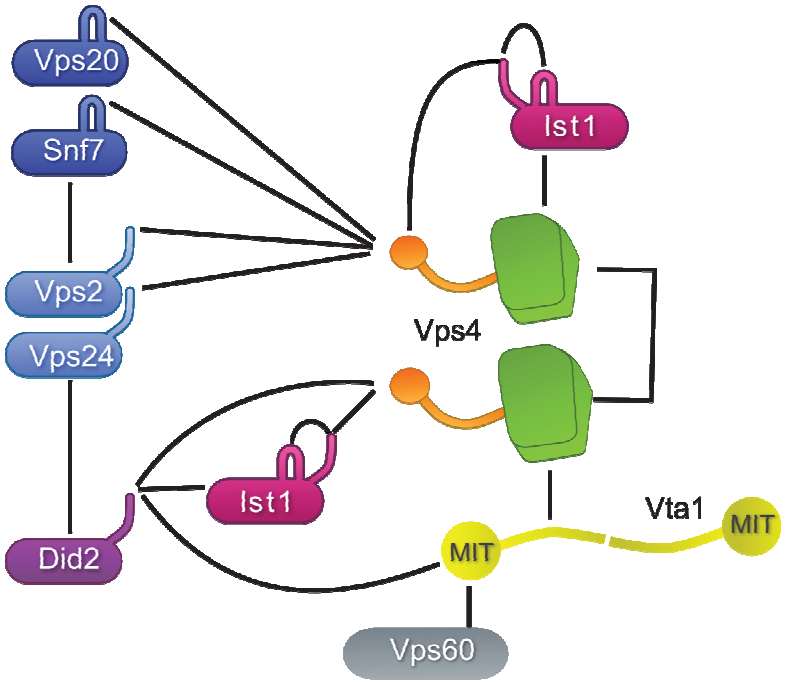

Figure 1-6. Network of interactions between Vps4 and ESCRT-III proteins based on previously published *in vitro* and *in vivo* studies (Chapter 2 and [86]).

activity [117]. In addition, binding of the C-terminal region of Ist1 to MIT domains also stimulated ATPase activity of Vps4 [85]. This increase in ATPase activity as a result of ESCRT-III-binding to MIT domains [118] could be explained by three possible mechanisms – stabilization of the Vps4 oligomer, direct relief of the autoinhibitory interactions through the MIT domain/linker region [119] with the ATPase cassette and conformational changes in the ATPase cassette [117].

The fully assembled Vps4 oligomer contains at least twelve MIT domains (dodecamer model) contributed by Vps4 and twelve MIT domains contributed by Vta1. Potentially, all twenty-four MIT domains can interact with ESCRT-III proteins Ist1, Did2, Vps60, Vps20, Snf7, Vps2 and Vps24. Therefore, recruitment

of the Vps4 to ESCRT-III, assembly into a functional oligomer, including regulation of its ATPase activity, is a result of a large protein network consisting of ESCRT-III core proteins and ESCRT-III associated proteins. Functional analysis of the ESCRT-III interactions with Vps4 is described in Chapter 2.

References

1. Palade, G. Intracellular aspects of the process of protein synthesis. *Science* **189**, 347 -358 (1975).

2. Lee, M.C.S., Miller, E.A., Goldberg, J., Orci, L. & Schekman, R. Bi-directional protein transport between the ER and Golgi. *Annual Review of Cell and Developmental Biology* **20**, 87-123 (2004).

3. Stenmark, H. Rab GTPases as coordinators of vesicle traffic. *Nat. Rev. Mol. Cell Biol.* **10**, 513-525 (2009).

4. Bröcker, C., Engelbrecht-Vandré, S. & Ungermann, C. Multisubunit tethering complexes and their role in membrane fusion. *Curr. Biol.* **20**, R943-952 (2010).

5. Epp, N., Rethmeier, R., Krämer, L. & Ungermann, C. Membrane dynamics and fusion at late endosomes and vacuoles--Rab regulation, multisubunit tethering complexes and SNAREs. *Eur. J. Cell Biol.* **90**, 779-785 (2011).

6. Hofmann, M.W. *et al.* Self-interaction of a SNARE transmembrane domain promotes the hemifusion-to-fusion transition. *J. Mol. Biol.* **364**, 1048-1060 (2006).

7. Sztul, E. & Lupashin, V. Role of tethering factors in secretory membrane traffic. *Am. J. Physiol., Cell Physiol.* **290**, C11-26 (2006).

8. Pelham, H.R. SNAREs and the specificity of membrane fusion. *Trends Cell Biol.* **11**, 99-101 (2001).

9. Antonin, W., Fasshauer, D., Becker, S., Jahn, R. & Schneider, T.R. Crystal structure of the endosomal SNARE complex reveals common structural principles of all SNAREs. *Nat. Struct. Biol.* **9**, 107-111 (2002).

10. Rothman, J.E. & Warren, G. Implications of the SNARE hypothesis for intracellular membrane topology and dynamics. *Curr. Biol.* **4**, 220-233 (1994).

11. Ungermann, C. & Langosch, D. Functions of SNAREs in intracellular membrane fusion and lipid bilayer mixing. *J. Cell. Sci.* **118**, 3819-3828 (2005).

12. Rathore, S.S., Ghosh, N., Ouyang, Y. & Shen, J. Topological arrangement of the intracellular membrane fusion machinery. *Mol. Biol. Cell* **22**, 2612-2619 (2011).

13. Phillipson, B.A. *et al.* Secretory Bulk Flow of Soluble Proteins Is Efficient and COPII Dependent. *The Plant Cell Online* **13**, 2005 -2020 (2001).

14. Katzmann, D.J., Odorizzi, G. & Emr, S.D. Receptor downregulation and multivesicular-body sorting. *Nat. Rev. Mol. Cell Biol* **3**, 893-905 (2002).

15. Miller, E., Antonny, B., Hamamoto, S. & Schekman, R. Cargo selection into COPII vesicles is driven by the Sec24p subunit. *EMBO J.* **21**, 6105-6113 (2002).

16. Barlowe, C. COPII: a membrane coat that forms endoplasmic reticulum-derived vesicles. *FEBS Lett.* **369**, 93-96 (1995).

17. Storrie, B. Maintenance of Golgi apparatus structure in the face of continuous protein recycling to the endoplasmic reticulum: making ends meet. *Int. Rev. Cytol.* **244**, 69-94 (2005).

18. Bednarek, S.Y., Orci, L. & Schekman, R. Traffic COPs and the formation of vesicle coats. *Trends Cell Biol.* **6**, 468-473 (1996).

19. Ren, Y. *et al.* A structure-based mechanism for vesicle capture by the multisubunit tethering complex Dsl1. *Cell* **139**, 1119-1129 (2009).

20. Spang, A. & Schekman, R. Reconstitution of retrograde transport from the Golgi to the ER in vitro. *J. Cell Biol.* **143**, 589-599 (1998).

21. Wang, C.-W., Hamamoto, S., Orci, L. & Schekman, R. Exomer: a coat complex for transport of select membrane proteins from the trans-Golgi network to the plasma membrane in yeast. *The Journal of Cell Biology* **174**, 973 -983 (2006).

22. Novick, P. *et al.* Interactions between Rabs, tethers, SNAREs and their regulators in exocytosis. *Biochem. Soc. Trans.* **34**, 683-686 (2006).

23. Hertzog, M. & Chavrier, P. Cell polarity during motile processes: keeping on track with the exocyst complex. *Biochem. J.* **433**, 403-409 (2011).

24. Beck, T., Schmidt, A. & Hall, M.N. Starvation induces vacuolar targeting and degradation of the tryptophan permease in yeast. *J. Cell Biol.* **146**, 1227-1238 (1999).

25. Robinson, M.S. & Bonifacino, J.S. Adaptor-related proteins. *Curr. Opin. Cell Biol.* **13**, 444-453 (2001).

26. Shih, S.C. *et al.* Epsins and Vps27p/Hrs contain ubiquitin-binding domains that function in receptor endocytosis. *Nat Cell Biol* **4**, 389-393 (2002).

27. Reider, A. *et al.* Syp1 is a conserved endocytic adaptor that contains domains involved in cargo selection and membrane tubulation. *EMBO J.* **28**, 3103-3116 (2009).

28. Dores, M.R., Schnell, J.D., Maldonado-Baez, L., Wendland, B. & Hicke, L. The function of yeast epsin and Ede1 ubiquitin-binding domains during receptor internalization. *Traffic* **11**, 151-160 (2010).

29. Katzmann, D.J., Babst, M. & Emr, S.D. Ubiquitin-dependent sorting into the multivesicular body pathway requires the function of a conserved endosomal protein sorting complex, ESCRT-I. *Cell* **106**, 145-155 (2001).

30. Belgareh-Touzé, N. *et al.* Versatile role of the yeast ubiquitin ligase Rsp5p in intracellular trafficking. *Biochem. Soc. Trans.* **36**, 791-796 (2008).

31. Stringer, D.K. & Piper, R.C. A single ubiquitin is sufficient for cargo protein entry into MVBs in the absence of ESCRT ubiquitination. *J. Cell Biol.* **192**, 229-242 (2011).

32. Huang, F., Goh, L.K. & Sorkin, A. EGF receptor ubiquitination is not necessary for its internalization. *Proc. Natl. Acad. Sci. U.S.A.* **104**, 16904-16909 (2007).

33. Piper, R.C., Bryant, N.J. & Stevens, T.H. The membrane protein alkaline phosphatase is delivered to the vacuole by a route that is distinct from the VPS-dependent pathway. *J. Cell Biol.* **138**, 531-545 (1997).

34. Ooi, C.E., Dell'Angelica, E.C. & Bonifacino, J.S. ADP-Ribosylation factor 1 (ARF1) regulates recruitment of the AP-3 adaptor complex to membranes. *J. Cell Biol.* **142**, 391-402 (1998).

35. Odorizzi, G., Cowles, C.R. & Emr, S.D. The AP-3 complex: a coat of many colours. *Trends Cell Biol* **8**, 282-288 (1998).

36. Black, M.W. & Pelham, H.R. A selective transport route from Golgi to late endosomes that requires the yeast GGA proteins. *J. Cell Biol.* **151**, 587-600 (2000).

37. Shiba, T. *et al.* Molecular mechanism of membrane recruitment of GGA by ARF in lysosomal protein transport. *Nat Struct Mol Biol* **10**, 386-393 (2003).

38. Scott, P.M. *et al.* GGA proteins bind ubiquitin to facilitate sorting at the trans-Golgi network. *Nat Cell Biol* **6**, 252-259 (2004).

39. Seaman, M.N.J., Michael McCaffery, J. & Emr, S.D. A Membrane Coat Complex Essential for Endosome-to-Golgi Retrograde Transport in Yeast. *The Journal of Cell Biology* **142**, 665 -681 (1998).

40. Bonifacino, J.S. & Hurley, J.H. Retromer. *Curr. Opin. Cell Biol.* **20**, 427-436 (2008).

41. Henne, W.M., Buchkovich, N.J. & Emr, S.D. The ESCRT pathway. *Dev. Cell* **21**, 77-91 (2011).

42. Losko, S., Kopp, F., Kranz, A. & Kölling, R. Uptake of the ATP-binding cassette (ABC) transporter Ste6 into the yeast vacuole is blocked in the doa4 Mutant. *Mol. Biol. Cell* **12**, 1047-1059 (2001).

43. Luhtala, N. & Odorizzi, G. Bro1 coordinates deubiquitination in the multivesicular body pathway by recruiting Doa4 to endosomes. *J. Cell Biol* **166**, 717-729 (2004).

44. Wickner, W. Membrane fusion: five lipids, four SNAREs, three chaperones, two nucleotides, and a Rab, all dancing in a ring on yeast vacuoles. *Annu. Rev. Cell Dev. Biol.* **26**, 115-136 (2010).

45. Hickey, C.M. & Wickner, W. HOPS initiates vacuole docking by tethering membranes before trans-SNARE complex assembly. *Mol. Biol. Cell* **21**, 2297-2305 (2010).

46. Stevens, T.H., Rothman, J.H., Payne, G.S. & Schekman, R. Gene dosage-dependent secretion of yeast vacuolar carboxypeptidase Y. *J. Cell Biol.* **102**, 1551-1557 (1986).

47. Rothman, J.H., Howald, I. & Stevens, T.H. Characterization of genes required for protein sorting and vacuolar function in the yeast Saccharomyces cerevisiae. *EMBO J.* **8**, 2057-2065 (1989).

48. Rothman, J.H. & Stevens, T.H. Protein sorting in yeast: mutants defective in vacuole biogenesis mislocalize vacuolar proteins into the late secretory pathway. *Cell* **47**, 1041-1051 (1986).

49. Bankaitis, V.A., Johnson, L.M. & Emr, S.D. Isolation of yeast mutants defective in protein targeting to the vacuole. *Proceedings of the National Academy of Sciences* **83**, 9075 -9079 (1986).

50. Banta, L.M., Robinson, J.S., Klionsky, D.J. & Emr, S.D. Organelle assembly in yeast: characterization of yeast mutants defective in vacuolar biogenesis and protein sorting. *J. Cell Biol.* **107**, 1369-1383 (1988).

51. Raymond, C.K., Howald-Stevenson, I., Vater, C.A. & Stevens, T.H. Morphological classification of the yeast vacuolar protein sorting mutants: evidence for a prevacuolar compartment in class E vps mutants. *Mol. Biol. Cell* **3**, 1389-1402 (1992).

52. Vida, T.A., Huyer, G. & Emr, S.D. Yeast vacuolar proenzymes are sorted in the late Golgi complex and transported to the vacuole via a prevacuolar endosome-like compartment. *J. Cell Biol.* **121**, 1245-1256 (1993).

53. Odorizzi, G., Babst, M. & Emr, S.D. Fab1p PtdIns(3)P 5-kinase function essential for protein sorting in the multivesicular body. *Cell* **95**, 847-858 (1998).

54. Coonrod, E.M. & Stevens, T.H. The yeast vps class E mutants: the beginning of the molecular genetic analysis of multivesicular body biogenesis. *Mol. Biol. Cell* **21**, 4057-4060 (2010).

55. Curtiss, M., Jones, C. & Babst, M. Efficient cargo sorting by ESCRT-I and the subsequent release of ESCRT-I from multivesicular bodies requires the subunit Mvb12. *Mol. Biol. Cell* **18**, 636-645 (2007).

56. Babst, M., Katzmann, D.J., Snyder, W.B., Wendland, B. & Emr, S.D. Endosome-associated complex, ESCRT-II, recruits transport machinery for protein sorting at the multivesicular body. *Dev. Cell* **3**, 283-289 (2002).

57. Babst, M., Katzmann, D.J., Estepa-Sabal, E.J., Meerloo, T. & Emr, S.D. Escrt-III: an endosome-associated heterooligomeric protein complex required for mvb sorting. *Dev. Cell* **3**, 271-282 (2002).

58. Caballe, A. & Martin-Serrano, J. ESCRT Machinery and Cytokinesis: the Road to Daughter Cell Separation. *Traffic* no-no (2011).doi:10.1111/j.1600-0854.2011.01244.x

59. Martin-Serrano, J. & Neil, S.J.D. Host factors involved in retroviral budding and release. *Nat. Rev. Microbiol.* **9**, 519-531 (2011).

60. Filimonenko, M. *et al.* The selective macroautophagic degradation of aggregated proteins requires the PI3P-binding protein Alfy. *Mol. Cell* **38**, 265-279 (2010).

61. Theos, A.C. *et al.* Dual loss of ER export and endocytic signals with altered melanosome morphology in the silver mutation of Pmel17. *Mol. Biol. Cell* **17**, 3598-3612 (2006).

62. Bilodeau, P.S., Urbanowski, J.L., Winistorfer, S.C. & Piper, R.C. The Vps27p Hse1p complex binds ubiquitin and mediates endosomal protein sorting. *Nat. Cell Biol.* **4**, 534-539 (2002).

63. Raiborg, C. *et al.* Hrs sorts ubiquitinated proteins into clathrin-coated microdomains of early endosomes. *Nat Cell Biol* **4**, 394-398 (2002).

64. Bilodeau, P.S., Winistorfer, S.C., Kearney, W.R., Robertson, A.D. & Piper, R.C. Vps27-Hse1 and ESCRT-I complexes cooperate to increase efficiency of sorting ubiquitinated proteins at the endosome. *J. Cell Biol.* **163**, 237-243 (2003).

65. Katzmann, D.J., Stefan, C.J., Babst, M. & Emr, S.D. Vps27 recruits ESCRT machinery to endosomes during MVB sorting. *J. Cell Biol* **162**, 413-423 (2003).

66. Raiborg, C., Rusten, T.E. & Stenmark, H. Protein sorting into multivesicular endosomes. *Curr. Opin. Cell Biol.* **15**, 446-455 (2003).

67. Prag, G. *et al.* The Vps27/Hse1 complex is a GAT domain-based scaffold for ubiquitin-dependent sorting. *Dev. Cell* **12**, 973-986 (2007).

68. Bilodeau, P.S., Urbanowski, J.L., Winistorfer, S.C. & Piper, R.C. The Vps27p Hse1p complex binds ubiquitin and mediates endosomal protein sorting. *Nat. Cell Biol.* **4**, 534-539 (2002).

69. Shields, S.B. & Piper, R.C. How Ubiquitin Functions with ESCRTs. *Traffic* (2011).doi:10.1111/j.1600-0854.2011.01242.x

70. Ren, X. & Hurley, J.H. Structural basis for endosomal recruitment of ESCRT-I by ESCRT-0 in yeast. *EMBO J.* **30**, 2130-2139 (2011).

71. Teo, H., Veprintsev, D.B. & Williams, R.L. Structural insights into endosomal sorting complex required for transport (ESCRT-I) recognition of ubiquitinated proteins. *J. Biol. Chem.* **279**, 28689-28696 (2004).

72. Teo, H. *et al.* ESCRT-I core and ESCRT-II GLUE domain structures reveal role for GLUE in linking to ESCRT-I and membranes. *Cell* **125**, 99-111 (2006).

73. Kostelansky, M.S. *et al.* Molecular architecture and functional model of the complete yeast ESCRT-I heterotetramer. *Cell* **129**, 485-498 (2007).

74. Shields, S.B. *et al.* ESCRT ubiquitin-binding domains function cooperatively during MVB cargo sorting. *J. Cell Biol.* **185**, 213-224 (2009).

75. Teis, D., Saksena, S., Judson, B.L. & Emr, S.D. ESCRT-II coordinates the assembly of ESCRT-III filaments for cargo sorting and multivesicular body vesicle formation. *EMBO J* **29**, 871-883 (2010).

76. Im, Y.J., Wollert, T., Boura, E. & Hurley, J.H. Structure and function of the ESCRT-II-III interface in multivesicular body biogenesis. *Dev. Cell* **17**, 234-243 (2009).

77. Teis, D., Saksena, S. & Emr, S.D. Ordered assembly of the ESCRT-III complex on endosomes is required to sequester cargo during MVB formation. *Dev. Cell* **15**, 578-589 (2008).

78. Bajorek, M. *et al.* Structural basis for ESCRT-III protein autoinhibition. *Nat. Struct. Mol. Biol* **16**, 754-762 (2009).

79. Shim, S., Kimpler, L.A. & Hanson, P.I. Structure/function analysis of four core ESCRT-III proteins reveals common regulatory role for extreme C-terminal domain. *Traffic* **8**, 1068-1079 (2007).

80. Lata, S. *et al.* Structural basis for autoinhibition of ESCRT-III CHMP3. *J. Mol. Biol* **378**, 818-827 (2008).

81. Lin, Y., Kimpler, L.A., Naismith, T.V., Lauer, J.M. & Hanson, P.I. Interaction of the mammalian endosomal sorting complex required for transport (ESCRT) III protein hSnf7-1 with itself, membranes, and the AAA+ ATPase SKD1. *J. Biol. Chem.* **280**, 12799-12809 (2005).

82. Babst, M., Wendland, B., Estepa, E.J. & Emr, S.D. The Vps4p AAA ATPase regulates membrane association of a Vps protein complex required for normal endosome function. *EMBO J* **17**, 2982-2993 (1998).

83. Nickerson, D.P., West, M. & Odorizzi, G. Did2 coordinates Vps4-mediated dissociation of ESCRT-III from endosomes. *J. Cell Biol* **175**, 715-720 (2006).

84. Azmi, I. *et al.* Recycling of ESCRTs by the AAA-ATPase Vps4 is regulated by a conserved VSL region in Vta1. *J. Cell Biol* **172**, 705-717 (2006).

85. Dimaano, C., Jones, C.B., Hanono, A., Curtiss, M. & Babst, M. Ist1 regulates Vps4 localization and assembly. *Mol. Biol. Cell* **19**, 465-474 (2008).

86. Shestakova, A. *et al.* Assembly of the AAA ATPase Vps4 on ESCRT-III. *Mol. Biol. Cell* **21**, 1059-1071 (2010).

87. Yeo, S.C.L. *et al.* Vps20p and Vta1p interact with Vps4p and function in multivesicular body sorting and endosomal transport in Saccharomyces cerevisiae. *J. Cell. Sci* **116**, 3957-3970 (2003).

88. Xiao, J. *et al.* Structural basis of Vta1 function in the multivesicular body sorting pathway. *Dev. Cell* **14**, 37-49 (2008).

89. Yu, Z., Gonciarz, M.D., Sundquist, W.I., Hill, C.P. & Jensen, G.J. Cryo-EM structure of dodecameric Vps4p and its 2:1 complex with Vta1p. *J. Mol. Biol* **377**, 364-377 (2008).

90. Lata, S. *et al.* Structure and function of ESCRT-III. *Biochem. Soc. Trans* **37**, 156-160 (2009).

91. Bajorek, M. *et al.* Biochemical analyses of human IST1 and its function in cytokinesis. *Mol. Biol. Cell* **20**, 1360-1373 (2009).

92. Bodon, G. *et al.* Charged multivesicular body protein-2B (CHMP2B) of the endosomal sorting complex required for transport-III (ESCRT-III)

polymerizes into helical structures deforming the plasma membrane. *The Journal of Biological Chemistry* (2011).doi:10.1074/jbc.M111.283671

93. Ghazi-Tabatabai, S. *et al.* Structure and disassembly of filaments formed by the ESCRT-III subunit Vps24. *Structure* **16**, 1345-1356 (2008).

94. Hanson, P.I., Roth, R., Lin, Y. & Heuser, J.E. Plasma membrane deformation by circular arrays of ESCRT-III protein filaments. *J. Cell Biol.* **180**, 389-402 (2008).

95. Wollert, T., Wunder, C., Lippincott-Schwartz, J. & Hurley, J.H. Membrane scission by the ESCRT-III complex. *Nature* **458**, 172-177 (2009).

96. Wollert, T. & Hurley, J.H. Molecular mechanism of multivesicular body biogenesis by ESCRT complexes. *Nature* **464**, 864-869 (2010).

97. Babst, M., Sato, T.K., Banta, L.M. & Emr, S.D. Endosomal transport function in yeast requires a novel AAA-type ATPase, Vps4p. *EMBO J* **16**, 1820-1831 (1997).

98. Hurley, J.H. & Yang, D. MIT domainia. *Dev. Cell* **14**, 6-8 (2008).

99. Hill, C.P. & Babst, M. Structure and function of the membrane deformation AAA ATPase Vps4. *Biochimica Et Biophysica Acta* (2011).doi:10.1016/j.bbamcr.2011.08.017

100. Ogura, T. & Wilkinson, A.J. AAA+ superfamily ATPases: common structure--diverse function. *Genes Cells* **6**, 575-597 (2001).

101. Erzberger, J.P. & Berger, J.M. Evolutionary relationships and structural mechanisms of AAA+ proteins. *Annu Rev Biophys Biomol Struct* **35**, 93-114 (2006).

102. Hanson, P.I. & Whiteheart, S.W. AAA+ proteins: have engine, will work. *Nat. Rev. Mol. Cell Biol.* **6**, 519-529 (2005).

103. Zhao, C., Smith, E.C. & Whiteheart, S.W. Requirements for the catalytic cycle of the N-ethylmaleimide-Sensitive Factor (NSF). *Biochimica Et Biophysica Acta* (2011).doi:10.1016/j.bbamcr.2011.06.003

104. Hartman, J.J. & Vale, R.D. Microtubule disassembly by ATP-dependent oligomerization of the AAA enzyme katanin. *Science* **286**, 782-785 (1999).

105. Scott, A. *et al.* Structural and mechanistic studies of VPS4 proteins. *EMBO J* **24**, 3658-3669 (2005).

106. Gonciarz, M.D. *et al.* Biochemical and structural studies of yeast Vps4 oligomerization. *J. Mol. Biol* **384**, 878-895 (2008).

107. Davies, J.M., Brunger, A.T. & Weis, W.I. Improved structures of full-length p97, an AAA ATPase: implications for mechanisms of nucleotide-dependent conformational change. *Structure* **16**, 715-726 (2008).

108. Hartmann, C. *et al.* Vacuolar protein sorting: two different functional states of the AAA-ATPase Vps4p. *J. Mol. Biol* **377**, 352-363 (2008).

109. Landsberg, M.J., Vajjhala, P.R., Rothnagel, R., Munn, A.L. & Hankamer, B. Three-dimensional structure of AAA ATPase Vps4: advancing structural insights into the mechanisms of endosomal sorting and enveloped virus budding. *Structure* **17**, 427-437 (2009).

110. Scheuring, S. *et al.* Mammalian cells express two VPS4 proteins both of which are involved in intracellular protein trafficking. *J. Mol. Biol* **312**, 469-480 (2001).

111. Babst, M., Sato, T.K., Banta, L.M. & Emr, S.D. Endosomal transport function in yeast requires a novel AAA-type ATPase, Vps4p. *EMBO J.* **16**, 1820-1831 (1997).

112. Obita, T. *et al.* Structural basis for selective recognition of ESCRT-III by the AAA ATPase Vps4. *Nature* **449**, 735-739 (2007).

113. Stuchell-Brereton, M.D. *et al.* ESCRT-III recognition by VPS4 ATPases. *Nature* **449**, 740-744 (2007).

114. Scott, A. *et al.* Structure and ESCRT-III protein interactions of the MIT domain of human VPS4A. *Proc. Natl. Acad. Sci. U.S.A* **102**, 13813-13818 (2005).

115. Kieffer, C. *et al.* Two distinct modes of ESCRT-III recognition are required for VPS4 functions in lysosomal protein targeting and HIV-1 budding. *Dev. Cell* **15**, 62-73 (2008).

116. Stuchell-Brereton, M.D. *et al.* ESCRT-III recognition by VPS4 ATPases. *Nature* **449**, 740-744 (2007).

117. Azmi, I.F. *et al.* ESCRT-III family members stimulate Vps4 ATPase activity directly or via Vta1. *Dev. Cell* **14**, 50-61 (2008).

118. Davies, B.A., Azmi, I.F. & Katzmann, D.J. Regulation of Vps4 ATPase activity by ESCRT-III. *Biochem. Soc. Trans* **37**, 143-145 (2009).

119. Merrill, S.A. & Hanson, P.I. Activation of human VPS4A by ESCRT-III proteins reveals ability of substrates to relieve enzyme autoinhibition. *J. Biol. Chem* **285**, 35428-35438 (2010).

CHAPTER 2

ASSEMBLY OF THE AAA ATPASE VPS4 ON ESCRT-III

Mol Biol Cell. 2010 Mar 15;21(6):1059-71. Epub 2010 Jan 28.

Assembly of the AAA ATPase Vps4 on ESCRT-III.

Shestakova A, Hanono A, Drosner S, Curtiss M, Davies BA,
Katzmann DJ, Babst M.

Assembly of the AAA ATPase Vps4 on ESCRT-III

Anna Shestakova,* Abraham Hanono,* Stacey Drosner,*† Matt Curtiss,* Brian A. Davies,‡ David J. Katzmann,‡ and Markus Babst*

*Department of Biology, University of Utah, Salt Lake City, UT 84112-9202; and ‡Department of Biochemistry and Molecular Biology, Mayo Clinic College of Medicine, Rochester, MN 55905

Submitted July 15, 2009; Revised January 6, 2010; Accepted January 19, 2010
Monitoring Editor: Sandra Lemmon

Vps4 is a key enzyme that functions in endosomal protein trafficking, cytokinesis, and retroviral budding. Vps4 activity is regulated by its recruitment from the cytoplasm to ESCRT-III, where the protein oligomerizes into an active ATPase. The recruitment and oligomerization steps are mediated by a complex network of at least 12 distinct interactions between Vps4, ESCRT-III, Ist1, Vta1, and Did2. The order of events leading to active, ESCRT-III–associated Vps4 is poorly understood. In this study we present a systematic in vivo analysis of the Vps4 interaction network. The data demonstrated a high degree of redundancy in the network. Although no single interaction was found to be essential for the localization or activity of Vps4, certain interactions proved more important than others. The most significant among these were the binding of Vps4 to Vta1 and to the ESCRT-III subunits Vps2 and Snf7. In our model we propose the formation of a recruitment complex in the cytoplasm that is composed of Did2-Ist1-Vps4, which upon binding to ESCRT-III recruits Vta1. Vta1 in turn is predicted to cause a rearrangement of the Vps4 interactions that initiates the assembly of the active Vps4 oligomer.

INTRODUCTION

Plasma membrane proteins are continuously endocytosed and either sorted into the multivesicular body (MVB) pathway for eventual degradation in the lysosome (vacuole in yeast) or recycled to the plasma membrane. Thus, modulation of surface protein trafficking is an important regulatory element for numerous cellular responses, such as growth factor receptor function, nutrient uptake, cell–cell communication and the immune response (for review, see Piper and Katzmann, 2007; Davies *et al.*, 2009; Raiborg and Stenmark, 2009; Saksena and Emr, 2009). Ubiquitination of endosomal cargo proteins initiates their sorting into the MVB pathway where they are sequestered into vesicles formed when the outer/limiting endosomal membrane invaginates into the lumen of the compartment, giving the structure a multivesicular appearance. MVBs then fuse with lysosomes, delivering the vesicles into the lumen of the hydrolytic compartment for degradation. The proper recognition and sorting of ubiquitinated cargoes requires the coordinated interaction of the Vps4 ATPase and the ESCRT (endosomal-sorting complex required for transport) protein complexes that work in sequence to mediate MVB protein sorting and vesicle formation events (for review, see Babst, 2005; Hurley and Emr, 2006; Williams and Urbe, 2007). Current models suggest that an initial cargo-sorting event occurs when the ubiquitinated cargo is recognized by the ESCRT-0 and ESCRT-I complexes on the cytoplasmic side of the MVB membrane. ESCRT-I subsequently activates ESCRT-II, which, in turn, initiates the formation of ESCRT-III. This latter step is thought to concentrate cargo and recruit additional factors, including Vps4. Vps4 is an AAA (ATPase associated with various cellular activities)-type ATPase that releases ESCRT-III from the MVB membrane for additional sorting events, which is the final discernable step in the MVB-sorting process. In the absence of Vps4 function, the ESCRT machinery accumulates on the endosome, and vesicle formation is inhibited.

The formation of MVB vesicles requires membrane deformation and fusion steps that utilize a reversed topology compared with other vesicle formation events in the cell (e.g., clathrin- and COP-mediated vesicle formation). Interestingly, the ESCRT machinery has been implicated in two other membrane fusion events with reverse topology. Retroviruses such as HIV-1 form new virus particles at the plasma membrane by an ESCRT-dependent budding event, and the final step in cytokinesis requires the ESCRT-dependent abscission of the plasma membrane in order to form two separate cells (Garrus *et al.*, 2001; VerPlank *et al.*, 2001; Spitzer *et al.*, 2006; Carlton and Martin-Serrano, 2007; Morita *et al.*, 2007; McDonald and Martin-Serrano, 2009).

The assembly of ESCRT-III on endosomal membranes has been suggested to both concentrate cargo and deform the membrane, two essential steps in formation of MVB vesicles (Babst *et al.*, 2002; Hanson *et al.*, 2008; Wollert *et al.*, 2009). Yeast ESCRT-III is composed of four subunits (Vps2, Vps20, Vps24, Snf7), each of which has at least one homologue in mammalian cells. These four subunits are predicted to have similar three-dimensional structures (Muziol *et al.*, 2006). In the cytoplasm the ESCRT-III subunits are in a "closed" inactive conformation that inhibits complex formation. On the endosomal membrane, however, the ESCRT-III subunits seem to switch to an "open" conformation that promotes the

This article was published online ahead of print in *MBC in Press* (http://www.molbiolcell.org/cgi/doi/10.1091/mbc.E09–07–0572) on January 28, 2010.

† Present address: Nelson Laboratories, 6280 S. Redwood Road, Murray, UT 84123.

Address correspondence to: Markus Babst (babst@biology.utah.edu).

Abbreviations used: AAA, ATPase associated with various cellular activities; ESCRT, endosomal-sorting complex required for transport; MIM1/2, MIT-interacting motif 1/2; MIT, microtubule-interacting and transport; MVB, multivesicular body.

formation of ESCRT-III and allows interactions with other ESCRT-III–associated factors (Shim *et al.*, 2007; Lata *et al.*, 2008; Bajorek *et al.*, 2009b). Within ESCRT-III the four subunits form two functionally distinct subcomplexes (Babst *et al.*, 2002). The Vps20–Snf7 subcomplex interacts with the endosomal membrane and with ESCRT-II, the complex that initiates ESCRT-III formation. The second subcomplex, Vps2–Vps24, is recruited by Vps20–Snf7 and thus functions downstream of the Vps20–Snf7 subcomplex. Although recent studies provided new insights into the arrangement of the subunits within ESCRT-III (Saksena *et al.*, 2009), the overall structure of ESCRT-III remains to be determined.

Vps4 belongs to the large protein family of AAA-type ATPases (for review, see Lupas and Martin, 2002). These proteins function as mechano-enzymes that, in most studied cases, use the energy of ATP hydrolysis to induce conformational changes in the bound substrate. Vps4 is composed of an N-terminal substrate-binding domain, called the MIT (microtubule interacting and transport) domain, one central AAA domain (hallmark of type-1 AAA ATPases), and a C-terminal region that is involved in Vps4 dimerization (Babst *et al.*, 1998; Scott *et al.*, 2005a; Gonciarz *et al.*, 2008; Vajjhala *et al.*, 2008). Vps4 uses energy from ATP hydrolysis to disassemble ESCRT-III, thereby recycling the ESCRT-III subunits for additional rounds of MVB cargo sorting. The disassembly reaction is initiated by the recruitment of Vps4 monomers or dimers from the cytoplasm to ESCRT-III, where they assemble into the active oligomeric ATPase (Babst *et al.*, 1998). Because of its dynamic nature the structural analysis of the Vps4 oligomer has been problematic and controversial. However recent studies indicate that the Vps4 oligomer is composed of 12 subunits that assemble into two hexameric rings in a tail-to-tail (antiparallel) orientation (Yu *et al.*, 2008; Landsberg *et al.*, 2009). Both the recruitment of Vps4 and the consequent disassembly reaction require the interaction of the Vps4 MIT domain with the ESCRT-III substrate. This interaction is mediated by two distinct motifs, termed MIMs (MIT-interacting motifs), found in the ESCRT-III subunits. MIM1 motifs are located in the very C-terminus of subunits Vps2 and Vps24, whereas MIM2 motifs are found in the C-terminal regions of the Vps20 and Snf7 subunits (Obita *et al.*, 2007; Stuchell-Brereton *et al.*, 2007; Kieffer *et al.*, 2008; Shim *et al.*, 2008). These two motifs bind to distinct surfaces of the MIT domain, allowing both types of interactions to occur simultaneously. Phenotypic analyses have indicated that both types of MIM motifs are important for proper Vps4 activity, but it remains unknown if all four potential yeast ESCRT-III MIM sites are functional.

Both recruitment and assembly of Vps4 are aided by additional factors that seem to ensure proper localization and timing of the disassembly reaction. Ist1 and Did2 have been implicated in the recruitment of Vps4 to ESCRT-III, whereas Vta1 has been shown to support the assembly and ATPase activity of Vps4 (Yeo *et al.*, 2003; Shiflett *et al.*, 2004; Azmi *et al.*, 2006; Lottridge *et al.*, 2006; Nickerson *et al.*, 2006; Azmi *et al.*, 2008; Dimaano *et al.*, 2008; Rue *et al.*, 2008). A fourth factor, Vps60, seems to function together with Vta1 at late stage of Vps4 activation; however, its precise role remains unknown (Ward *et al.*, 2005; Azmi *et al.*, 2008; Rue *et al.*, 2008; Shim *et al.*, 2008). Together, Vps4, ESCRT-III, Did2, Ist1, and Vta1 form a complex network of interactions that leads to the formation of an active ATPase complex and the disassembly of ESCRT-III. Although much is known about each of these interactions individually, the temporal arrangement of the interactions and how they work together to achieve the disassembly reaction is poorly understood. We present a detailed in vivo analysis of the interactions known to be involved in the recruitment and assembly steps of Vps4.

MATERIALS AND METHODS

Antibodies

The anti-HA (hemagglutinin) mAb used for immunoprecipitations and Western blotting was purchased from Covance (Princeton, NJ). The antisera against Vps4, Snf7, and Vps24 were previously described (Babst *et al.*, 1998). The antiserum against Vps20 was a gift from Scott D. Emr (Cornell University, Ithaca, NY).

Strains and Media

Saccharomyces cerevisiae strains used in this work are listed in Table 1. To maintain plasmids, yeast strains were grown in corresponding complete synthetic dropout medium (Sherman *et al.*, 1979). Wild-type, integrated, and knockout strains were grown in rich YPD medium (yeast extract-peptone-dextrose). Yeast gene knockouts were constructed as previously described (Baudin *et al.*, 1993).

DNA Manipulations

Plasmids used in this study are listed in Table 1. All plasmids were constructed using standard cloning techniques. Plasmids obtained by PCR-based cloning techniques were confirmed by DNA sequencing. Point mutations were introduced using Stratagene QuikChange Site-Directed Mutagenesis Kit (Agilent Technologies, La Jolla, CA). The pRS4XX shuttle vectors used in this study have been described previously (Christianson *et al.*, 1992). pEGFP-C1 was from Clontech Laboratories (Palo Alto, CA). MIT-green fluorescent protein (GFP) was constructed by fusing EGFP to the Eco47III site of *VPS4*. *GFP-VPS4*$^{\Delta}$MIT-type constructs were obtained by fusing a fragment containing the *PRC1* promoter and GFP of pGO36 into the Eco47III site of a *VPS4*-containing plasmid.

Procedures

Fluorescence microscopy was performed on a deconvolution microscope (DeltaVision, Applied Precision, Issaquah, WA). The distribution of MIT-GFP was quantified from deconvoluted Z-stack projections of cells using an open-source GIMP 2.6.6 program (www.gimp.org). To achieve a more uniform level of protein expression in cells MIT-GFP was expressed from a *CPS1* promoter (pMC48 and pMC50). The percent signal on endosomes was calculated by dividing endosomal fluorescence intensity by total cellular fluorescence intensity. Using an unpaired *t* test, p values were calculated using Instat software. Subcellular fractionation experiments were performed as described previously (Dimaano *et al.*, 2008), except for subcellular fractionation experiments localizing Vps4, where spheroplasted cells were lysed by osmotic stress in Pop buffer (100 mM KCl, 50 mM KAc, 20 mM PIPES, pH 6.8, 5 mM $MgAc_2$, 100 mM sorbitol) containing 0.1 mM AEBSF and Complete protease inhibitor cocktail (Roche Molecular Biochemicals, Indianapolis, IN). When localizing ESCRT-III components, spheroplasts were lysed by douncing with 15–20 strokes in a glass homogenizer in PBS containing Complete protease inhibitor cocktail. Immunoprecipitation experiments were performed as described previously (Babst *et al.*, 2002). For in vitro binding experiments glutathione *S*-transferase (GST) fusion proteins were expressed in *Escherichia coli* and purified by affinity purification using standard methods on glutathione-Sepharose 4 Fast Flow resin (GE Healthcare Bio-Sciences AB, Uppsala, Sweden). The purification of Vps4^{E233Q}, Ist1, and Vta1 were previously described (Babst *et al.*, 1998; Azmi *et al.*, 2006; Dimaano *et al.*, 2008). To test the interaction between proteins in vitro, 40 μg of purified GST fusion protein was prebound to ~15-μl bead volume of glutathione-Sepharose 4 Fast Flow resin. Equimolar amounts of purified test proteins were then added to the resin in GST pulldown buffer (100 mM KAc, 5 mM $MgAc_2$, 20 mM HEPES, pH 7.4) to a final volume of 150 μl and incubated for 10 min at room temperature with gentle mixing; 1 mM ATP or ADP was included as indicated. An unbound sample was taken, and the bound protein was washed extensively in GST pulldown buffer. The bound protein was eluted by boiling for 5 min in SDS-PAGE sample buffer (2% SDS, 0.1 M Tris, pH 6.8, 10% glycerol, 0.01% bromophenol blue, 5% ß-mercaptoethanol), and 10 μl of each sample was separated by SDS-PAGE and stained by Coomassie Brilliant Blue. The liquid overlay assay was performed as previously described (Darsow *et al.*, 2000).

RESULTS

The recruitment of Vps4 subunits from the cytoplasm to ESCRT-III and the consequent oligomerization of Vps4 into the active dodecameric state are not well understood. The study of this process is complicated by the number of Vps4 interactions that have been reported, some of which overlap and compete with each other (Figure 1A). Furthermore, many Vps4 interaction studies have been performed in vitro

Table 1. Strains and plasmids used in this study

Strain or plasmid	Descriptive name	Genotype or description	Reference or source
Strain[a]			
SEY6210	WT	MATα *leu2-3,112 ura3-52 his3-Δ200 trp1-Δ901 lys2-801 suc2-Δ9*	Robinson *et al.* (1988)
BHY10	WT *CPY-I*	SEY6210, CPY-INVERTASE::*LEU2 ura3-52 his3-Δ200 trp1-Δ901 lys2-801 suc2-Δ9*	Horazdovsky *et al.* (1994)
MBY2	*vps4Δ CPY-I*	BHY10, *VPS4::TRP1*	Babst *et al.* (1997)
MBY3	*vps4Δ*	SEY6210, *VPS4::TRP1*	Babst *et al.* (1997)
MBY16	*vps4Δ vps36Δ*	SEY62010.1, *VPS4::TRP1, VPS36::HIS3*	Babst *et al.* (2002)
MBY28	*vps2Δ*	SEY6210, *VPS2::HIS3*	Babst *et al.* (2002)
BWY102	*vps24Δ*	SEY6210, *VPS24::HIS3*	Babst *et al.* (2002)
MBY37	*vps4Δ vps20Δ*	MBY3, VPS20::HIS3	Babst *et al.* (2002)
JPY50	*vps4Δ vta1Δ*	MBY4, *VTA1::HIS3*	Azmi *et al.* (2006)
MCY3	*vps4Δ ist1Δ*	MBY3, *IST1::HIS3*	Dimaano *et al.* (2008)
EEY1-3	*vps20Δ CPY-I*	BHY10, *VPS20::HIS3*	This study
EEY2-1	*vps20Δ*	6210, *VPS20::HIS3*	Babst *et al.* (2002)
EEY8	*snf7Δ CPY-I*	BHY10, *SNF7::HIS3*	This study
EEY9	*snf7Δ*	SEY6210, *SNF7::HIS3*	Babst *et al.* (2002)
EEY12	*vps4Δ snf7Δ*	MBY3, *SNF7::HIS3*	Babst *et al.* (2002)
EEY26-1	*vps4Δ did2Δ*	MBY3, *DID2::HIS3*	Dimaano *et al.* (2008)
ASY4	*vps4Δ vps2Δ vps24*	6210.1, *VPS4::TRP1, VPS2::HIS3, VPS24::HIS3*	This study
ASY5	*vps2Δ vps24Δ*	SEY6210, *VPS24::HIS3, VPS2::HIS3*	This study
ASY8	*vps2Δ CPY-I*	BHY10, *VPS2::G418*	This study
ASY9	*vps24Δ CPY-I*	BHY10, *VPS24::G418*	This study
ASY12	*vps2Δ vps24Δ CPY-I*	ASY8, *VPS24::HIS3*	This study
ASY16	*vps4Δ vps20Δ snf7Δ*	MBY37, *SNF7::G418*	This study
ASY19	*snf7Δ vps20Δ CPY-I*	EEY1-3, *SNF7::G418*	This study
ASY20	*vps4Δ vps20Δ snf7Δ ist1Δ*	ASY16, *IST1::URA3*	This study
E. coli: XL1-blue		recA1 endA1 gyrA96 thi-1 hsdR17 supE44 relA1 lac [F′ proAB lacIqZΔM15 Tn10(tetr)]	Stratagene (La Jolla, CA)
Plasmids			
pAS22	*vps2(ΔC)-HA*	*URA3* (pRS416) *vps2(ΔC)-HA*	This study
pAS23	*vps24(ΔC)-HA*	*URA3* (pRS416) *vps24(ΔC)-HA*	This study
pAS28	*vps2(ΔC)-HA*	*LEU2* (pRS415) *vps2(ΔC)-HA*	This study
pAS42	*vps2(ΔC)-HA, vps24(ΔC)-HA*	*TRP1* (pRS414) *vps2(ΔC)-HA, vps24(ΔC)-HA*	This study
pAS44	MIT-GFP	*URA3* (pRS426) *vps4*(MIT)-GFP	This study
pAS47	*vps2(ΔC)-HA, vps24(ΔC)-HA*	*URA3* (pRS416) *vps2(ΔC)-HA, vps24(ΔC)-HA*	This study
pAS51	GFP-*vps4*(ΔMIT*(E233Q, S377A)*)	*URA3* (pRS416) *GFP-vps4*(ΔMIT*(E233Q, S377A)*)	This study
pAS58	*vps2(ΔC)-HA, vps24(ΔC)-HA*	*LEU2* (pRS415) *vps2(ΔC)-HA, vps24(ΔC)-HA*	This study
pAS59	MIT*(L64D)*-GFP	*URA3* (pRS426) *vps4*(MIT *(L64D)*)-GFP	This study
pAS62	*vps4* (ΔMIT*(E233Q)*)	*URA3* (pRS416) *vps4*(ΔMIT*(E233Q)*)	This study
pAS72	*snf7(L199D)*	*LEU2* (pRS415) *snf(L199D)*	This study
pAS74	*vps20(L188D)*	*LEU2* (pRS415) *vps20(L188D)*	This study
pAS76	*vps20(L188D)-HA*	*URA3* (pRS416) *vps20(L188D)-HA*	This study
pAS79	*vps4(S377A)*	*URA3* (pRS416) *vps4(S377A)*	This study
pMB4	*VPS4*	*HIS3* (pRS413) *VPS4*	Babst *et al.* (1997)
pMB66	*vps4(E233Q)*	*HIS3* (pRS413) *vps4(E233Q)*	Babst *et al.* (1998)
pMB168	*VPS20-HA*	*URA3* (pRS416) *VPS20-HA*	Babst *et al.* (2002)
pMB341	GFP-*vps4*(ΔMIT*(E233Q)*)	*URA3* (pRS416) *P(CPY)*-GFP-*vps4*(ΔMIT*(E233Q)*)	This study
pMB343	*vps4(E233Q)*–GFP	*URA3* (pRS416) *vps4(E233Q)-HA*-GFP	This study
pMB370	*vps4(L64D, E233Q)*-GFP	*URA3* (pRS416) *vps4(L64D, E233Q)-HA*-GFP	This study
pMB380	*vps4(I18D, E233Q)*-GFP	*URA3* (pRS416) *vps4(I18D, E233Q)-HA*-GFP	This study

Continued

Table 1. *Continued*

Strain or plasmid	Descriptive name	Genotype or description	Reference or source
pMB393	*snf7(L199D), vps20(L188D)*	*URA3* (pRS416) snf*7(L199D), vps20(L188D)*	This study
pMB394	*snf7(L199D), vps20(L188D)*	*LEU2* (pRS415) *snf7(L199D), vps20(L188D)*	This study
pPN3	*VPS20*	*LEU2* (pRS415) *VPS20*	This study
pVPS4(I18D)	*vps4(I18D)*	*URA3* (pRS416) *vps4(I18D)*	This study
pVPS4(L64D)	*vps4(L64D)*	*URA3* (pRS416) *vps4(L64D)*	This study
pVPS4(I18D, E233Q)	*vps4(I18D, E233Q)*	*URA3* (pRS416) *vps4(I18D, E233Q)*	This study
pVPS4(L64D, E233Q)	*vps4(L64D, E233Q)*	*URA3 (pRS416) vps4(L64D, E233Q)*	This study
pGO45	GFP-*CPS*	*URA3*(pRS426) GFP-*CPS1*	Odorizzi *et al.* (1998)
pMC48	MIT-GFP	*URA3*(pRS416) *P(CPS1)-vps4*(MIT)-GFP	This study
pMC50	MIT*(I18D)*-GFP	*URA3 (pRS416) P(CPS1)-vps4*(MIT*(I18D)*)-GFP	This study
pAH31	GST-*DID2*	*(pGEX-KG)* GST-*DID2*	This study
pAH32	GST-*CT(DID2)*	*(pGEX-KG)* GST-*DID2(113-204)*	This study
pMB411	GST-*vps20(C)*	*(pGEX-KG)* GST-*vps20(101-221)*	This study
pMB412	GST-*snf7(C, L199D)*	*(pGEX-KG)* GST-*snf7(101-240)(L199D)*	This study
pMB413	GST-*snf7(C)*	*(pGEX-KG)* GST-*snf7(101-240)*	This study
pMB414	GST-*vps20(C, L188D)*	*(pGEX-KG)* GST-*snf7(101-221)(L188D)*	This study
pAS85	*snf7(L199D), vps20(L188D),* MIT-GFP	*LEU2* (pRS415) *snf7(L199D), vps20(L188D),* P(*CPS1*)-MIT-GFP	This study

[a] All strains are *Saccharomyces cerevisiae* are except the one marked *E. coli.*

in the presence of only one or a few of the ESCRT factors, which raises questions of the relevance of these observations for the in vivo situation. Therefore we dissected the Vps4 interactions in vivo by expressing different truncated or mutated forms of Vps4 in a variety of ESCRT deletion strains (see Table 2). These data resulted in a model for the recruitment and assembly of Vps4 on MVBs (Figure 1B).

Analysis of the Vps4 MIT Interactions

The MIT domain of Vps4 has been shown to interact with six different proteins of the ESCRT machinery: the four subunits of ESCRT-III (Vps2, Vps20, Vps24, Snf7) and two factors that are related to ESCRT-III subunits and have been implicated in the endosomal recruitment of Vps4, Did2, and Ist1 (Figure 1A; Shim *et al.*, 2007; Azmi *et al.*, 2008; Dimaano *et al.*, 2008; Kieffer *et al.*, 2008; Xiao *et al.*, 2008). These six factors bind via two distinct binding motifs, MIM1 and MIM2, to two different surface areas of the MIT domain (Figure 1C). This arrangement allows the MIT domain to simultaneous bind to MIM1 and MIM2. To test which of the MIT interactions are involved in the recruitment of Vps4 to ESCRT-III, we expressed a MIT-GFP fusion construct in yeast strains deleted for *VPS4* alone or in combination with other ESCRT mutations. These yeast cells were analyzed by fluorescence microscopy, and the resulting pictures were judged by the ratio of MIT-GFP signal localized either to the cytoplasm or to the aberrant endosomes formed in these mutant strains (class E compartments; Figure 2A). Enlarged examples of the microscopy pictures are shown in Supplemental Figure 1. Furthermore, for a subset of MIT-GFP localization experiments, the ratio of endosomal-to-cytoplasmic localization was quantified (Figure 2B).

Previous studies have shown that *vps4*Δ cells accumulate ESCRT-III and its associated proteins Did2 and Ist1 on endosomal membranes (Babst *et al.*, 2002; Nickerson *et al.*, 2006; Dimaano *et al.*, 2008). Thus the majority of MIT-GFP localized to class E compartments in cells deleted for *VPS4* and to cytoplasm in wild-type cells (Figure 2, A and B, 1 and 2). Additional deletions of *DID2* or *IST1* resulted in a partial redistribution of MIT-GFP to the cytoplasm (Figure 2, A and B, 7 [$p < 0.0001$] and 8 [$p < 0.0001$]). This result is consistent with previously published models in which Did2 and Ist1 function together in the recruitment of Vps4 (Dimaano *et al.*, 2008; Rue *et al.*, 2008). In contrast, deletion of *VTA1* did not interfere with recruitment of the MIT domain (Figure 2, A and B, 9) supporting a later role for this Vps4-interacting protein.

The ESCRT-III subunits Vps2 and Vps24 both contain C-terminal MIM1 interaction sites (Obita *et al.*, 2007; Stuchell-Brereton *et al.*, 2007). To study the effect of loss of MIM1, 3′ truncations of *VPS2* and *VPS24* were constructed that lacked the codons for the last 11 amino acids (*vps2*$^{\Delta C}$, *vps24*$^{\Delta C}$, Figure 1C, Table 2). These mutations did not affect stability or MVB recruitment of Vps2 and Vps24 (Figure 2C, lanes 3–6). A partial redistribution of MIT-GFP to the cytoplasm was observed in *vps4*Δ strains that lacked the Vps2 MIM1 motif (Figure 2, A and B, 5; $p < 0.0001$). The loss of Vps24 MIM1 had no effect on MIT-GFP localization (Figure 2A, 6). However, when combined with *vps2*$^{\Delta C}$ the deletion of Vps24 MIM1 showed a small but significant increase in MIT-GFP relocalization (Figure 2, A and B, 4; $p < 0.0048$). These data indicated that, although both MIM1 sites are functional, the Vps2 MIM1 site is more important for Vps4 recruitment than the Vps24 MIM1 motif.

Deletion of both *VPS2* and *VPS24* abolished MIT-GFP recruitment (Figure 2A, 3), which can be explained by the fact that this strain not only lacks the ESCRT-III MIM1 sites but in addition does not properly localize the other two MIM1-containing proteins Did2 and Ist1 (Nickerson *et al.*, 2006; Dimaano *et al.*, 2008). Similarly, a mutation in the MIT domain shown in mammalian Vps4 to block the MIT–MIM1 interaction (MIT^{L64D}; Figure 1C; Stuchell-Brereton *et al.*, 2007) did not localize to class E compartments of *vps4*Δ cells, supporting the idea that loss of all MIM1 sites both in ESCRT-III as well as in the recruitment factors Did2 and Ist1 abolishes recruitment of MIT-GFP (Figure 2A, 14).

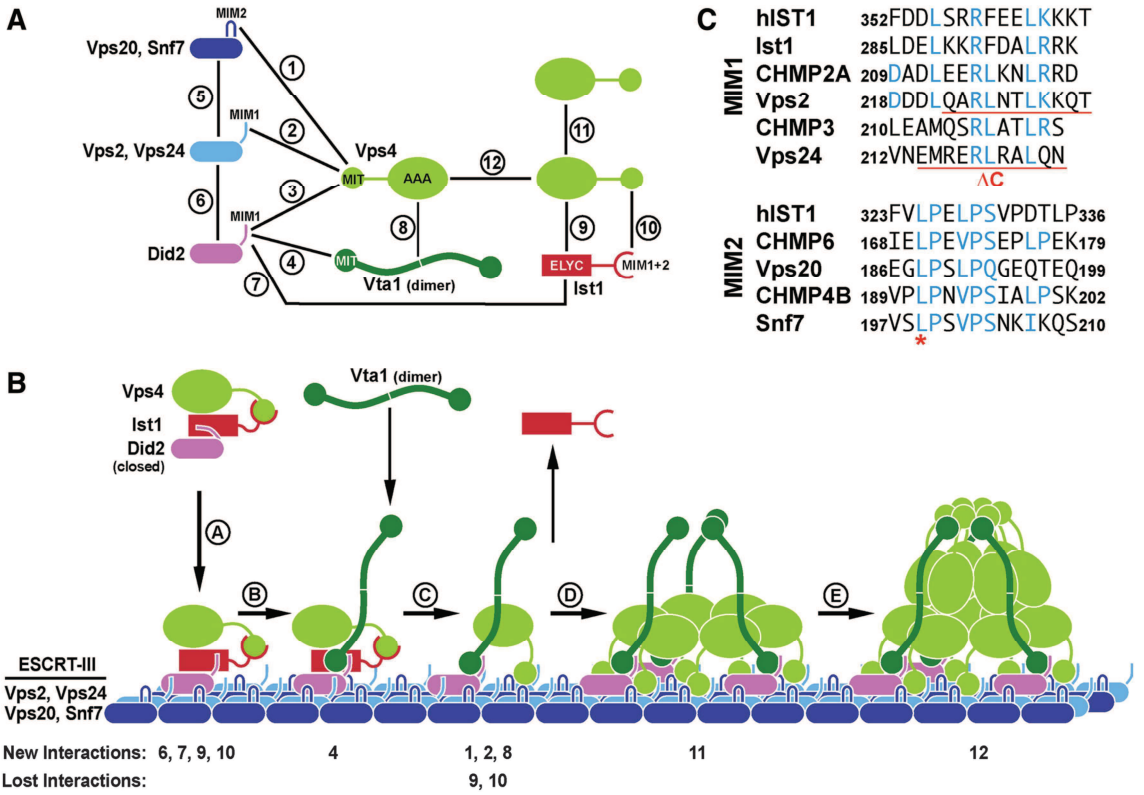

Figure 1. Interactions between Vps4 and its substrate and regulators. (A) Vps4 interaction network based on previous studies (Scott *et al.*, 2005b; Azmi *et al.*, 2008; Kieffer *et al.*, 2008; Bajorek *et al.*, 2009a; Xiao *et al.*, 2009). (B) Model for the recruitment and assembly of Vps4. The numbers indicating New Interactions or Lost Interactions refer to the numbers in A. (C) Alignments of the putative MIM1 and MIM2 motifs of yeast and mammalian ESCRT-III subunits (yeast Ist1 does not contain an obvious MIM2 consensus sequence). Mutations used in this study are marked in red.

To test the effect of loss of Vps2 and Vps24 MIM1 motifs on the recruitment of full-length Vps4, we fractionated cell extracts by centrifugation, separating the soluble, cytoplasmic pool of Vps4 (S) from the endosomal fraction found in the pellet (P). As previously observed, in wild-type cells the ATP-locked mutant Vps4^{E233Q} accumulated in the pellet fraction, indicating efficient recruitment of Vps4^{E233Q} to ESCRT-III (Figure 2C, lanes 1 and 2; Babst *et al.*, 1998). Similarly, mutant strains that lacked the MIM1 motif of either Vps2 or Vps24 efficiently recruited Vps4^{E233Q} to membranes (Figure 2C, lanes 3–6). The lack of both MIM1 sites caused a partial redistribution of Vps4^{E233Q} to the soluble fraction, whereas Vps2$^{\Delta C}$ or Vps24$^{\Delta C}$ remained in the membrane-bound pellet fraction (Figure 2C, lanes 7 and 8). These results supported the notion that the ESCRT-III MIM1 motifs are functionally redundant. However, the recruitment defects observed by cell fractionation were less severe than the MIT-GFP localization phenotypes, which can be explained by the presence of Vps4–Vps4 and Vps4–Vta1 interactions that stabilize ESCRT-III–associated Vps4 oligomers (see below).

We tested the importance of the MIM2 interaction motifs in Vps4 recruitment by mutating a conserved leucine residue of the Vps20 and Snf7 MIM2 sites (L188D in Vps20 and L199D in Snf7) that has been previously shown to be important for the MIM2–MIT interaction of the mammalian ESCRT system (Figure 1C; Kieffer *et al.*, 2008). The effect of these mutations on the interaction with yeast Vps4 was first analyzed in vitro using immobilized GST-fusion proteins containing the C-terminal half of either Snf7 or Vps20. Sepharose beads presenting either wild-type or mutant versions of the fusion proteins were incubated with recombinant Vps4^{E233Q} in the presence of either ATP or ADP. The

Table 2. Mutations used in this study

Name	Mutation	Affected interactions (see Figure 1A)
Vps4^{I18D}	Ile(18) to Asp	1, 10
Vps4^{L64D}	Leu(64) to Asp	2, 10
Vps4$^{\Delta MIT}$	aa 2-87 deleted	1, 2, 10
Vps4^{S377A}	Ser(377) to Ala	8
Vps4^{E233Q}	Glu(233) to Gln	None (ATP locked)
Vps2$^{\Delta C}$	aa 222-end deleted	2
Vps24$^{\Delta C}$	aa 214-end deleted	2
Vps20^{L188D}	Leu(188) to Asp	1
Snf7^{L199D}	Leu(199) to Asp	1

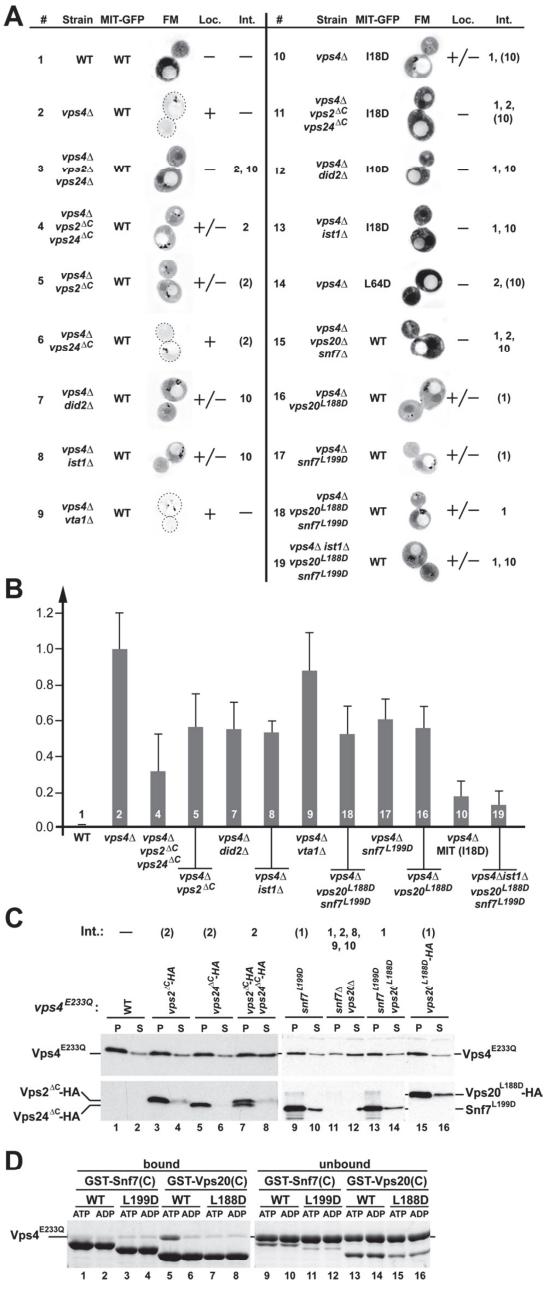

Figure 2. MIM1 and MIM2 interactions contribute to the recruitment of Vps4 to ESCRT-III. (A) Fluorescence microscopy analysis of the Vps4 MIT domain fused to GFP (MIT-GFP). The wild-type, MIM1 mutant (L64D), or MIM2 mutant (I18D) version of MIT-GFP was expressed in different yeast strains (see Table 1), and the extent of endosomal localization was determined (Loc.). For better visualization the fluorescence microscopy pictures were inverted and the intensity was adjusted to the individual brightness range (black is the brightest signal). Vps4 interactions affected by the different mutations are listed (Int., numbers are based on the interactions in Figure 1A). Numbers in parentheses indicate partially disrupted interactions. (B) Quantification of endosome-localized MIT-GFP relative to wild type (0.0) and *vps4*Δ (1.0). The data shown represent the results of at least 15 individually analyzed cells. Numbers refer to the experiment number in A. (C) Subcellular fractionation of different yeast strains expressing $vps4^{E233Q}$ into soluble, cytoplasmic fraction (S) and pelletable, membrane-associated fraction (P). Fractions were analyzed by Western blot using antibodies specific for Vps4 (top panels), Snf7 (bottom panel, lanes 9–14) and the HA-tag (bottom panels, lanes 1–8 and 15–16). Vps4 interactions affected by the different mutations are listed (Int., numbers are based on the interactions in Figure 1A). Numbers in parentheses indicate partially disrupted interactions. (D) In vitro Vps4 interaction studies using wild-type and MIM2 mutant forms of GST-Vps20(C) (fusion of GST with C-terminal half of Vps20) or GST-Snf7(C) immobilized on GSH-Sepharose. $Vps4^{E233Q}$ was added in the presence of ATP or ADP to immobilized proteins; bound and unbound fractions were analyzed by SDS-PAGE and Coomassie staining.

resulting bound and unbound fractions were then analyzed by SDS-PAGE (Figure 2D). Wild-type, but not L188D Vps20 was able to bind to Vps4 in presence of ATP (lane 5), demonstrating that the mutation indeed inhibited the Vps20 MIM2–MIT interaction. In contrast, neither wild-type nor mutant Snf7 bound to Vps4 under the conditions tested. These results are consistent with previously published data from both yeast and mammalian systems that suggested a preferred interaction of Vps4 with Vps20 rather than Snf7 (Azmi *et al.*, 2008; Kieffer *et al.*, 2008).

When expressed in yeast, the mutant proteins $Vps20^{L188D}$ and $Snf7^{L199D}$ were stable and efficiently recruited to endosomal membranes, indicating that the mutations did not interfere with normal protein folding (Figure 2C, lanes 9–10 and 15–16). However, when analyzed by SDS-PAGE the L199D mutation in Snf7 resulted in an apparent size shift, possibly because of the additional negative charge (Figure 3B, lanes 19–22). Mutation of each of the MIM2 motifs resulted in partial loss of MIT-GFP recruitment to ESCRT-III (Figure 2, A and B, 16 [$p < 0.0001$] and 17 [$p < 0.0001$]). Similarly, the combination of both mutations impaired endosomal localization of MIT-GFP (Figure 2, A and B, 18; $p < 0.0001$). Together, these data indicated that both ESCRT-III MIM2 motifs are important for MIT recruitment even though the in vitro data suggested only a minor role of Snf7 in the interaction of ESCRT-III with Vps4 (Figure 2D).

To test the effect of Snf7 and Vps20 MIM2 mutations on the recruitment of full-length Vps4, we performed subcellular fractionation experiments. MIM2 mutations in either Snf7 or Vps20 or the combination of both did not significantly redistribute Vps4 into the cytoplasmic fraction (Figure 2C, lanes 9–10 and 13–16). This result suggested, as observed with MIT-GFP, that MIM1 interactions play a more important role in the recruitment of Vps4 than the MIM2 motifs. Deletion of both *SNF7* and *VPS20* resulted in a relocalization of $Vps4^{E233Q}$ to the cytoplasm, which is likely caused by the loss of endosomal ESCRT-III and its associated proteins in this strain (Figure 2C, lanes 11 and 12).

The function of the MIM2 interaction was further analyzed by mutating the MIM2-binding site in the MIT domain of Vps4. A previous study indentified the valine at position 13 of human VPS4A as a crucial amino acid for the interaction between MIM2 and the MIT domain (Kieffer *et al.*, 2008). However, the corresponding mutation in yeast Vps4 (V14D) resulted in an unstable protein, suggesting that this mutation might interfere with protein folding (Supplemental Figure 2). Therefore we changed isoleucine at position 18 to aspartate, a mutation that based on published NMR analysis is predicted to interfere with the MIM2 interaction (Kieffer *et*

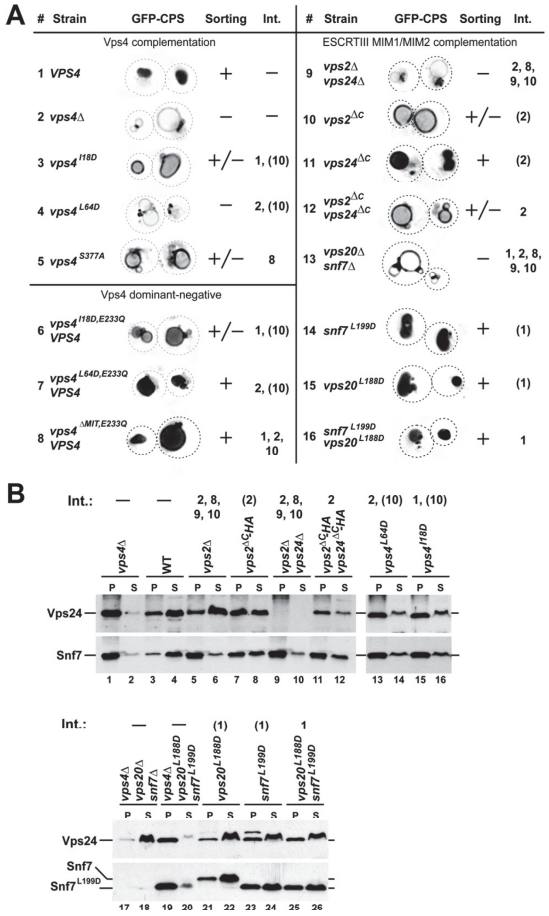

Figure 3. Phenotypic analysis of mutations affecting Vps4 interactions. (A) Fluorescence microscopy analysis of yeast strains expressing GFP-CPS. The efficiency of GFP-CPS sorting into the lumen of the vacuole is indicated (+, +/−, −). Vps4 interactions affected by the different mutations are listed. (B) Subcellular fractionation of yeast strains into soluble (S) and membrane-associated pellet fractions (P). The samples were analyzed by Western blot using antibodies specific for Vps24 and Snf7. Vps4 interactions affected by the different mutations are listed. (A and B) Int., numbers are based on the interactions in Figure 1A, and numbers in parentheses indicate partially disrupted interactions.

Table 3. CPY-invertase secretion

Strain	Secretion (%)	Affected Vps4 interactions (Figure 1A)
Complementation		
Wild type	0 ± 0	None
vps4Δ	100 ± 8	All
$vps4^{I18D}$	59 ± 8	1, 10
$vps4^{L64D}$	73 ± 4	2, 10
$vps4^{S377A}$	12 ± 0	8
$vps2^{\Delta C}$	30 ± 10	2
$vps24^{\Delta C}$	27 ± 6	2
$vps2^{\Delta C}$, $vps24^{\Delta C}$	48 ± 0	2
$snf7^{L199D}$	3 ± 1	1
$vps20^{L188D}$	3 ± 2	1
$snf7^{L199D}$, $vps20^{L188D}$	−1 ± 1	1
Dominant-negative		
VPS4	0 ± 0	None
$vps4^{E233Q}$, *VPS4*	100 ± 3	None
$vps4^{I18D,\ E233Q}$, *VPS4*	68 ± 5	1, 10
$vps4^{L64D,\ E233Q}$, *VPS4*	10 ± 0	2, 10
$vps4^{\Delta MIT,\ E233Q}$, *VPS4*	−7 ± 0	1, 2, 10

al., 2008). The I18D mutation impaired Vps4 function without affecting in vivo protein stability (Figure 3, 3, and Table 3; Supplemental Figure 2). The mutation strongly inhibited the recruitment of MIT-GFP to class E compartments of *vps4*Δ cells (Figure 2, A and B, 10; $p < 0.0001$), which is a more dramatic MIT recruitment phenotype than observed in the double MIM2 mutant strain ($vps4\Delta\ vps20^{L188D}\ snf7^{L199D}$, Figure 2A, 18). A likely explanation for this result is that the I18D MIT mutation not only affected the interaction with ESCRT-III but also the binding to the recruitment factor Ist1 (interactions 1 and 10, Figure 1A). Consistent with this idea we observed an increased recruitment defect when the $vps20^{L188D}\ snf7^{L199D}$ mutations were combined with a deletion of *IST1* (Figure 2, A and B, 19; $p < 0.0001$). However, deletion of *IST1* caused a complete loss of MIT^{I18D}-GFP recruitment to the endosome, which is a more severe phenotype than observed in the $vps20^{L188D}\ snf7^{L199D}\ ist1\Delta$ strain (Figure 2A, 13 and 19). This result suggested either the existence of an additional unknown MIM2 motif or the possibility that the I18D mutation might affect the MIM1-interaction site of the MIT domain. Combining the I18D MIT mutation with strains lacking Did2 or the MIM1-binding sites in ESCRT-III resulted in loss of MIT-GFP recruitment (Figure 2A, 11 and 12), which suggested that MIM1 and MIM2 interactions act synergistically in the recruitment of Vps4.

The in vivo analysis of MIT domain localization to ESCRT-III has demonstrated a high level of redundancy in the Vps4 recruitment system. Not one of the tested MIT interactions has been found to be essential for recruitment. Only mutations that interfere with at least two of the known MIT interactions are able to disrupt binding of the MIT domain to ESCRT-III. Furthermore, the MIM1 and MIM2 interactions act cooperatively in the recruitment of the MIT domain, suggesting that both interactions occur simultaneously on ESCRT-III. In contrast to the microscopy analysis, subcellular fractionations have shown that in *vps4*Δ MIT-GFP localizes to the soluble, cytoplasmic fraction (data not shown). This result suggested that binding of the MIT domain to ESCRT-III is too weak to maintain the MIT–ESCRT-III interaction during the fractionation procedure, an observation that fits well with the micromolar affinities found in vitro for MIT–MIM interactions (Obita *et al.,* 2007; Stuchell-Brereton *et al.,* 2007; Kieffer *et al.,* 2008).

Functional Redundancy among the ESCRT-III MIM Motifs

The MIT-GFP localization studies revealed redundancy in the function of the different MIT interaction motifs in Vps4 recruitment. To test if the ESCRT-III MIM sites are also functionally redundant in regard to MVB cargo sorting, we analyzed potential trafficking phenotypes in strains that lack either one or both of the ESCRT-III MIM1 or MIM2 motifs. Newly synthesized carboxypeptidase S (CPS) is a type I transmembrane protein that traffics via the MVB pathway to the vacuolar lumen where it functions as a vacuolar hydro-

lase (Odorizzi *et al.,* 1998). Fluorescence microscopy of wild-type cells expressing GFP-tagged CPS (GFP-CPS) showed mainly staining of the vacuolar lumen (Figure 3A, 1). In contrast, ESCRT mutants lacked luminal staining of the vacuole but instead accumulated GFP-CPS in aberrant endosomes, the class E compartments, and the limiting membrane of the vacuole (Figure 3A, 2). Cells that expressed the MIM1 mutant form of *VPS2*, $vps2^{\Delta C}$, exhibited a partial GFP-CPS sorting phenotype, whereas the loss of the *VPS24* MIM1 motif showed no obvious MVB trafficking defect (Figure 3A, 10 and 11). Loss of both MIM1 motifs resulted in a sorting defect similar than that of the $vps2^{\Delta C}$ mutant strain, consistent with the MIT-GFP localization studies that indicated the Vps2 MIM1 motif plays a more important role in Vps4 recruitment (Figure 3A, 12).

The Vps4 L64D mutation caused a severe GFP-CPS sorting defect indicating that the loss of all MIM1 interactions blocked Vps4 function (Figure 3A, 4). In contrast, the MIM2-interaction mutant $Vps4^{I18D}$ only partially inhibited the activity of Vps4 (Figure 3A, 3), which is consistent with the observed partial loss of MIT^{I18D}-GFP recruitment to endosomes (Figure 2, A and B, 10). However, single and double mutants of the ESCRT-III MIM2 motifs resulted in normal GFP-CPS trafficking, further supporting the notion that mutants with weak MIT-localization defects show correspondingly weak (or no) MVB-trafficking phenotypes (Figure 3A, 14–16).

The soluble fusion protein CPY-invertase is synthesized and translocated at the endoplasmic reticulum, transported by the sorting receptor Vps10 from the *trans*-Golgi to a MVB and finally delivered to the vacuole. ESCRT mutants impair the recycling of Vps10 back to the *trans*-Golgi, thereby limiting the transport function of this receptor. As a consequence, ESCRT mutants secrete a portion of newly synthesized CPY-invertase, a phenotype that can be detected by a colorimetric assay (Table 3; Paravicini *et al.,* 1992).

The CPY-invertase assay revealed similar functional redundancies of the ESCRT-III MIM1 motifs as observed by the analysis of GFP-CPS trafficking, although there was no clear difference in phenotypic severity between the $vps2^{\Delta C}$ and $vps24^{\Delta C}$ mutants. Loss of the Vps2 or Vps24 MIM1 motif resulted in a modest secretion phenotype ($vps2^{\Delta C}$ and $vps24^{\Delta C}$, ~30% secretion relative to the secretion of *vps4*Δ), whereas loss of both motifs caused a more severe phenotype (~50% secretion relative to *vps4*Δ). Mutation of the Vps4 MIM1 interaction site ($Vps4^{L64D}$) further enhanced CPY-invertase secretion (~70% secretion), consistent with the idea that this mutation interferes with all potential Vps4 MIM1 interactions, including those with Did2 and Ist1.

In contrast to the MIM1 mutants, the ESCRT-III MIM2 mutant strains did not secrete CPY-invertase (Table 3). However, mutating the Vps4 MIM2 interaction site ($Vps4^{I18D}$) caused detectable secretion (~60% secretion, Table 3), suggesting that loss of MIM2 interactions both on ESCRT-III and Ist1 together resulted in a synthetic phenotype (interactions 1 and 10, Figure 1A). Together, the phenotypic characterization of the different MIM mutants suggested that MIM1 interactions are more important for Vps4 function than the MIM2 interactions. However, we cannot exclude the possibility that the mutations in the MIM2 motifs retain some functionality.

The immediate consequence of the loss of Vps4 function is the accumulation of ESCRT-III on endosomes (Babst *et al.,* 1997). Therefore, we analyzed the effect of the MIM mutations on the localization of ESCRT-III subunits by fractionating cell extracts into soluble and membrane-associated pellet. In wild-type cells the majority of Vps24 and Snf7 localized to the soluble cytoplasmic pool (S), whereas deletion of *VPS4* resulted in the accumulation of both proteins in the pellet fraction (P; Figure 3B, lanes 1–4). Similarly, deleting *VPS2* alone or in combination with *VPS24* caused a shift of Snf7 pool to the pellet fraction, consistent with the published function of Vps2/Vps24 in Vps4 activity (Figure 3B, lanes 5–6 and 9–10; Babst *et al.,* 2002). In contrast, the majority of Vps24 was found in the soluble fraction in *vps2*Δ cells, which can be explained by the observation that Vps2 and Vps24 required each other for proper ESCRT-III assembly (Figure 3B, lanes 5 and 6; Babst *et al.,* 2002). Deletion of the *VPS2* MIM1 motif resulted in partial accumulation of both Vps24 and Snf7 ($vps2^{\Delta C}$-*HA*; Figure 3B, lanes 7 and 8), consistent with the partial trafficking phenotype associated with this strain. The additional deletion of the *VPS24* MIM1 motif further impaired but did not block the Vps4-dependent disassembly of ESCRT-III (cf. $vps2^{\Delta C}$-*HA* $vps24^{\Delta C}$-*HA* with *vps4*Δ in Figure 3B, lanes 1–2 and 11–12), suggesting that the remaining MIM2 sites were sufficient to maintain some Vps4 activity. Consistent with the observed redundancy among the MIM1/2 interactions we found that mutating either the MIM1 or the MIM2 interaction site in Vps4 only partially inhibited ESCRT-III disassembly (Figure 3B, lanes 13–16).

Loss of the Vps20–Snf7 subcomplex in *vps4*Δ caused the redistribution of Vps24 to the soluble, cytoplasmic fraction, an expected result based on previous publications (lanes 17 and 18, Figure 3B; Babst *et al.,* 2002). Additional expression of $vps20^{L188D}$ and $snf7^{L199D}$ in this strain restored ESCRT-III accumulation on endosomal membranes, indicating that the mutations in MIM2 did not interfere with the assembly of this protein complex (lanes 19 and 20, Figure 3B). However the mutation of the Snf7 MIM2 motif partially impaired the recycling of ESCRT-III from membranes whereas the corresponding mutation in Vps20 did not interfere with the Vps4-dependent disassembly reaction (lanes 21–26, Figure 3B). These observations suggested that although both MIM2 motifs of ESCRT-III are involved in the binding of the Vps4 MIT domain only Snf7 MIM2 seems to play an important role in the ESCRT-III disassembly reaction.

In summary the fractionation experiments indicated that MIM1 and MIM2 motifs of ESCRT-III act together not only in the recruitment of Vps4 but also in the subsequent ESCRT-III disassembly reaction. Both type of MIT interactions are important for Vps4 activity and loss of MIM1 or MIM2 affect recycling of both ESCRT-III subcomplexes, Vps20/Snf7 and Vps2/Vps24.

Characterization of the Vps4 AAA Domain Interactions

We tested the role of the Vps4 AAA domain interactions on the recruitment of the ATPase to the endosome in vivo by analyzing the localization of an ATP-locked Vps4 protein in which the MIT domain had been exchanged with GFP (GFP-$Vps4^{\Delta MIT,E233Q}$). The only known binding partners of this protein are Vta1, Ist1, and Vps4 itself (interactions 8, 9, 11, and 12 in Figure 1A). In *vps4*Δ cells GFP-$Vps4^{\Delta MIT,E233Q}$ localized mainly to class E compartments (Figure 4A, 1), indicating that the MIT domain is not essential for the localization of Vps4 to endosomes. Loss of the AAA-Ist1 interaction did not affect the recruitment of GFP-$Vps4^{\Delta MIT,E233Q}$ to ESCRT-III (*vps4*Δ*ist1*Δ, Figure 4A, 4), which is consistent with previous reports that described a rather weak interaction (Dimaano *et al.,* 2008). In contrast, cells that lacked Vta1 were not able to recruit GFP-$Vps4^{\Delta MIT,E233Q}$ to ESCRT-III (Figure 4A, 3). Similarly, lack of Did2 abolished endosomal recruitment of GFP-$Vps4^{\Delta MIT,E233Q}$ (Figure 4A, 2). Because Did2 has been shown to be important for endosomal local-

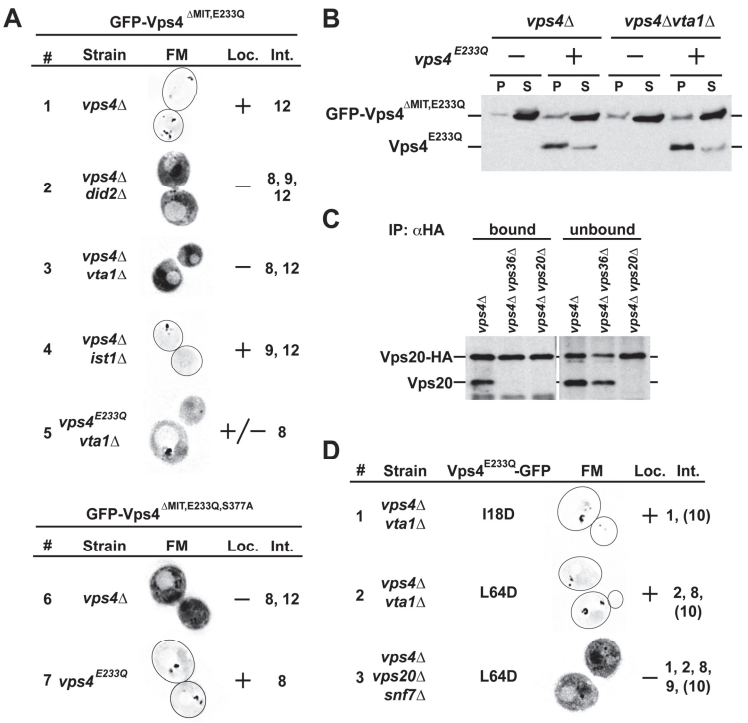

Figure 4. Localization of mutant Vps4 proteins. (A) Localization of MIT-deleted Vps4 (GFP-Vps4$^{\Delta MIT,E233Q}$ and GFP-Vps4$^{\Delta MIT,E233Q,S377A}$) in different yeast mutant strains (see Table 1) determined by fluorescence microscopy (FM). (A and D) The extent of observed endosomal localization is indicated (Loc.). Vps4 interactions affected by the different mutations are listed. Int., numbers are based on the interactions in Figure 1A. (B) Endosomal recruitment of MIT-deleted Vps4 in the presence or absence of full-length Vps4 protein determined by subcellular fractionation and Western blot analysis (S, soluble; P, pellet). (C) Immunoprecipitation of Vps20-HA from detergent-solubilized membrane fractions. The resulting bound and unbound samples were analyzed by Western blot using anti-Vps20 antiserum. (D) Fluorescence microscopy (FM) analysis of GFP-tagged full-length Vps4 protein in different mutant strains (Table 1). Numbers in parentheses indicate partially disrupted interactions.

ization of Vta1, the mislocalization of GFP-Vps4$^{\Delta MIT,E233Q}$ in *vps4*Δ *did2*Δ is likely due to a lack of ESCRT-III–associated Vta1 in this strain (Azmi *et al.*, 2008).

To further corroborate the role of Vta1 in GFP-Vps4$^{\Delta MIT,E233Q}$ localization, the previously published mutation S377A was introduced into the beta-loop of Vps4, a mutation predicted to interfere with Vta1 binding (Scott *et al.*, 2005b). When expressed in yeast, the Vps4^{S377A} mutant protein was stable and present at normal levels, indicating that the mutation did not interfere with protein folding (Supplemental Figure 2). As expected, the mutation resulted in a partial GFP-CPS and a weak CPY-invertase trafficking phenotype (Figure 3A, 5, and Table 3), similar to the phenotype observed in cells deleted for *VTA1* (Azmi *et al.*, 2006; Saksena *et al.*, 2009). When introduced into GFP-Vps4$^{\Delta MIT,E233Q}$, the resulting mutant construct GFP-Vps4$^{\Delta MIT,E233Q,S377A}$ did not localize to endosomes in *vps4*Δ cells (Figure 4A, 6), which is consistent with the loss of Vta1 interaction. Together, the data supported the model that Vta1 localizes to ESCRT-III via Did2 and that the ESCRT-III–associated pool of Vta1 is sufficient to recruit MIT-deleted Vps4.

Introducing full-length Vps4^{E233Q} into *vps4*Δ*vta1*Δ cells partially restored endosomal localization of GFP-Vps4$^{\Delta MIT,E233Q}$ (*vps4^{E233Q} vta1*Δ; Figure 4A, 5). Similarly the presence of Vps4^{E233Q} suppressed the localization defect of Vps4$^{\Delta MIT,E233Q,S377A}$ (Figure 4A, 7). These results indicated that Vps4-Vps4 interactions were sufficient to recruit the ATPase to ESCRT-III.

In contrast to the microscopy studies, subcellular fractionation experiments GFP-Vps4$^{\Delta MIT,E233Q}$ localized almost exclusively to the soluble, cytoplasmic fraction in presence or absence of either Vps4^{E233Q} or Vta1 (Figure 4B). This discrepancy is likely caused by the dissociation of GFP-Vps4$^{\Delta MIT,E233Q}$ during the fractionation procedure, suggesting that the lack of the MIT domain weakened the interaction not only between Vps4 and ESCRT-III but also the interactions within the Vps4 oligomer.

In summary, the localization studies using MIT-deleted Vps4 suggested that Vps4 could be recruited to ESCRT-III either via binding to Vta1 or via interactions with other ESCRT-III–associated Vps4 subunits. However, loss of the MIT domain resulted in reduced stability of the ESCRT-III–associated Vps4 oligomer.

Vps4 Oligomer and ESCRT-III Make Multiple Contacts

Recently, a model for the ESCRT-III structure has been proposed that suggested a single linear polymer consisting of the ordered assembly of one subunit of Vps20, followed by ~10 subunits of Snf7, followed by about three subunits of Vps2, and finished by about two Vps24 proteins (Teis *et al.*, 2008; Saksena *et al.*, 2009). It is difficult to model how this linear arrangement of ESCRT-III subunits would allow the simultaneous interaction of both MIM motifs with the Vps4 MIT domains, which based on our observations are critical for the Vps4-dependent ESCRT-III disassembly. Therefore, the predicted ESCRT-III composition was tested using immunoprecipitation experiments to determine if ESCRT-III indeed contains a single Vps20 subunit. For this purpose we expressed HA-tagged *VPS20* (*VPS20-HA*) and untagged *VPS20* in the same strain, immunoprecipitated Vps20-HA from detergent-solubilized membranes and analyzed the resulting samples by Western blot using anti-Vps20 antiserum. The result demonstrated that Vps20 coimmunoprecipitated

with Vps20-HA from *vps4*Δ cells, a mutant strain that accumulates ESCRT-III on the endosomal membrane (Figure 4C). In contrast, *vps4*Δ cells that lacked either the ESCRT-II subunit Vps36 or Vps20 itself did not show coimmunoprecipitation of Vps20 with Vps20-HA. These results indicated that ESCRT-III contains at least two subunits of Vps20, suggesting a more complex structure for ESCRT-III than previously proposed.

A more complex ESCRT-III structure could allow for several MIT domains of a Vps4 oligomer to contact ESCRT-III simultaneously via both MIM1 and MIM2 interactions, a model that is supported by our localization studies of full-length Vps4. The microscopy data indicated that Vps4^{E233Q}-GFP localized to endosomes efficiently even in presence of only the MIM1 or MIM2 interaction (I18D or L64D mutant in *vps4*Δ *vta1*Δ, Figure 4D). This observation is in contrast to the studies of MIT-GFP shown in Figure 2A, which demonstrated that the loss of MIM1 or MIM2 severely inhibited the localization of the MIT domain to endosomes. Only deletion of the Snf7-Vps20 subcomplex, which results in a complete loss of ESCRT-III on endosomes, blocked the localization of Vps4^{E233Q}-GFP to endosomes (*vps4*Δ *vps20*Δ *snf7*Δ, Figure 4D).

Together, the data indicated that the binding of full-length Vps4 to ESCRT-III is less sensitive to loss of MIT interactions than observed with a single MIT domain. This difference is likely due to the oligomerization of full-length Vps4 that allows the formation of several MIT-ESCRT-III interactions per Vps4 complex. These multiple interactions would act additively, thereby dramatically enhancing overall affinity of Vps4 to its substrate.

Indications for Functionally Distinct Ring Structures in the Vps4 Oligomer

The Vps4^{E233Q} mutant protein is unable to hydrolyze the bound ATP and exhibits a dominant negative phenotype in vivo (Babst *et al.*, 1998). This dominant-negative effect is likely caused by the assembly of the Vps4^{E233Q} mutant proteins together with wild-type Vps4 into the oligomeric structure, thereby inhibiting the function of the assembled protein complex. Interestingly, both CPY-invertase secretion assays and GFP-CPS sorting analysis indicated that deletion of the MIT domain eliminated the dominant-negative phenotype of Vps4^{E233Q} (*vps4*$^{\Delta}$MIT,E233Q, Figure 3A, 8, and Table 3) even though microscopy studies demonstrated that Vps4^{E233Q} lacking the MIT domain is recruited to ESCRT-III via binding to full-length Vps4 (Figure 4A, 5 and 7). Similarly, mutations in the MIT domain that interfere with binding to ESCRT-III and Ist1 (L64D and I18D) suppressed the dominant-negative phenotype of Vps4^{E233Q} (Table 3 and Figure 3A, 6 and 7). Because our data suggested that the MIT domain plays an important role in the initial recruitment of Vps4 to ESCRT-III, we speculate that without the MIT domain Vps4 is preferentially incorporated into the second, ESCRT-III-distal ring of the Vps4 oligomer. If correct, this would argue that the function of the Vps4 oligomer is not inhibited by the presence of ATP-locked subunits in the second ring but is blocked by the presence of Vps4^{E233Q} in the ESCRT-III–bound ring.

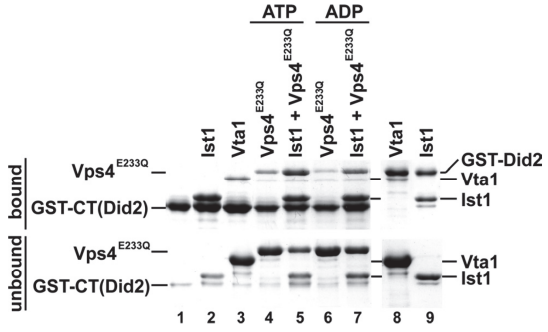

Figure 5. Ist1 and Did2 form a stable complex. GST-tagged full-length Did2 (GST-Did2) or C-terminal half of Did2 [GST-CT(Did2)] was immobilized on GSH-Sepharose, and purified Ist1, Vta1, or Vps4^{E233Q} protein was added. The resulting bound and unbound fractions were analyzed by SDS-PAGE and Coomassie staining.

Binding of Vps4, Vta1, and Ist1 to Did2

Did2 binds to Vps4, Vta1, and Ist1 via its C-terminal MIM1 motif (Figure 1A; Howard *et al.*, 2001; Stuchell-Brereton *et al.*, 2007; Azmi *et al.*, 2008; Bajorek *et al.*, 2009b; Xiao *et al.*, 2009). To compare the strength of these interactions, in vitro GST pulldown experiments were performed. GST fused to Did2 was purified and immobilized on GSH-Sepharose. Recombinant Ist1 or Vta1 was added in a one-to-one ratio to the immobilized GST-Did2 and bound and unbound fractions were analyzed by SDS-PAGE. In these experiments, Ist1 bound with an approximate 1:1 ratio to Did2 (Figure 5, lane 9). In contrast, the binding of Vta1 to GST-Did2 was inefficient, and a majority of the protein was found in the unbound fraction (Figure 5, lane 8). Because Vps4 and GST-Did2 comigrate in SDS-PAGE gels, additional interaction studies were performed using the C-terminal half of Did2 [CT(Did2), amino acids 113-204]. Similar to the results observed with full-length Did2, GST-CT(Did2) bound very efficiently to Ist1, but only small amounts of Vta1 were detected in the bound fraction (Figure 5, lanes 2 and 3). The hydrolysis mutant Vps4^{E233Q} bound poorly to GST-CT-(Did2) both in the presence of ATP and ADP (Figure 5, lanes 4 and 6). However, the presence of Ist1 increased the amount of Did2-bound Vps4^{E233Q} (Figure 5, lanes 5 and 7). This increase in Vps4 binding was more pronounced in the presence of ATP compared with ADP, which is consistent with the previously observed nucleotide dependence of the Vps4-Ist1 interaction (Dimaano *et al.*, 2008). These results suggested that in the presence of Ist1 the observed Vps4-Did2 interaction is not direct but mediated by Ist1.

Together, the in vitro binding studies suggested that Ist1 has much higher affinity to Did2 than Vta1 or Vps4. Therefore, we predicted that in the cytoplasm Ist1 is the preferred binding partner of Did2. Furthermore, previous studies have shown that high cytoplasmic levels of Did2 interfere with endosomal localization of Ist1, supporting the notion that Did2 binds to Ist1 in vivo in the cytoplasm (Dimaano *et al.*, 2008). In contrast, high Did2 expression levels did not affect the endosomal localization of Vta1 or Vps4 (data not shown). In the presence of ATP, Vps4 demonstrated a high-affinity for Ist1 (Figure 5; Dimaano *et al.*, 2008), which suggested that in the cytoplasm Did2, Ist1, and Vps4 might form a complex that is then recruited to ESCRT-III. However, attempts to obtain direct evidence for the presence of this complex in the cytoplasm by coimmunoprecipitation experiments or gel filtration analysis were not successful (data not shown), which might be a consequence of the transient nature of the Vps4-Ist1-Did2 complex.

DISCUSSION

The recruitment of Vps4 to ESCRT-III is mediated to a large extent by interactions between the Vps4 MIT domain and the four subunits of ESCRT-III, as well as Ist1 and Did2. All six proteins interact with the MIT domain via MIM1 or MIM2 motifs, which bind to two different surface areas of the MIT domain (Figure 1, A and C). These interactions are rather weak, with K_d values in the micromolar range (Stuchell-Brereton *et al.*, 2007; Kieffer *et al.*, 2008), suggesting that several interactions act synergistically to achieve Vps4 recruitment and assembly.

The binding of Ist1 to Did2 is required for the localization of Ist1 to ESCRT-III (Dimaano *et al.*, 2008; Rue *et al.*, 2008). Overexpression of *DID2* results in accumulation of Ist1 together with Did2 in the cytoplasm, indicating that the Did2-Ist1 interaction is not limited to ESCRT-III but can occur in solution (Dimaano *et al.*, 2008). This observation is consistent with our in vitro data demonstrating the formation of a stable interaction between Ist1 and full-length Did2, which suggested that this interaction occurs in the closed conformation of cytoplasmic Did2 (in contrast to the open conformation of ESCRT-III–associated Did2; Figure 5). Therefore, we propose that Ist1 and Did2 interact in the cytoplasm and that this complex binds to Vps4, which facilitates its recruitment to ESCRT-III. In this complex the C-terminal MIM1 and MIM2 motifs of Ist1 bind to the Vps4 MIT domain, whereas the Ist1 ELYC domain interacts with both Did2 and the AAA domain of Vps4 (interactions 7, 9, and 10, Figure 1A). This trimeric complex is recruited to ESCRT-III via the interaction between Did2 and the Vps2–Vps24 subcomplex (step A in Figure 1B). In this model the direct interaction between Vps4 and Did2 implicated in previous studies, does not play a role in Vps4 recruitment (interaction 3, Figure 1A).

One of the two MIT domains of Vta1 has been shown to bind to the MIM1 motif of Did2 (Azmi *et al.*, 2008). This motif is accessible in the open, or ESCRT-III–associated conformation of Did2. Therefore, we predict that Vta1 is recruited to the ESCRT-III–associated Did2-Ist1-Vps4 complex (step B in Figure 1B). This recruitment might initialize the assembly of Vps4 from the Ist1-Did2–bound state into the active oligomeric form. Because Ist1 apparently competes with Vta1 and ESCRT-III for Vps4 binding (Figure 1A), we propose that Vps4 assembly requires rearrangement of the existing Vps4 interactions (step C in Figure 1B). The MIT domain switches from the MIM1 and MIM2 interactions with Ist1 to MIM1 and MIM2 interactions with ESCRT-III (MIM1 of Vps2–Vps24 subcomplex and MIM2 of Vps20–Snf7 subcomplex). The Vps4 AAA domain changes its interaction from the Ist1 ELYC domain to the dimerization domain of Vta1 (VHL domain; Azmi *et al.*, 2006). These rearrangements replace the recruiting factor Ist1 with the assembly factor Vta1 and the substrate ESCRT-III.

In contrast to cytokinesis, which requires Ist1 function (Agromayor *et al.*, 2009; Bajorek *et al.*, 2009a), the MVB pathway showed only minor defects in *ist1*Δ cells (Dimaano *et al.*, 2008). This observation suggested that at the MVB, Vps4 can be directly recruited by ESCRT-III– and Did2-associated Vta1 (step C bypassing A and B in Figure 1B). This redundancy seems to be common in the Vps4 system of the MVB pathway. For example, only the loss of two or more Vps4 MIT interactions severely impaired the recruitment and function of Vps4 (Figures 2 and 3, Table 3). Mainly, the phenotypic severity of the different MIT and ESCRT-III interaction mutants followed the severity of the MIT-GFP recruitment defects observed in these strains. Exceptions were the MIM2 mutations in Vps20 and Snf7 that resulted in reduced endosomal recruitment of MIT-GFP and increased accumulation of ESCRT-III, but no obvious effects on MVB trafficking.

Based on our mutational analysis, all four potential ESCRT-III MIT interaction motifs are functional. However, loss of Vps2 MIM1 or Snf7 MIM2 resulted in more severe phenotypes than observed with mutations in the MIT interaction motifs of Vps24 and Vps20, suggesting that Vps2 and Snf7 contain the major Vps4-binding sites. This finding contradicted in vitro data, indicating Vps20 as a major binding partner for Vps4 (Figure 2D, Azmi *et al.*, 2008; Kieffer *et al.*, 2008) and demonstrated the importance for in vivo studies to determine the relevance of interactions observed in vitro.

The high level of redundancy in the Vps4 recruitment system is further illustrated by the fact that Vps4 lacking the MIT domain is still able to localize to endosomes. Our data showed that MIT deleted Vps4 was able to localize to MVBs by binding to Vta1 that has been localized via Did2 to ESCRT-III (Figure 4). However, the deletion of the MIT domain resulted in loss of Vps4 function, suggesting the MIT domain functions not only in Vps4 localization but also in the ESCRT-III disassembly reaction.

Our data indicated that efficient recruitment of Vps4 and subsequent ESCRT-III disassembly required MIM1 and MIM2 MIT interactions to occur simultaneously, an observation that has strong implications in the ESCRT-III structure. A recently published model of ESCRT-III proposed a single linear polymer of ~16 subunits (Teis *et al.*, 2008; Saksena *et al.*, 2009). However, our results indicated a more complex structure for ESCRT-III (Figure 4C), a structure that should allow for the simultaneous binding of several Vps4 MIT domains to ESCRT-III MIM1 and MIM2 motifs.

Vps4 oligomerizes into a complex composed of 12 subunits which form two six-membered rings in a tail-to-tail arrangement (Yu *et al.*, 2008; Landsberg *et al.*, 2009). Based on this structure, one ring interacts via the N-terminal MIT domains with ESCRT-III, whereas the second ring seems to have no direct contact with the substrate, a functional difference that is reflected in the different subunit arrangements of the two rings (Yu *et al.*, 2008). ATP-locked $Vps4^{E233Q}$ is a dominant-negative mutant protein that assembles with wild-type Vps4 and blocks its activity (Babst *et al.*, 1998). However, deletion or mutation of the MIT domain suppressed the dominant-negative phenotype of $Vps4^{E233Q}$ even though the protein was recruited together with full-length Vps4 to the endosomal membrane (Figures 3A and 4A, Table 3). Because the MIT domain plays an important role in the initial recruitment of Vps4 to ESCRT-III, we speculate that the mutant MIT versions of Vps4 predominantly assemble via Vps4–Vps4 and Vps4–Vta1 interactions in the second, ESCRT-III-distal Vps4 ring (Figure 1B, step E). If correct, this model would imply that the presence of ATP-locked $Vps4^{E233Q}$ in the second ring does not interfere with the function of the overall complex. The second, non-ESCRT-III–associated ring might mainly play a structural or regulatory role and thus is not directly involved in the ATP-dependent dissociation reaction. Similarly, type-II AAA ATPases, such as NSF/Sec18 and p97/Cdc48, have been shown to contain two functionally distinct AAA domain rings (reviewed in Erzberger and Berger, 2006). The N-terminal AAA ring hydrolyzes ATP, providing the energy for the disassembly or unfolding of the bound substrate. The second, C-terminal AAA ring, plays a structural role and does not hydrolyze the bound nucleotide.

Together, our studies resulted in a model of the Vps4 interaction network that underlies the recruitment and oli-

gomerization of the ATPase. Both types of interactions, MIM1 and MIM2, play a role in these activities and work together to accomplish the recycling of ESCRT-III subunits and the formation of MVB vesicles. These built-in redundancies ensure the robustness of the system and highlight the importance of Vps4 in the proper function of endosomal protein trafficking and cytokinesis, two essential cellular processes.

ACKNOWLEDGMENTS

We thank Tamara Darsow, Vladimir Lupashin, and Charles Jones for critical reading of the manuscript. We thank Wes Sundquist and Jack Skalicky for assistance with designing the MIT point mutations. This work has been supported by Grant R01 GM074171 from the National Institutes of Health (NIH) and Grant 0530210N from the American Heart Association. D.J.K. and B.A.D. are supported by Grant R01 GM073024 from the NIH.

REFERENCES

Agromayor, M., Carlton, J. G., Phelan, J. P., Matthews, D. R., Carlin, L. M., Ameer-Beg, S., Bowers, K., and Martin-Serrano, J. (2009). Essential role of hIST1 in cytokinesis. Mol. Biol. Cell *20*, 1374–1387.

Azmi, I., Davies, B., Dimaano, C., Payne, J., Eckert, D., Babst, M., and Katzmann, D. J. (2006). Recycling of ESCRTs by the AAA-ATPase Vps4 is regulated by a conserved VSL region in Vta1. J. Cell Biol. *172*, 705–717.

Azmi, I. F., Davies, B. A., Xiao, J., Babst, M., Xu, Z., and Katzmann, D. J. (2008). ESCRT-III family members stimulate Vps4 ATPase activity directly or via Vta1. Dev Cell *14*, 50–61.

Babst, M. (2005). A protein's final ESCRT. Traffic *6*, 2–9.

Babst, M., Katzmann, D. J., Estepa-Sabal, E. J., Meerloo, T., and Emr, S. D. (2002). Escrt-III: an endosome-associated heterooligomeric protein complex required for mvb sorting. Dev. Cell *3*, 271–282.

Babst, M., Sato, T. K., Banta, L. M., and Emr, S. D. (1997). Endosomal transport function in yeast requires a novel AAA-type ATPase, Vps4p. EMBO J. *16*, 1820–1831.

Babst, M., Wendland, B., Estepa, E. J., and Emr, S. D. (1998). The Vps4p AAA ATPase regulates membrane association of a Vps protein complex required for normal endosome function. EMBO J. *17*, 2982–2993.

Bajorek, M., Morita, E., Skalicky, J. J., Morham, S. G., Babst, M., and Sundquist, W. I. (2009a). Biochemical analyses of human IST1 and its function in cytokinesis. Mol. Biol. Cell *20*, 1360–1373.

Bajorek, M., Schubert, H. L., McCullough, J., Langelier, C., Eckert, D. M., Stubblefield, W. M., Uter, N. T., Myszka, D. G., Hill, C. P., and Sundquist, W. I. (2009b). Structural basis for ESCRT-III protein autoinhibition. Nat. Struct. Mol. Biol. *16*, 754–762.

Baudin, A., Ozier Kalogeropoulos, O., Denouel, A., Lacroute, F., and Cullin, C. (1993). A simple and efficient method for direct gene deletion in *Saccharomyces cerevisiae*. Nucleic Acids Res. *21*, 3329–3330.

Carlton, J. G., and Martin-Serrano, J. (2007). Parallels between cytokinesis and retroviral budding: a role for the ESCRT machinery. Science *316*, 1908–1912.

Christianson, T. W., Sikorski, R. S., Dante, M., Shero, J. H., and Hieter, P. (1992). Multifunctional yeast high-copy-number shuttle vectors. Gene *110*, 119–122.

Darsow, T., Odorizzi, G., and Emr, S. D. (2000). Invertase fusion proteins for analysis of protein trafficking in yeast. Methods Enzymol. *327*, 95–106.

Davies, B. A., Lee, J. R., Oestreich, A. J., and Katzmann, D. J. (2009). Membrane protein targeting to the MVB/lysosome. Chem. Rev. *109*, 1575–1586.

Dimaano, C., Jones, C. B., Hanono, A., Curtiss, M., and Babst, M. (2008). Ist1 regulates vps4 localization and assembly. Mol. Biol. Cell *19*, 465–474.

Erzberger, J. P., and Berger, J. M. (2006). Evolutionary relationships and structural mechanisms of AAA+ proteins. Annu. Rev. Biophys. Biomol. Struct. *35*, 93–114.

Garrus, J. E., *et al.* (2001). Tsg101 and the vacuolar protein sorting pathway are essential for HIV-1 budding. Cell *107*, 55–65.

Gonciarz, M. D., Whitby, F. G., Eckert, D. M., Kieffer, C., Heroux, A., Sundquist, W. I., and Hill, C. P. (2008). Biochemical and structural studies of yeast Vps4 oligomerization. J. Mol. Biol. *384*, 878–895.

Hanson, P. I., Roth, R., Lin, Y., and Heuser, J. E. (2008). Plasma membrane deformation by circular arrays of ESCRT-III protein filaments. J. Cell Biol. *180*, 389–402.

Horazdovsky, B. F., Busch, G. R., and Emr, S. D. (1994). VPS21 encodes a rab5-like GTP binding protein that is required for the sorting of yeast vacuolar proteins. EMBO J. *13*, 1297–1309.

Howard, T. L., Stauffer, D. R., Degnin, C. R., and Hollenberg, S. M. (2001). CHMP1 functions as a member of a newly defined family of vesicle trafficking proteins. J. Cell Sci. *114*, 2395–2404.

Hurley, J.H., and Emr, S.D. (2006). The ESCRT Complexes: Structure and Mechanism of a Membrane-Trafficking Network. Annu Rev Biophys Biomol Struct. *35*, 277–298.

Kieffer, C., Skalicky, J. J., Morita, E., De Domenico, I., Ward, D. M., Kaplan, J., and Sundquist, W. I. (2008). Two distinct modes of ESCRT-III recognition are required for VPS4 functions in lysosomal protein targeting and HIV-1 budding. Dev. Cell *15*, 62–73.

Landsberg, M. J., Vajjhala, P. R., Rothnagel, R., Munn, A. L., and Hankamer, B. (2009). Three-dimensional structure of AAA ATPase Vps *4*, advancing structural insights into the mechanisms of endosomal sorting and enveloped virus budding. Structure *17*, 427–437.

Lata, S., Roessle, M., Solomons, J., Jamin, M., Gottlinger, H. G., Svergun, D. I., and Weissenhorn, W. (2008). Structural basis for autoinhibition of ESCRT-III CHMP3. J. Mol. Biol. *378*, 818–827.

Lottridge, J. M., Flannery, A. R., Vincelli, J. L., and Stevens, T. H. (2006). Vta1p and Vps46p regulate the membrane association and ATPase activity of Vps4p at the yeast multivesicular body. Proc. Natl. Acad. Sci. USA *103*, 6202–6207.

Lupas, A. N., and Martin, J. (2002). AAA proteins. Curr. Opin. Struct. Biol. *12*, 746–753.

McDonald, B., and Martin-Serrano, J. (2009). No strings attached: the ESCRT machinery in viral budding and cytokinesis. J. Cell Sci. *122*, 2167–2177.

Morita, E., Sandrin, V., Chung, H. Y., Morham, S. G., Gygi, S. P., Rodesch, C. K., and Sundquist, W. I. (2007). Human ESCRT and ALIX proteins interact with proteins of the midbody and function in cytokinesis. EMBO J. *26*, 4215–4227.

Muziol, T., Pineda-Molina, E., Ravelli, R. B., Zamborlini, A., Usami, Y., Gottlinger, H., and Weissenhorn, W. (2006). Structural basis for budding by the ESCRT-III factor CHMP3. Dev. Cell *10*, 821–830.

Nickerson, D. P., West, M., and Odorizzi, G. (2006). Did2 coordinates Vps4-mediated dissociation of ESCRT-III from endosomes. J. Cell Biol. *175*, 715–720.

Obita, T., Saksena, S., Ghazi-Tabatabai, S., Gill, D. J., Perisic, O., Emr, S. D., and Williams, R. L. (2007). Structural basis for selective recognition of ESCRT-III by the AAA ATPase Vps4. Nature *449*, 735–739.

Odorizzi, G., Babst, M., and Emr, S. D. (1998). Fab1p PtdIns(3)P 5-kinase function essential for protein sorting in the multivesicular body. Cell *95*, 847–858.

Paravicini, G., Horazdovsky, B. F., and Emr, S. D. (1992). Alternative pathways for the sorting of soluble vacuolar proteins in yeast: a *vps35* null mutant missorts and secretes only a subset of vacuolar hydrolases. Mol. Biol. Cell *3*, 415–427.

Piper, R. C., and Katzmann, D. J. (2007). Biogenesis and Function of Multivesicular Bodies. Annu Rev Cell Dev Biol. *23*, 519–547.

Raiborg, C., and Stenmark, H. (2009). The ESCRT machinery in endosomal sorting of ubiquitylated membrane proteins. Nature *458*, 445–452.

Robinson, J. S., Klionsky, D. J., Banta, L. M., and Emr, S. D. (1988). Protein sorting in *Saccharomyces cerevisiae*: isolation of mutants defective in the delivery and processing of multiple vacuolar hydrolases. Mol. Cell. Biol. *8*, 4936–4948.

Rue, S. M., Mattei, S., Saksena, S., and Emr, S. D. (2008). Novel Ist1-Did2 complex functions at a late step in multivesicular body sorting. Mol. Biol. Cell *19*, 475–484.

Saksena, S., and Emr, S. D. (2009). ESCRTs and human disease. Biochem. Soc. Trans. *37*, 167–172.

Saksena, S., Wahlman, J., Teis, D., Johnson, A. E., and Emr, S. D. (2009). Functional reconstitution of ESCRT-III assembly and disassembly. Cell *136*, 97–109.

Scott, A., Chung, H. Y., Gonciarz-Swiatek, M., Hill, G. C., Whitby, F. G., Gaspar, J., Holton, J. M., Viswanathan, R., Ghaffarian, S., Hill, C. P., and Sundquist, W. I. (2005a). Structural and mechanistic studies of VPS4 proteins. EMBO J. *24*, 3658–3669.

Scott, A., Gaspar, J., Stuchell-Brereton, M. D., Alam, S. L., Skalicky, J. J., and Sundquist, W. I. (2005b). Structure and ESCRT-III protein interactions of the MIT domain of human VPS4A. Proc. Natl. Acad. Sci. USA *102*, 13813–13818.

Sherman, F., Fink, G. R., and Lawrence, L. W. (1979). Methods in Yeast Genetics: A Laboratory Manual, Cold Spring Harbor, NY: Cold Spring Harbor Laboratory Press.

Shiflett, S. L., Ward, D. M., Huynh, D., Vaughn, M. B., Simmons, J. C., and Kaplan, J. (2004). Characterization of Vta1p, a class E Vps protein in *Saccharomyces cerevisiae*. J. Biol. Chem. *279*, 10982–10990.

Shim, S., Kimpler, L. A., and Hanson, P. I. (2007). Structure/function analysis of four core ESCRT-III proteins reveals common regulatory role for extreme C-terminal domain. Traffic *8*, 1068–1079.

Shim, S., Merrill, S. A., and Hanson, P. I. (2008). Novel interactions of ESCRT-III with LIP5 and VPS4 and their implications for ESCRT-III disassembly. Mol. Biol. Cell *19*, 2661–2672.

Spitzer, C., Schellmann, S., Sabovljevic, A., Shahriari, M., Keshavaiah, C., Bechtold, N., Herzog, M., Muller, S., Hanisch, F. G., and Hulskamp, M. (2006). The *Arabidopsis* elch mutant reveals functions of an ESCRT component in cytokinesis. Development *133*, 4679–4689.

Stuchell-Brereton, M. D., Skalicky, J. J., Kieffer, C., Karren, M. A., Ghaffarian, S., and Sundquist, W. I. (2007). ESCRT-III recognition by VPS4 ATPases. Nature *449*, 740–744.

Teis, D., Saksena, S., and Emr, S. D. (2008). Ordered assembly of the ESCRT-III complex on endosomes is required to sequester cargo during MVB formation. Dev. Cell *15*, 578–589.

Vajjhala, P. R., Nguyen, C. H., Landsberg, M. J., Kistler, C., Gan, A. L., King, G. F., Hankamer, B., and Munn, A. L. (2008). The Vps4 C-terminal helix is a critical determinant for assembly and ATPase activity and has elements conserved in other members of the meiotic clade of AAA ATPases. FEBS J. *275*, 1427–1449.

VerPlank, L., Bouamr, F., LaGrassa, T. J., Agresta, B., Kikonyogo, A., Leis, J., and Carter, C. A. (2001). Tsg101, a homologue of ubiquitin-conjugating (E2) enzymes, binds the L domain in HIV type 1 Pr55(Gag). Proc. Natl. Acad. Sci. USA *98*, 7724–7729.

Ward, D. M., Vaughn, M. B., Shiflett, S. L., White, P. L., Pollock, A. L., Hill, J., Schnegelberger, R., Sundquist, W. I., and Kaplan, J. (2005). The role of LIP5 and CHMP5 in multivesicular body formation and HIV-1 budding in mammalian cells. J. Biol. Chem. *280*, 10548–10555.

Williams, R. L., and Urbe, S. (2007). The emerging shape of the ESCRT machinery. Nat. Rev. Mol. Cell Biol. *8*, 355–368.

Wollert, T., Wunder, C., Lippincott-Schwartz, J., and Hurley, J. H. (2009). Membrane scission by the ESCRT-III complex. Nature *458*, 172–177.

Xiao, J., Chen, X. W., Davies, B. A., Saltiel, A. R., Katzmann, D. J., and Xu, Z. (2009). Structural basis of Ist1 function and Ist1-Did2 interaction in the mVB pathway and cytokinesis. Mol. Biol. Cell. *20*, 3514–3524.

Xiao, J., Xia, H., Zhou, J., Azmi, I. F., Davies, B. A., Katzmann, D. J., and Xu, Z. (2008). Structural basis of Vta1 function in the multivesicular body sorting pathway. Dev. Cell *14*, 37–49.

Yeo, S. C., *et al.* (2003). Vps20p and Vta1p interact with Vps4p and function in multivesicular body sorting and endosomal transport in *Saccharomyces cerevisiae*. J. Cell Sci. *116*, 3957–3970.

Yu, Z., Gonciarz, M. D., Sundquist, W. I., Hill, C. P., and Jensen, G. J. (2008). Cryo-EM structure of dodecameric Vps4p and its 2:1 complex with Vta1p. J. Mol. Biol. *377*, 364–377.

CHAPTER 3

FUNCTIONAL AND BIOCHEMICAL STUDIES OF THE LINKER REGION OF THE VPS4 PROTEIN

Abstract

Disassembly of the endosome-associated ESCRT-III by the Vps4 ATPase is believed to be a final step in the formation of intralumenal MVB vesicles. Vps4 consists of three domains – the N-terminal MIT domain (1-79) that binds ESCRT-III, the C-terminal ATPase cassette (123-437) that promotes oligomerization and the ATP hydrolysis and linker region (79-123). MIT-mediated recruitment of Vps4 by ESCRT-III promotes homooligomerization of the Vps4 ATPase cassettes into a double-stacked ring structure forming a central cavity or pore that is essential for the Vps4 function. It is not clear if MIT domains function in the recruitment step or if they contribute together with the pore region in solubilization of the ESCRT-III. This study is aimed at identifying the role of the linker region in providing flexibility of movement to the MIT domains of Vps4. We used a serial deletion/mutation approach to identify length of the linker region that supports function of Vps4 *in vivo*. Deletion of the linker region was demonstrated to stimulate ATPase activity of the Vps4. At the same time, linker length was demonstrated to be largely dispensable for the function of Vps4 in the MVB. Our results suggest that Vps4 function is only partially compromised by the short linker region, suggesting that MIT domains do not require a wide range of movement and therefore work together with a pore region in processing substrate.

Introduction

Vps4 ATPase and ESCRT protein complexes (ESCRT-0, I, II and III) are known to function in a variety of cellular processes that require membrane deformation and scission events, thereby promoting formation of MVBs in yeast and metazoans, cell division in archea and mammalian cells as well as budding of the HIV-1 viral particle [1] [2] [3]. In general, ESCRTs function by physically deforming membranes and promoting vesicle formation (MVB) and scission events (cytokinesis and HIV-1 budding). ESCRT- 0, I, II and III protein complexes assemble on membranes in the sequential manner.

ESCRT-III core and accessory proteins (Ist1, Did2) continuously cycle from a soluble inactive or "closed" form to a membrane-bound active or "open" form. C-terminal regions of ESCRT-III proteins contain MIT Interacting Motifs (MIMs) that mediate binding to MIT domains of Vps4 and therefore regulate recruitment of Vps4. Upon membrane recruitment, ESCRT-III proteins acquire an open conformation that exposes their C-termini for interaction with Vps4. Polymerization of the ESCRT-III complex composed of Vps20, Snf7, Vps2 and Vps24 is believed to promote membrane deformation and scission as demonstrated by their ability to induce vesicle formation *in vitro* [4] and deform plasma membrane *in vivo* [5]. *In vivo* ESCRT-III polymer needs to be removed from the membranes to allow for further rounds of ESCRT-dependent membrane deformation events. Recruitment of Vps4 ATPase is believed to be the final step that solubilizes ESCRT-III, therefore promoting membrane scission.

Yeast Vps4 is a soluble, nonessential AAA+ ATPase that consists of 437 amino acids forming two functionally and structurally separate domains – an N-

terminal substrate interacting or MIT domain (1-79 amino acids) and a C-terminal single (class I) nucleotide binding/hydrolyzing ATPase domain composed of large and small subdomains (123-437 amino acids) (Figure 3-1-A). Almost ten percent of the Vps4 amino acid sequence belongs to the linker region, which forms an unstructured stretch of 44 amino acids connecting MIT and ATPase domains (Figure 3-1-B).

ATP binding drives oligomerization of Vps4 and promotes assembly of the functional ATPase that is capable of ATP hydrolyses. Two adjacent subunits of Vps4 comprise a “bipartite” nucleotide-binding pocket and therefore, ATP binding promotes oligomerization [6]. Structural studies of the mouse Vps4 (SKD1/Vps4B) revealed nucleotide-dependent conformational change within the ATPase cassette demonstrated by a 20° rotation between lar ge and small ATPase subdomains [7]. Most of AAA+ ATPases, as demonstrated for NSF, p97 and ClpB, function as closed hexameric rings, although other arrangements are known (ClpP forms a seven-fold symmetry). The class I ATPases ClpX, spastin, and katanin contain a single ATPase cassette per subunit and assemble into a single-ring structure. In contrast, class II ATPases NSF, p97, and ClpB contain two ATPase cassettes and assemble into a hexameric ring in which two ATPase domains form two separate rings. Vps4, in contrast to other Class I ATPases, assembles into a double-stacked ring oligomer thereby mimicking assembly of the Class II ATPases. Based on the published data from cryo electron microscopy (cryoEM), size-exclusion chromatography, negative-stain transmission electron microscopy (TEM) and multiangle laser light scattering

A

B

```
yVPS4   78 EANAAKKSPSAGSGSNGGNKKISQEEGEDNGGEDNKKLRGALSSAI 123
hVps4B  80 EKKA-QKPVKEGQPSPADEKGNDSDGEGESDDPEKKKLQNQLQGAI 126
hVps4A  78 EKHG-KKPVKENQ-----SEGKGSDSDSEGDNPEKKKLQEQLMGAV 118
pVps4   78 NNQISSKSRVSNGNVEGSNSPTANEALDS----DAKKLRSALTSAI 120
eVps4   78 -KTQ-KKPVKDGK-------------DDSDEDEDKKKFQDKLSGAI 110
```

C

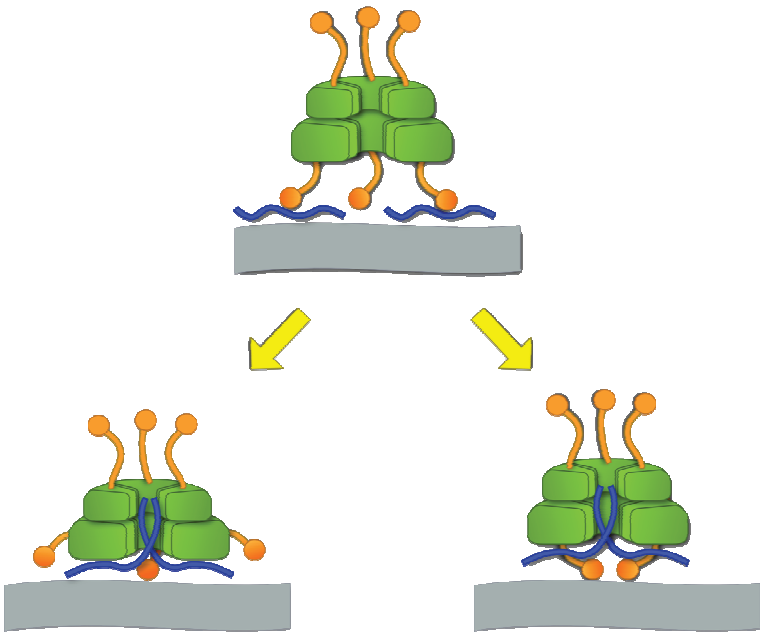

Figure 3-1. Linker region of Vps4. A. Domain structure of the Vps4 ATPase. MIT domain is depicted in orange; linker region and ATPase domain are in grey and green, respectively. B. Alignment of the linker region. Conserved amino acids are highlighted with black. Y – *Saccharomyces cerevisiae*, h – *Homo sapiens*, p – *Schizosaccharomyces pombe*, e – *Caenorhabditis elegans*. C. Possible mechanism of the ESCRT-III (blue rods) disassembly by the Vps4 ATPase. MIT domains are tucked away from the pore region (left); MIT domains process substrate together with the pore (right).

(MALLS), Vps4 was proposed to assemble into a dodecamer consisting of two stacked tail-to-tail hexameric rings [8] [9] or a tetradecamer consisting of two heptameric rings [10].

In vivo, function of the Vps4 ATPase is regulated through its recruitment to the endosome-associated ESCRT-III. Most of the interactions are mediated by the Vps4 MIT domains that bind to the C-terminal MIM regions in ESCRT-III proteins core subunits and the ESCRT-III-associated proteins Did2 and Ist1. In our recent publication [11] we summarized functionally important interactions between Vps4 and ESCRT-III proteins. Our model suggests that the assembly of the Vps4 oligomer on the ESCRT-III-enriched membranes is initiated by the recruitment of the cytosolic complex composed of Vps4-Did2-Ist1. Further on, binding of Vta1 releases Ist1 and drives oligomerization of the Vps4 into a substrate-interacting hexameric ring. A second hexameric ring is assembled on top of the substrate-interacting ring, thus forming a fully functional dodecameric Vps4 ATPase [12].

In vitro correlation between oligomerization and ATPase activity of Vps4 was demonstrated to be dependent on the binding to Ist1 and Vta1. Ist1 negatively regulates ATPase by preventing Vps4 oligomerization [13]. Interaction with Vta1 promotes oligomerization of Vps4 and therefore results in the increase in the ATPase activity [14] [15]. There is evidence that ATPase activity of Vps4 increases as a result of binding to its substrate ESCRT-III proteins, as judged by the binding to Vps2 [14] and CHMP2 [16]. Vps2/CHMP2 bind to Vps4 through MIT domains and therefore are not proposed to contribute in stabilization of the Vps4

oligomer. Alternatively, interactions of MIT domains with a substrate are proposed to promote ATPase activity by disrupting possible autoinhibitory interactions of the MIT domain and/or linker region with the ATPase domain, or by promoting conformational change within the Vps4 N-terminus that results in the increase in the ATPase activity by promoting conformational change within the ATPase domain of Vps4.

Based on the published data of the structure of the MIT and ATPase domains, the linker region was assigned to be 44 amino acids stretching from the end of the MIT and beginning of the ATPase domains (Figure 3-1-A) [17]. Alignment analysis of the linker region revealed that linker length is preserved in different Vps4 species and, strikingly, human Vps4A has a 5 amino acids shorter linker than human Vps4B and *S. cerevisiae* Vps4 homologs. To date, function of the linker region of Vps4 is poorly understood, although there is a limited body of published data that addresses the possible role of the Vps4 linker in the ATPase activity [16] and substrate binding [18] [19].

Insight into linker function comes from the studies of the mutations within the linker region of the p97 AAA ATPase that were identified as the cause of the abnormal function of p97 [18]. p97, structurally similar to Vps4 ATPase, is composed of the N-terminus, linker region and two ATPase cassettes. Mutations in the linker region of p97 resulted in the higher exchange rate of ATP/ADP [18]. The crystal structure of p97 linker mutants revealed that mutations in the linker region led to the change in the conformation of the N-terminus, which resulted in the change of the conformation of the ATPase cassette promoting a higher rate

of nucleotide exchange. Importantly, it was conformational change of the N-terminus that rendered p97 nonfunctional and affected affinity to nucleotide binding since reciprocal mutations resulted in the similar conformational change of N-terminus. These data suggest that linker indirectly affects nucleotide exchange rate of the ATPase cassette by allowing conformational change in the N-terminus of p97.

Recently, Dr. Hanson's group published an article describing the role of the linker as a direct autoinhibitory element in the human hVps4A protein [16]. In addition, binding of the ESCRT-III protein CHMPII/Vps2 to the N-terminus of hVps4A stimulated its ATPase activity. Substrate-mediated increase in the ATPase activity can be explained in two ways. CHMP2 binding to Vps4 MIT promoted conformation change within the MIT domain and/or linker region that resulted in the increase in ATPase activity either indirectly via inducing conformational change within ATPase cassette or directly via disrupting autoinhibitory interaction of MIT/Linker with ATPase domain.

As demonstrated by Dr. Xu's group, ATP binding also promoted rotation of the N-terminal substrate-interacting domain of yeast Vps4 [20]. As the result of the MIT rotation, the linker region became more sensitive to the protease treatment, suggesting that the MIT domain and linker undergo conformational changes in an ATP-dependent manner. On the other hand, binding of ATP to the ATPase domain promoted conformational changes in the linker region and MIT domain, as judged by the enhanced substrate binding (Vps2) to Vps4 [19].

A mechanism of ESCRT-III solubilization by the Vps4 ATPase is currently

not known. Similar to other related AAA+ ATPases ClpX [21] and RecA-like RNA helicase [22] , Vps4 ATPase might apply pulling force on the substrate by threading ESCRT-III polymer through the pore, resulting in its solubilization (Figure 3-1). In agreement with the threading mechanism, the pore region of Vps4 was demonstrated to be important for the function of the Vps4 [23]. It is believed that MIT domains function in the recruitment step only and are being moved away from the pore region upon interaction with the substrate. This mechanism predicts that the linker region that connects MIT and ATPase domains provides flexibility of the movement of MIT domains (Figure 3-1-C). We hypothesized that the length of the linker region is important for the proper positioning/movement of the MIT domains and therefore is important in the function of the Vps4 ATPase.

In an effort to establish a role of the linker in the function of Vps4, we performed functional and biochemical analysis of the series of mutations within the linker region of Vps4. We demonstrated that the length of the linker region is not essential for the function of the Vps4 ATPase. Deletion of the linker region results in the increased ATPase activity of Vps4 and affects size of the intralumenal MVB vesicles.

Materials and methods

Reagents and antibodies. Monoclonal anti-GFP was purchased from Covance (Princeton, NJ). The antisera against Vps4 and Snf7 were previously described [24].

Strains and medium. *Saccharomyces cerevisiae* and *E. coli* strains used

in this work are listed in Table 3-1. To maintain plasmids, strains were grown in corresponding complete synthetic dropout medium. Yeast gene knockouts were constructed as previously described [11].

DNA manipulations. Plasmids used in this study are listed in Table 3-1. Plasmids were constructed using standard cloning techniques. All mutations were confirmed by sequencing. Point mutations and some of the deletions in the linker region of *VPS4* were introduced using mutagenic primers as recommended by (Aglient Technologies, La Jolla, CA). Some deletions were generated by means of amplifying upstream and downstream regions of *VPS4* omitting the desired region of deletion, introducing a BamHI site (translates Glycine and Threonine (+GT) to connect the two regions. Linker mutant alleles of *VPS4* were expressed from the endogenous *VPS4* promoter in a low copy number vector pRS416.

Live-cell fluorescence microscopy was performed on a deconvolution microscope (Delta Vision, Applied Precision, Issaquah, WA) as previously described [11].

Subcellular fractionation experiments were performed as previously described [11]. When localizing Vps4 proteins cells were lysed by osmotic stress in pop buffer and when localizing ESCRT-III subunits cells were lysed by douncing. Both procedures were performed in the presence of protease inhibitors (PMSF 10 µg/ml and complete inhibitor cocktail) (Roche Molecular Biochemicals, Indianapolis, IN). Immunoblotting was performed by running denatured samples on SDS-PAGE and transferring on nitrocellulose membrane [11]. Signal was

Table 3-1. Plasmids, yeast strains and E. coli used in this study.

Strain or Plasmid	Descriptive name	Vector	Reference
Plasmids			
pMB118	*GFP-CPS*	*URA3* (pRS416)	[25]
pMB103	*Vps4(E233Q)*	*URA3* (pRS416)	[26]
pMB28	*VPS4*	*URA3* (pRS416)	[24]
pVps4(V14D)	*Vps4(V14D)*	*URA3* (pRS416)	[11]
pVps4(W206,M207A)	*Vps4(W206A,M207A)*	*URA3* (pRS416)	D. Katzmann
pAS86	*vps4(Δ85-95)*	*URA3* (pRS416)	This study
pAS87	*vps4(Δ85-106+GT)*	*URA3* (pRS416)	This study
pAS88	*Vps4(long)*	*URA3* (pRS416)	This study
pAS90	*vps4(Δ85-112+GT)*	*URA3* (pRS416)	This study
pAS91	*vps4(Δ85-115+GT)*	*URA3* (pRS416)	This study
pAS92	*vps4 (Δ85-120+GT)*	*URA3* (pRS416)	This study
pAS93	*vps4(Δ85-115+GT,E233Q)*	*URA3* (pRS416)	This study
pAS94	*vps4(Δ85-120+GT,E233Q)*	*URA3* (pRS416)	This study
pAS95	*vps4(Δ85-115+GT)-HA-EGFP*	*URA3* (pRS416)	This study
pAS96	*vps4(Δ85-115+GT,E233Q)-HA-EGFP*	*URA3* (pRS416)	This study
pAS97	*vps4(Δ85-120+GT,E233Q)-HA-EGFP*	*URA3* (pRS416)	This study
pAS98	*vps4(Δ85-120+GT)-HA-EGFP*	*URA3* (pRS416)	This study
pAS109	*vps4(Δ85-118+GT)*	*URA3* (pRS416)	This study
pAS111	*vps4(L119A)*	*URA3* (pRS416)	This study

Table 3-1. continued

Strain or Plasmid	Descriptive name	Vector	Reference
Plasmids			
pAS112	*vps4(E205K)*	*URA3* (pRS416)	This study
pAS113	*vps4(K209E)*	*URA3* (pRS416)	This study
pAS114	*vps4(Δ78-118+GT)*	*URA3* (pRS416)	This study
pAS115	*vps4(Δ83-118+GT)*	*URA3* (pRS416)	This study
pAS116	*vps4(Δ79-118+GT*	*URA3* (pRS416)	This study
pAS117	*vps4(Δ81-118+GT)*	*URA3* (pRS416)	This study
pAS118	*vps4(Δ84-118+GT)*	*URA3* (pRS416)	This study
pAS120	*vps4(Δ85-118+GT,E233Q)*	*LEU2 (pRS415)*	This study
pAS121	*vps4(Δ78-118+GT,E233Q)*	*LEU2 (pRS415)*	This study
pAS125	*vps4(Δ79-118)*	*URA3* (pRS416)	This study
pAS126	*vps4(Δ82-118)*	*URA3* (pRS416)	This study
pAS127	*vps4(Δ79-118,E233Q)*	*URA3* (pRS416)	This study
pAS128	*vps4(Δ82-118,E233Q)*	*URA3* (pRS416)	This study
pMB54	*GST-VPS4*	*(pGEX-KG)*	[15]
pAS133	*GST- vps4(Δ78-118+GT)*	*(pGEX-KG)*	This study
pAS136	*GST- vps4(Δ79-118)*	*(pGEX-KG)*	This study
Strains			
MBY3	*Δvps4*	*SEY6210, VPS4:TRP1*	[24]

Table 3-1. continued

Strain or Plasmid	Descriptive name	Vector	Reference
Strains			
EEY26-1	*Δvps4Δdid2*	*MBY3, DID2:HIS3*	[13]
MCY3	*Δvps4Δist1*	*MBY3, IST1:HIS3*	[13]
MCY7	*Δvps4Δvta1*	*MBY3, VTA1:HIS3*	[15]
EEY23	*Δvps4Δvps60*	*MBY3, VPS60:HIS3*	This study
ASY25	*Δvma4Δvps4*	*MBY3, VMA4:HIS3*	This study
Δbar1	*Δbar1*	*SEY 6210.1, BAR1:URA3, FOA*	This study
ASY26	*Δbar1Δvps4*	*Δbar1Δvps4*	This study
Δelm1	*Δelm1*	*BY4741, ELM1:G418*	This study
ASY27	*Δelm1Δvps4*	*Δelm1, VPS4:HIS3*	This study
ASY28	*Δelm1Δsnf7*	*Δelm1, VPS4:SNF7*	This study

visualized using secondary antibodies conjugated to near-infrared fluorescent molecules. Fluorescent signal was visualized and quantified using LiCOR infrared Odyssey scanner (LiCOR-Biotechnology, Lincoln, NB).

For the GFP-CPS maturation assay total cell lysates were prepared by lysis. Three ODV of yeast cells were incubated for 15 minutes in 1 ml of 0.1 N NaOH containing PMSF 10 µg/ml, and cells were pelleted and boiled in 1XSB. Efficiency of GFP-CPS clipping was estimated by measuring intensity of a free GFP (~ 25 kDa) band per lane as a percent of total intensity corresponding to the area covering 45 – 25 kDa.

For the canavanine sensitivity assay, serial dilutions of yeast cells were plated on selection plates lacking arginine and containing 4 µg/ml canavanine. Cell growth was assayed after 3 days of growth at 30 ℃.

For the transmission electron microscopy, ASY24 (*Δvma4Δvps4*) were grown in the selective medium to maintain plasmids – pMB28, pAS91 and pAS88. A total of 50 OD of 0.4 OD_{600} was gathered by spinning in the clinical centrifuge. Cells were fixed in 2 ml of fix buffer (3% Glutaraldehyde, 0.1 M NaCacodilate pH 7.4, 5 mM $CaCl_2$, 5 mM $MgCl_2$, 2.5% sucrose) for 1 hour at 25℃ with gentle agitation. Cells were fashed in 10 0mM cacodylate buffer, pH 7.4 and shipped for EM analysis (Johns Hopkins, Electron microscopy center). After samples were embedded, they were sectioned using a LEICA Ultracut UCT Ultramicrotome. Samples were post-stained with UA and Lead Citrate http://iicxserve.jhu.edu/groups/integratedimagingcenteruserwiki/wiki/75980/Poststaining_Sections.html. iTEM software was used to aid in morphometry analysis

http://www.resaltatech.com/item_overview.htm.

Recombinant Vps4 proteins were expressed as a fusion to GST (Gluthatione S-transferase). GST-Vps4 fusion proteins were expressed in *Escherichia coli* and purified by affinity purification using standard methods on glutathione-Sepharose 4 Fast Flow resin. After thrombin clipping, Vps4 protein was eluted using increasing salt gradient on anion exchanger using high pressure liquid chromatography (HPLC). Stock solutions of ~ 1mg/ml in 20% glycerol were kept in -80℃.

Vps4 ATPase assays were performed as previously described [26]. Set up 100 µl volume reactions containing 1 µM Vps4 (5 µg of protein per 100 µl) and 1 mM ATP (pH 7.0). Mix purified Vps4 protein with 20 µl 5X Reaction Buffer and water to a total of 95 µl; keep on ice. Add 5 µl of 20 mM ATP solution to each reaction, mix and continue incubation at 0˚C for ~3 minutes. Prepare eppendorf tubes containing 10 µl methanol; keep on ice (methanol evaporates fast). Add 10 µl of one of the reactions to a methanol-containing tube (time 0). Start the reactions by moving every one sample each 30 seconds from ice to 30˚C (add water to the heat block or use water bath). Stop reaction every 2 minutes by mixing 10 µl of each reaction with ice-cold methanol. Keep samples on ice; at the end of the assay, centrifuge eppendorf tubes for 10 minutes at 4˚C. Move 15 µl of supernatant to autoinjector-tubes; avoid pellet; check for airbubbles in the autoinjector-tubes. Analyze ATPase activity by running samples on Reverse Phase (RP) High Liquid Chromatography column (HPLC) (C18, 4.6 x 5 cm). Total run time is 5.5 minutes, ADP peaks first at 3.1 minutes, ATP peaks second

at 4.6 minutes. Determine the ratio of ADP/ATP of each sample; subtract the time 0 sample. Calculate Vps4 ATPase activity in ADP/Vps4/min: % ADP X 10 / minutes X uM(Vps4).

For alpha-factor synchronization, *Δbar1 and* ASY27 *Δbar1Δvps4* strains were grown to OD_{600} = 0.4. 1 ml of cells was washed and resuspended in 0.5 ml YPD containing 5 uM (50 µg/ml) α-factor. Cells were synchronized by shaking at 30℃ for 120 minutes. Cell morphology was monitored after 90 minutes of synchronization with 1000X DIC microscope. 90 µl of cell suspension were resuspended in 10 µl of 36% formaldehyde and fixed for 2 hours at 30℃; resuspend in 1 ml PBS (cells can be stored at +4℃). G1 arrested cells have characteristic pear-shaped or “schmoos” morphology. Cells are released from G1 arrest by washing and resuspending in 1 ml of fresh preconditioned medium. Monitor cell morphology by taking a sample of cells every 15 minutes after 60 minutes of recovery period. Resuspend 90 µl of cell suspension in 10 µl of 36% formaldehyde and fix for 2 hours at 30℃; resuspend in 1 ml PBS. To visualize nucleus, stain with DAPI diluted 1:1000 in PBS for 15 minutes, wash with PBS and resuspend cells in 100-50 µl PBS. Score cellular morphology with 1000X microscope under polarized light. Score nuclear morphology with fluorescent light (DAPI filter set).

Results and discussion

Linker region is not essential for cargo sorting into MVBs. All Vps4(linker mutants) were first tested for the complementation of the MVB sorting phenotype

in *Δvps4* strain by following GFP-CPS trafficking by means of the fluorescence microscopy. N-terminal fusion of GFP (green fluorescent protein) to the type II vacuolar peptidase CPS (Carboxypeptidase S) results in GFP-CPS that was published to undergo MVB sorting (Figure 1-3-B) [27]. The functional MVB pathway sorts GFP-CPS inside MVB and delivers GFP-CPS into vacuolar lumen (depicted with "+" sign in Table 3-2, row 1). Defect in the MVB pathway results in less GFP-CPS being delivered to the lumen, with GFP-CPS accumulated in the vacuolar membrane and/or Class E compartment (depicted by "-" sign in Table 3-2, row 2).

In brief, *Δvps4* strain was cotransformed with Vps4(linker mutations) and GFP-CPS. Transformants were grown in appropriate selection media to OD_{600} ~0.6 and visualized under a mercury lamp using FITC channel. We started with the identification of the C-terminal border of the linker region by extending deletion from the C-terminal end of the MIT domain (S85) toward the ATPase domain (I123). We found that Vps4(Δ85-118+GT), but not Vps4(Δ85-120+GT), was functional, suggesting that amino acids beyond A118 are important for the function of Vps4 (Table 3-2, rows 3 - 12). For instance, Leucine 119, conserved throughout Vps4 species, is the most N-terminal amino acid that has a defined structure in the crystal structure of the Vps4 ATPase domain [23]. Indeed, point mutation of Vps4(L119A) resulted in the defect in MVB sorting as judged by the GFP-CPS assay (Table 3-2, row 13). Thus, we defined Alanine 118 to be a C-terminal border of the linker region.

Table 3-2. Fluorescence microscopy of the GFP-CPS sorting in yeast expressing mutant Vps4 proteins.

#	Vps4 protein	Plasmid	Complementation	Dominant-negative
1	Vps4 (wild-type)	pMB28	+	-
2	Vps4(E233Q) Dominant-negative	pMB103	-	+
C-terminal border of the linker region				
3	Vps4(Δ89-95+GT)	pMB419	+	-
4	Vps4(Δ85-95+GT)	pAS86	+	-
5	Vps4(Δ85-106+GT)	pAS87	+	-
6	Vps4(Δ85-112+GT)	pAS90	+	-
7	Vps4(Δ85-115+GT)	pAS91	+	-
8	Vps4(Δ85-115+GT,E233Q)	pAS93		+
9	Vps4(Δ85-118+GT)	pAS109	+	-
10	Vps4(Δ85-118+GT,E233Q)	pAS120	-	-
11	Vps4(Δ85-120+GT)	pAS92	-	-
12	Vps4(Δ85-120+GT,E233Q)	pAS94		+/-
13	Vps4(L119A)	pAS111	+/-	-
N-terminal border of the linker region				
14	Vps4(Δ84-118+GT)	pAS118	+	-
15	Vps4(Δ83-118+GT)	pAS115	+	-

Table 3-2. continued

#	Vps4 protein	Plasmid	Complementation	Dominant-negative
16	Vps4(Δ82-118)	pAS126	+/--	-
17	Vps4(Δ82-118,E233Q)	pAS128		-
18	Vps4(Δ81-118+GT)	pAS117	++/-	-
	Minimal functional linker			
19	Vps4(Δ79-118+GT)	pAS116	+/--	-
20	Vps4(Δ79-118)	pAS125	-	-
21	Vps4(Δ79-118,E233Q)	pAS127	-	+
22	Vps4(Δ78-118+GT)	pAS114	-	-
23	Vps4(Δ78-118+GT,E233Q)	pAS121		+
24	Vps4(long)	pAS88	+	-

"+" - sorting into vacuolar lumen only (normal MVB function)

"-" - no sorting into vacuolar lumen (blocked MVB function)

empty – phenotype was not checked

"+/-" - equal lumen and limiting membrane

"+/--" - more limiting membrane less lumen

"++/-" - more lumen less limiting membrane

We went on to define an N-terminal border of the linker, by extending deletion upstream of the S85. Maximum deletion that produced fully functional Vps4 was Vps4(Δ83-118+GT) and even larger deletion up to Vps4(Δ79-118+GT) produced semifunctional Vps4 (Table 3-2, rows 14 - 21). Vps4(Δ78-118+GT) resulted in nonfunctional Vps4 that can be explained by the fact that E78 structurally belongs to the MIT domain and is therefore important for its function (although we did not generate a point mutation of Vps4E78A, we expect E78A to interfere with function of Vps4). Importantly, two amino acids that were introduced in Vps4(Δ79-118+GT), but not Vps4(Δ79-118), supported the function of the MVB. Therefore, we defined the linker region of Vps4 to consist of 40 amino acids starting at Alanine 79 and ending at Alanine 118 (Table 3-2, row 19).

We further challenged function of the Vps4 protein by inserting 11 amino acids (-GGGSGAGGSGG-) into its linker region, resulting in Vps4(long). Vps4(long) function was not compromised as judged by the GFP-CPS complementation assay (Table 3-2, row 24). The extended linker region of Vps4 did not interfere with the MVB sorting pathway, suggesting that longer linker supports functionality of the Vps4 oligomer.

Vps4 linker mutants were assayed for their ability to interfere with the function of the wild-type Vps4 by the GFP-CPS fluorescent microscopy assay. Vps4(linker mutations) did not interfere with the function of wild-type Vps4 (Table 3-2, dominant-negative column). Linker mutations were introduced into the dominant-negative Vps4 hydrolysis mutant (Vps4(E233Q), and the point mutation E233Q in the ATPase domain Walker A motif that abolishes ATP hydrolyses

rendering Vps4 nonfunctional. We determined that all Vps4 linker mutants combined with the E233Q were dominant-negative, except for the Vps4(Δ85-118+GT,E233Q) and Vps4(Δ82-118,E233Q) (Table 3-2, rows 10 and 17). We think that Vps4(Δ85-118+GT,E233Q) and Vps4(Δ82-118,E233Q) are not dominant-negative because they either do not incorporate into the wild-type Vps4 oligomer or do not interfere with the Vps4 oligomer function upon incorporation. Interaction of Vps4(Δ82-118,E233Q)/Vps4(Δ85-118+GT,E233Q) with Vps4(E233Q) can be further verified by the GST-pulldown of purified Vps4 proteins. Incorporation of Vps4(Δ82-118,E233Q)/Vps4(Δ85-118+GT,E233Q) into wild-type Vps4 oligomer can be demonstrated by measuring ATPase activity of a mixed population as ATPase activity was demonstrated to increase after addition of Vps4(E233Q) to wild-type Vps4 [28].

To ensure that defect in the complementation of the *Δvps4* MVB sorting defect is not due to low protein levels, protein expression of each Vps4(linker deletion) was verified by western blotting. All Vps4(linker mutations) were expressed properly, as demonstrated by the immunoblotting of total yeast lysate containing some of the Vps4(linker mutants) (Figure 3-2) and cyclohexamide chase experiments (Figure 3-2) (notice difference in size that correlates with the size of deletion).

We supplemented data obtained from the fluorescence microscopy of the GFP-CPS by a quantitative GFP-CPS maturation assay. CPS is synthesized as a type II integral glycosylated vacuolar hydrolase with a large luminal C-terminal catalytic domain and short cytosolic N-terminus. CPS is being sorted inside

Figure 3-2. Vps4(linker mutations) have defect in solubilization of ESCRT-III (Snf7). A. Total cell lysates from cells expressing Vps4(linker deletions) were immunoblotted with anti-Vps4 antibody (notice size difference that corresponds to the length of the deletion region). B. Vps4(linker deletions) produce stable proteins. Yeast cells expressing Vps4(linker deletions) were treated with cyclohexamide and chased for 60 minutes. Total cell lysates were prepared after 0 and 60 minutes of chase. Vps4(linker deletions) were visualized with anti-Vps4 antibody (V14D is published [11] to render Vps4(V14D) protein not stable). C. GFP-CPS is processed normally in functional Vps4(linker mutations). Yeast cells expressing GFP-CPS and Vps4(linker mutations) were lysed and immunoblotted with anti-GFP (green) and anti-Snf7 (red) antibodies. Functional MVBs result in accumulation of a fully cleaved free GFP (**), dysfunction of MVB results in accumulation of not fully cleaved intermediates of GFP-CPS (*). Fully cleaved GFP-CPS is quantified as a percent of free GFP (**) from the total of all GFP-CPS clipped forms ((**)/((**) + (*) + (*)). C. Redistribution of Snf7 to membrane fraction in cells expressing Vps4(linker deletions). Cells expressing Vps4(linker deletions) were subjected to subcellular fractionation; resulting soluble (S) and membrane (P) fractions were immunoblotted with anti-Vps4 and anti-Snf7. Accumulation of free GFP (~25 kDa) that is known to be resistant to proteolysis and therefore can be detected by immunoblotting with anti-GFP antibody.

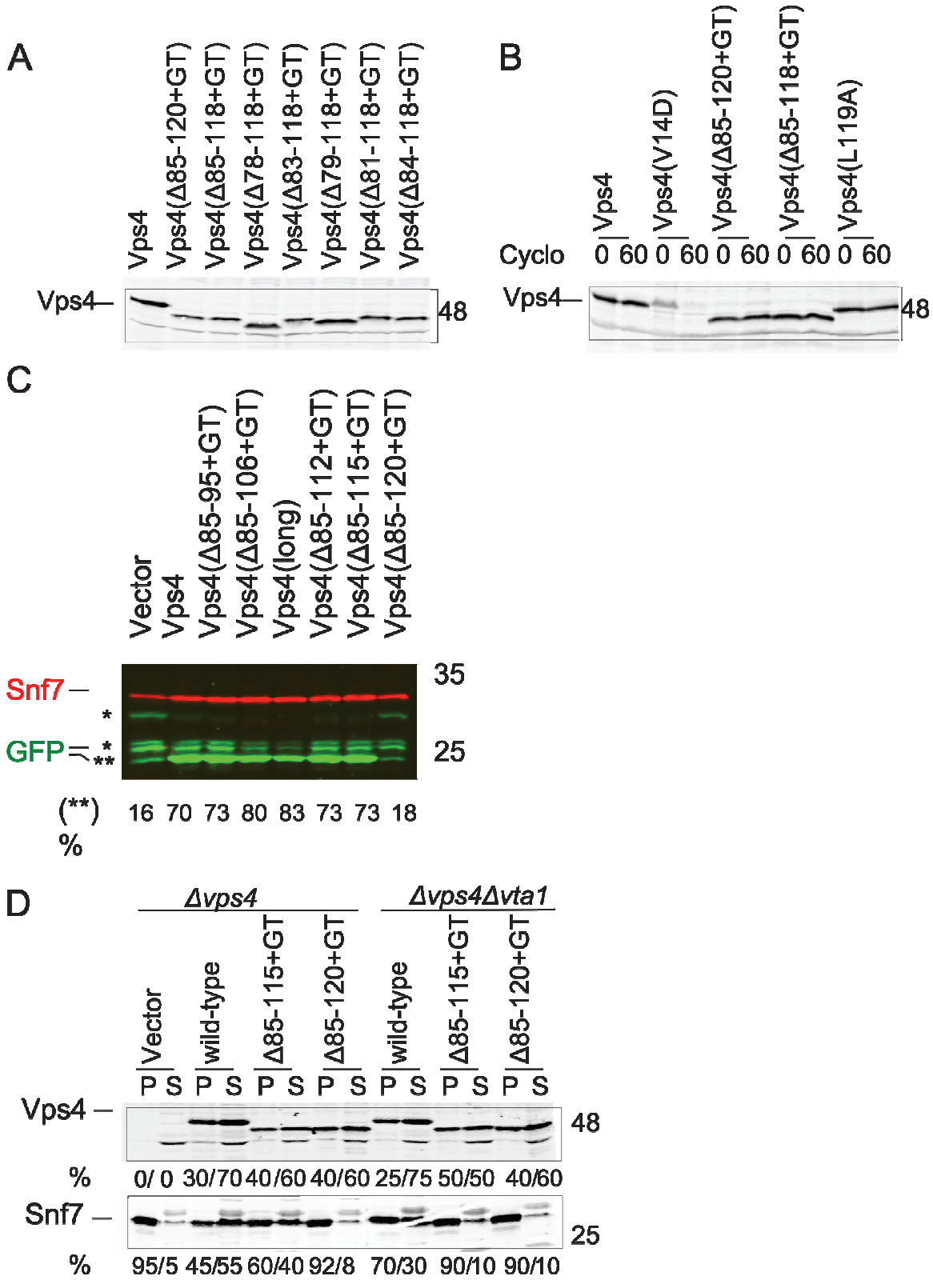
A
Vps4
Vps4(Δ85-120+GT)
Vps4(Δ85-118+GT)
Vps4(Δ78-118+GT)
Vps4(Δ83-118+GT)
Vps4(Δ79-118+GT)
Vps4(Δ81-118+GT)
Vps4(Δ84-118+GT)
Vps4—
48
B
Vps4
Vps4(V14D)
Vps4(Δ85-120+GT)
Vps4(Δ85-118+GT)
Vps4(L119A)
Cyclo
0 60 0 60 0 60 0 60 0 60
Vps4—
48
C
Vector
Vps4
Vps4(Δ85-95+GT)
Vps4(Δ85-106+GT)
Vps4(long)
Vps4(Δ85-112+GT)
Vps4(Δ85-115+GT)
Vps4(Δ85-120+GT)
Snf7 —
35
*
GFP =
*
**
25
(**) %
16 70 73 80 83 73 73 18
D
Δvps4
Δvps4Δvta1
Vector
wild-type
Δ85-115+GT
Δ85-120+GT
wild-type
Δ85-115+GT
Δ85-120+GT
P S P S P S P S P S P S P S
Vps4 —
48
%
0/ 0 30/70 40/60 40/60 25/75 50/50 40/60
Snf7 —
25
%
95/5 45/55 60/40 92/8 70/30 90/10 90/10

MVBs and upon delivery to the vacuolar lumen, its C-terminus is cleaved by Proteinase A at the transmembrane domain, producing mature CPS. Defect in the vacuolar delivery results in less efficient proteolytic maturation of CPS. Therefore, efficient vacuolar targeting of the N-terminally fused GFP-CPS results in accumulation of larger molecular-weight GFP-positive bands, which correspond to the inefficient clipping of CPS, indicating defect in vacuolar targeting/or vacuolar processing. Figure 3-2 shows the GFP-CPS clipping profile of cells expressing some of the Vps4 linker mutants together with GFP-CPS. Accumulation of the lower ~25 kDa GFP-positive band corresponds to the free GFP, suggesting that MVB sorting is functioning properly and GFP-CPS is being delivered into the vacuolar lumen (Figure 3-2 Vps4 lane, green band, depicted with double **). Accumulation of a larger-size GFP-positive bands suggests defect in the MVB sorting (vector and Vps4(Δ85-120+GT) depicted with single *). Accumulation of the free GFP GFP-CPS maturation assay confirmed that functional Vps4(linker mutations) supported MVB function.

Function of the Vps4 ATPase is regulated through its recruitment by ESCRT-III-associated proteins. Did2 is central in regulating Vps4 recruitment since Did2 binds directly to Vps4, ESCRT-III, Ist1 and Vta1. Deletion of Did2 abolishes membrane recruitment of Ist1 and partially blocks membrane localization of Vta1 and Vps60, which is mediated in part by the Vps4-Vta1-Vps60 interactions. Single deletions of *Δdid2, Δvta1 or Δvps60* produce intermediate GFP-CPS sorting phenotype or no phenotype (*Δist1*) (Table 3-3, row 1). Combination of *Δist1* (*Δist1Δvta1 or Δist1Δvps60)* or *Δdid2* (*Δdid2Δvps60*

Table 3-3. Fluorescence microscopy of the GFP-CPS sorting in yeast lacking Vps4-regulatory genes expressing different Vps4(linker mutations).

#	Vps4 protein	Yeast strains				
		Δvps4	*Δvps4 Δist1*	*Δvps4 Δdid2*	*Δvps4 Δvta1*	*Δvps4 Δvps60*
1	Vps4	+	+	+/-	+/-	+/-
2	Non-functional Vps4(linker deletion) Vps4(Δ85-120+GT)	-	-	-	-	-
	Functional Vps4(linker mutations)					
3	Vps4(Δ85-95+GT)	+		+/-	+/-	+/--
4	Vps4(Δ85-106+GT)	+	+	+/-	+/-	+/--
5	Vps4(long)	+		+/-	+/-	+/-
6	Vps4(Δ85-112+GT)	+	+/--	+/--	+/-	+/-
7	Vps4(Δ85-115+GT)					

"+" - sorting into vacuolar lumen only (normal MVB function)

"-" - no sorting into vacuolar lumen (blocked MVB function)

"+/-" - equal lumen and limiting membrane

"+/--" - more limiting membrane less lumen

empty – phenotype was not checked

or *Δdid2Δvta1)* shows extremely severe GFP-CPS phenotype, pointing at genetic interactions between those proteins [29]. Therefore, dysfunction of Vps4 might be the result of defect in interaction with its recruiting proteins Ist1, Did2, Vta1 and Vps60.

We used GFP-CPS fluorescence microscopy to assay if MVB sorting defect conferred by the deletion of the Vps4- regulatory genes is aggravated by the expression of the Vps4(linker mutations). Vps4(Δ85-115+GT) showed a synthetic phenotype with *Δist1* and *Δdid2*, indicating potential defective interaction with Vta1 and/or Vps60 (Table 3-3, row 6).

Shorter linker deletions Vps4(Δ85-95+GT) and Vps4(Δ85-106+GT) showed more severe MVB sorting defect in the absence of Vps60, suggesting possible defective interaction with Ist1 and/or Did2 (Table 3-3, rows 2 and 3). Noticeably, localization of chimeric protein Vps4(linker mutations)-GFP was similar to Vps4-GFP, suggesting that the recruitment step is not disrupted (data not shown). We extended the phenotypic analysis of the synthetic interactions using canavanine-sensitivity assay. This type of an assay was introduced by Dr. Emr's group as an indirect way to test the function of the MVB pathway [30]. The canavanine- sensitivity assay tests amount of the arginine transporter Can1 that accumulates on the plasma membrane. Level of the Can1 expression on the plasma membrane is regulated through its endocytosis, sorting into the MVB pathway and subsequent delivery to the vacuole for proteolysis. In cells with a defective MVB pathway, Can1 accumulates on the plasma membrane and therefore, the toxic arginine analog canavanine is transported in larger amount

into cells.

In brief, *Δvps4* cells containing an additional deletion of one of the Vps4 regulators were transformed with plasmids expressing the *vps4* linker mutants and grown to OD_{600} ~0.6. Serial dilutions were plated on appropriate minimal medium plates (to select for plasmid; devoid of arginine) containing 4 μg/ml canavanine. Cell growth was scored after 2 days of growth at 30℃ (Figure 3-3). Functional Vps4(linker deletion) mutants did not aggravate the growth phenotype of mutant *ΔistΔvps4* and *Δvta1Δvps4* cells. Most prominent defect in the cell growth was observed in *Δvps4Δdid2* and to a lesser extent *Δvps4Δvps60* mutant cells expressing Vps4(Δ85-112+GT) and Vps4(Δ85-115+GT). Did2 mediates recruitment of Vps4 through interaction with Ist1 and Vta1. Therefore, it appears possible to speculate that Vps4(Δ85-112+GT) and Vps4(Δ85-115+GT) cannot efficiently maintain Vta1 interaction in the absence of Did2.

Defects in the MVB sorting conferred by the mutations in the Vps4 linker region were further demonstrated by the analysis of the subcellular distribution of the Vps4 mutant proteins and the ESCRT-III subunit Snf7. Yeast cells expressing the Vps4 linker mutants were grown to OD_{600} ~0.6 and a total of 5 ODV cells were lysed and subjected to the subcellular fractionation by the differential centrifugation. The pellet fraction (P13) is enriched with vacuoles, endosomes and parts of the ER. The soluble fraction (S13) contains soluble proteins, vesicles and Golgi. The P13 and S13 fractions were separated on SDS-PAGE and analyzed by immunoblotting with anti-Vps4 and anti-Snf7 antibodies (Figure 3-2-D). ATP hydrolysis by the Vps4 ATPase results in solubilization of the

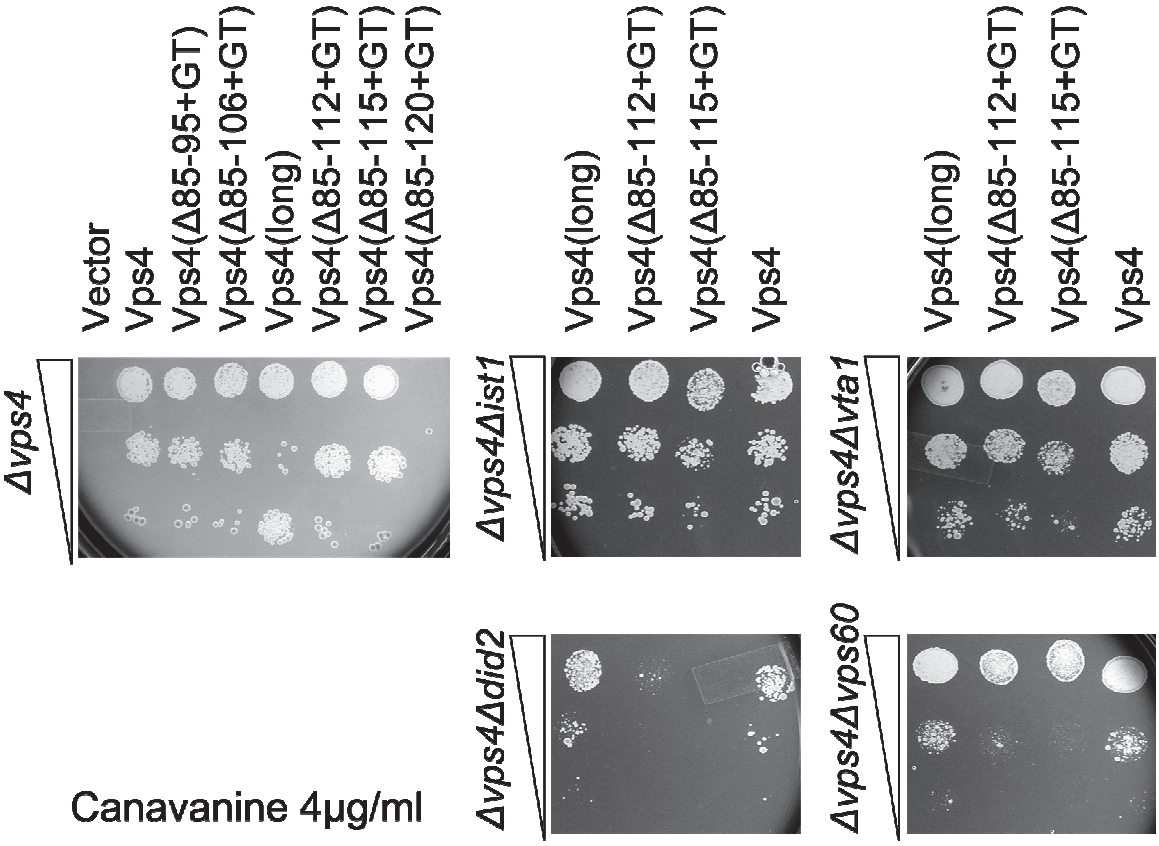

Figure 3-3. Functional Vps4(linker deletions) are more sensitive to the canavanine in the background of *Δdid2* or *Δvps60*. Serial dilutions of different yeast mutants (as indicated) expressing wild-type Vps4 and Vps4(linker mutations) were spotted on selective plates containing 4 μg/ml canavanine; plates were photographed after 2 days of growth at 30℃. *Δvps4* or *Δvps4* expressing nonfunctional Vps4(Δ85-120+GT) show no growth at 4 μg/ml canavanine (*Δvps4* panel). Deletion of *DID2* and *VPS60* confers higher canavanine sensitivity in cells expressing Vps4(Δ85-112+GT) and Vps4(Δ85-115+GT).

ESCRT-III complex and cycling of the Vps4 ATPase itself ON/OFF endosomal membrane. Therefore, normal function of the Vps4 ATPase results in predominant cytosolic (S13 fraction) distribution of ESCRT-III subunits and Vps4 itself [31]. On the other hand, the Vps4(E233Q) hydrolysis mutant is incapable of the solubilization of ESCRT-III, resulting in predominate membrane distribution (P13) of ESCRT-III and Vps4 [26]. Vps4 linker-deletion proteins are redistributed more to P13 compared to wild-type Vps4, suggesting a recycling defect of the Vps4 mutant proteins. Defect in the recycling of Vps4(Δ85-115+GT) and Vps4(Δ85-120+GT) correlates with redistribution of ESCRT-III subunit Snf7 to P13, indicating a defect in the disassembly of ESCRT-III by Vps4(Δ85-115+GT) and Vps4(Δ85-120+GT).

Vps4 mutants lacking linker region show higher ATPase activity. The linker region of hVps4A was proposed to act as an autoinhibitory element within Vps4 ATPase, as demonstrated by the direct correlation between deletion of the linker region and increase in the ATPase activity [16]. Therefore, we addressed the possibility that deletion of the linker region promotes ATPase activity of Vps4 by measuring ATPase activity of the wild-type and Vps4(linker deletions). We started ATPase analysis with two nonfunctional Vps4 (linker deletions) - Vps4(Δ78-118+GT) and Vps4(Δ79-118).

Recombinant *GST* (Gluthathione-S Transferase) – *VPS4* fusions were constructed using the pGEX-KG(Kan) vector. On average, 1000 ODs of cells yielded ~15-25 mg of recombinant fusion protein. The GST-tag was cleaved off with thrombin and Vps4 was purified using anion-exchange HPLC. For the

ATPase activity tests, we used a Vps4 concentration of 2 μM (10 μg per 100 μl) and 1mM ATP. The conversion of ATP to ADP was quantified using HPLC reversed-phase chromatography. Results of the ATPase activity test of Vps4 proteins are shown in Figure 3-4. Vps4 wild-type (Figure 3-4) hydrolyzed ATP at the rate of ~15 ADP/Vps4/minute, which is lower than previously published ATPase activity of Vps4 [26] and [24]. ATPase activity of wild-type Vps4 was published to be ~25 ADP/Vps4/minute at 1.5 μM Vps4. We attributed lower ATPase activity of wild-type Vps4 to suboptimal salt conditions in the reaction, a result of using a diluted protein stock solution. Vps4(Δ79-118) showed an increased ATPase activity (Figure 3-4) of 40 ADP/Vps4/minute. The decrease of Vps4(Δ79-118) ATP hydrolysis rate at later time points is likely a result of product inhibition. Vps4(Δ78-118) also showed residual ATPase activity of ~10 ADP/Vps4/minute, suggesting that, although Vps4(Δ78-118) is not functional, it oligomerizes and is capable of ATP hydrolyses (Figure 3-4).

Linker region regulates size of the MVB vesicles. Under normal conditions, MVBs form as spherical 100-200 nm in diameter membrane compartments that contain multiple vesicles with average size of 25-35 [32]. Disruption of the ESCRT machinery or Vps4 function abolishes MVB formation and results in the accumulation of an abnormal late-endosomal membrane compartment (class E compartment) that is characterized by the elongated stacks of endosomaly-derived cisternae devoid of intralumenal vesicles. Mutations in the proteins that regulate ATPase activity of Vps4 affect rate of the vesiculation and size of the intralumenal MVB vesicles, albeit preserving the MVB sorting pathway [13]. Using

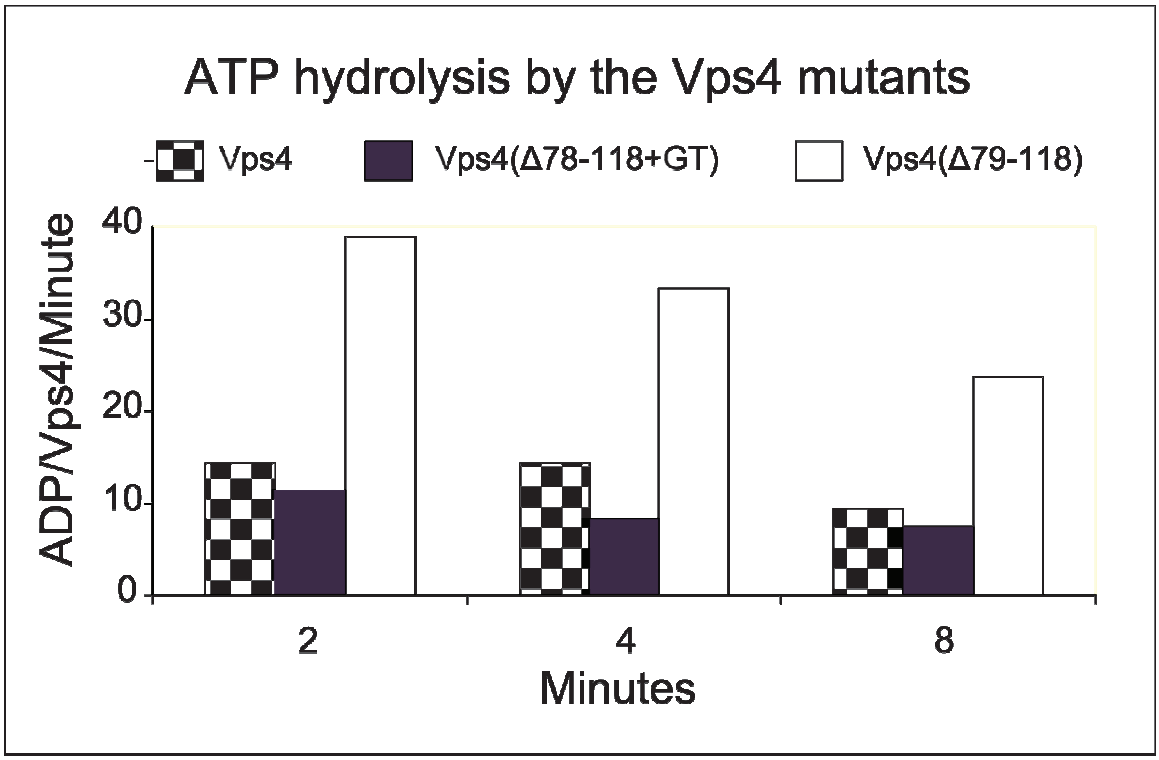

Figure 3-4. Vps4(Δ79-118) has higher ATPase activity than wild-type Vps4. ATPase activity of Vps4 proteins (2 μM) was assayed using reverse-phase HPLC. Reactions were stopped after 2, 4 and 8 minutes. ATPase activity was calculated as ADP per Vps4 per minute (ADP/Vps4/minute).

electron tomography, Greg Odorizzi's group published that the deletion of Vps4 regulators in yeast resulted in the formation of MVBs containing larger intralumenal vesicles, thus linking activity of Vps4 to MVB vesicle biogenesis. For example, deletion of *IST1*, a gene encoding the only negative regulator of the Vps4 ATPase activity, increased efficiency of vesiculation resulting in MVBs that are more densely-packed with intralumenal vesicles. Deletion of *VTA1*, a gene encoding a major positive regulator of the Vps4 ATPase activity, resulted in

MVBs that had less efficient vesiculation than wild-type MVB [32] [33].

We demonstrated before that removing 33 amino acids from the Vps4 linker (Vps4 Vps4(Δ85-118+GT)) or adding 11 amino acids to the linker (Vps4(long)) did not interfere with the MVB sorting pathway. Therefore we set up to test if changes in the linker size Vps4(Δ85-115+GT) and Vps4(long) change the size of the MVB vesicles using transmission electron microscopy (TEM). Vps4 linker mutants were expressed in *Δvma4* mutant background. *Δvma4* mutant strain lacks a functional vacuolar H+-ATPase (V-ATPase) which increases vacuolar pH and consequently renders vacuolar hydrolases less active [34]. As a result, MVB-derived vesicles accumulate in the vacuole of *Δvma4* mutant strains. Furthermore, a decrease in the phosphate transport into vacuolar lumen in *Δvma4* mutant results in less dense vacuoles under an electron microscope. Therefore, MVB vesicles can easily be detected in the vacuolar lumen of *Δvma4* mutants [30].

Samples of mutant yeast strain *Δvma4Δvps4* expressing wild-type Vps4, and two different linker mutations, Vps4(Δ85-115+GT) and Vps4(long), were fixed and shipped for the electron microscopy analysis to Dr. McCaffrey's group at John Hopkins University, Baltimore, MR (fixation procedure see Materials and Methods). Representative pictures of *Δvma4* cells expressing wild-type Vps4 are shown in Figure 3-5-A. Vacuoles have two types of vesicle population –smaller ~35 nm (arrows) vesicles that are derived from the MVB lumen and larger ~100 nm vesicles (arrowhead) that form as a result of microautophagy of the vacuolar membrane. MVB-derived vesicles are distributed homogeneously throughout the

Figure 3-5. Mutant Vps4(Δ85-115+GT) induces formation of larger intralumenal MVB vesicles. A. Representative pictures of the transmission electron microscopy of Δvma4Δvps4 yeast cells expressing Vps4, Vps4(Δ85-115+GT) and Vps4(long). a – yeast cell (V-vacuole, N – nucleus); b, c and d – magnified area of the vacuolar lumen/membrane of Vps4, Vps4(Δ85-115+GT) and Vps4(long), respectively (arrows - intralumenal MVB vesicles, arrowheads – microautophagy vesicles). Scale bar as indicated (notice different scale bar). B. Statistical analysis of the average size of the intralumenal MVB vesicles depicted in A. Vesicular morphometry of 11 cells per condition was performed at the electron microscopy facility using iTEM software http://www.resaltatech.com/item_overview.htm (John Hopkins, Integrated Imaging Center).

A

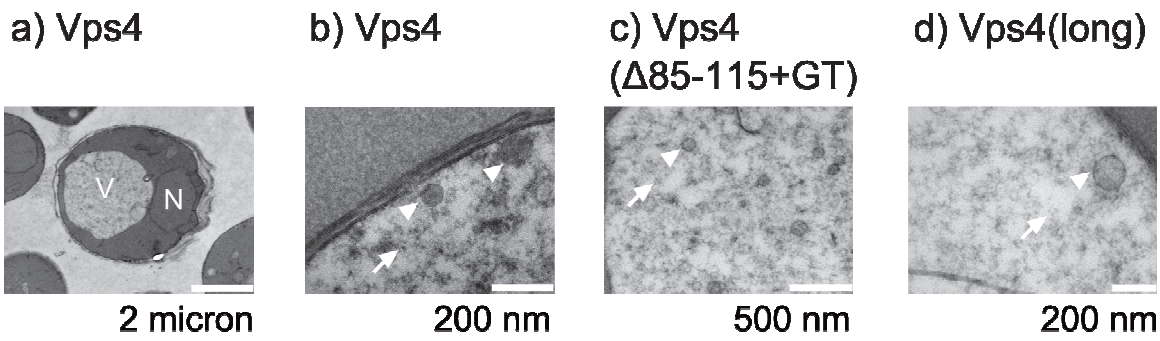
a) Vps4
b) Vps4
c) Vps4
(Δ85-115+GT)
d) Vps4(long)
V
N
2 micron
200 nm
500 nm
200 nm

B

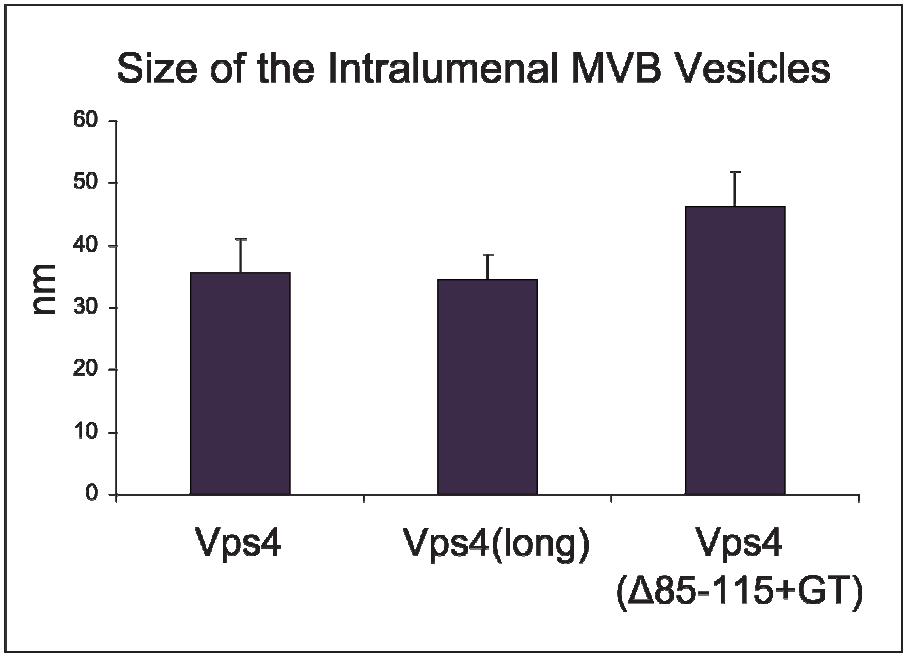
Size of the Intralumenal MVB Vesicles
nm
60
50
40
30
20
10
0
Vps4
Vps4(long)
Vps4
(Δ85-115+GT)

vacuolar lumen, whereas larger vesicles are distributed more to the periphery closer to the vacuolar membrane. Vesicular morphometry of 11 cells per condition was performed at the electron microscopy facility using iTEM software (http://www.resaltatech.com/item_overview.htm). Vesicular morphometry showed that the average vesicle size in cells expressing wild-type Vps4 and Vps4(long) was ~35 nm and in cells expressing Vps4(Δ85-118+GT) was ~46 nm (Figure 3-5-B). TEM of cells expressing Vps4(Δ85-115+GT) revealed a larger size of intralumenal MVB vesicles, defect in the MVB biogenesis that was not detected by the GFP-CPS fluorescence microscopy (Table 3-2, row 11).

The pore region 1 is important for the function of Vps4. There is an evidence to suggest that some of the AAA+ ATPases act by translocating their substrate through the central pore [35]. For instance, bacterial Rho transcription termination factor, an AAA+ RecA-family hexameric helicase, was recently demonstrated to pull RNA through the pore as the consequence of a coordinated ATP hydrolyses mechanism [22]. ClpX, a hexameric bacterial AAA^+ ATPase, was demonstrated to exert mechanical force on a protein substrate, thereby unfolding and translocating proteins into the ClpX-associated peptidase ClpP [21]. Crosslinking studies in ClpB(Hsp104), an AAA+ ATPase that solubilizes protein aggregates together with DnaK(Hsp70), revealed direct interactions between conserved hydrophopic residues of the pore with the protein substrate [36].

Finally, consistent with pore-threading mechanism, residues within the pore region have been shown to be functionally important in other AAA+ ATPases [37] [36] [38].

Vps4 uses ATP hydrolyses to solubilize ESCRT-III proteins [39]. It is conceivable that Vps4 utilizes a translocation mechanism through its central pore to perform this function. Crystal structure of yeast Vps4 ATPase domain demonstrated that the pore region contains two loop regions – pore loop 1 (206WMG208) and pore loop 2 "arginine-collar" (241RGEGESEASRR251) [23]. Mutation of corresponding hydrophobic residues in a pore loop motif 1 of hVps4A and hVps4B were shown to be functionally important for HIV-1 budding, supporting the role of the pore region in the function of hVps4 proteins [40].

We tested if the pore loop 1 region is important for the function of Vps4 in the yeast MVB sorting pathway. Vps4(W206A,M207A) abolished the MVB sorting pathway in yeast, as judged by the GFP-CPS sorting, indicating the functional significance of the pore loop 1 region (Table 3-4). We noticed that the pore loop 1 was surrounded by the two charged conserved residues Lys205 and Glu209. We reasoned that ionic interactions might be involved in the function of the pore region with its substrate and therefore introduction of the opposite charge might disrupt function of Vps4, presumably by disrupting interaction with the substrate. We introduced K205E and E209K mutations in Vps4. We found that Vps4(K205E) was not functional and resulted in a block of MVB formation, whereas Vps4(E209K) resulted in a partial defect in the MVB sorting (Table 3-4). The observed defect in the function of Vps4(W206A,M207A), Vps4(K205E) and Vps4(E209K) was not due to an inadequate expression of a protein, since immunoblotting with anti-Vps4 antibody showed protein level comparable to the wild-type Vps4 (data not shown). Mutations in the pore loop 1 might disrupt

Table 3-4. Fluorescence microscopy of the GFP-CPS sorting in yeast expressing Vps4(pore mutants).

Vps4(pore mutants)	Complementation	Dominant-negative
Vps4(W206A,M207A)	-	-
Vps4(E205K)	-	-
Vps4(K209E)	+/-	+

"+" - sorting into vacuolar lumen only (normal MVB function)

"-" - no sorting into vacuolar lumen (blocked MVB function)

substrate binding and therefore render Vps4 nonfunctional. Alternatively, pore mutants might cause defects in Vps4 oligomerization, ATPase hydrolysis or interaction with regulatory proteins. However, Vps4(W206A,M207A) was shown to oligomerize properly, indicating that defect in the Vps4 function is not due to its perturbed assembly [41].

Role of the Vps4 in the cytokinesis of budding yeast

There were two reasons that prompted us to test the importance of the Vps4 and its linker region in the cytokinesis of budding yeast. Since we demonstrated the Vps4 linker region to be dispensable for the MVB sorting pathway, we reasoned that the linker might be important for cytokinesis, another ESCRT-dependent process [42]. Although ESCRTs have not been reported to be involved in cytokinesis in budding yeast, the ESCRT-III protein complex and Vps4 have been shown to be essential for cytokinesis in certain archaea [43] and

mammalian cells [42]. Furthermore, it was recently published that Vps27 (ESCRT-0), Vps25 (ESCRT-II protein) and Vps4 have synthetic lethal genetic interactions with Elm1 kinase that modifies septin proteins, which are an essential part of the cytokinetic machinery of budding yeast [44].

Cytokinesis leads to the separation of mother and daughter cells through abscission. In eukaryotes, abscission involves coordinated sequence of dynamic events including contraction of an actomyosin ring, targeted membrane remodeling at the division site and plasma membrane fission, reviewed in [45 46 47] although mechanistic details of the abscission remain obscure [48]. Plasma membrane abscission is topologically similar to the formation of MVBs and HIV-1 budding – two processes that are promoted by the ESCRT-machinery. ESCRT machinery regulates the abscission step during cytokinesis in animal cells reviewed in [42]. For instance, ALIX and Tsg101 [49] localize to the midbody during cytokinesis. Depletion of either ESCRT-III subunit or hVps4A/B inhibited cytokinesis in mammalian cells [50]. ESCRT-III was demonstrated to induce membrane fission *in vitro* [51], and polymerize into filamentous structures *in vivo* [52]. Finally, components of the ESCRT-III complex were proposed to promoting fission of the plasma membrane by forming subcortical filaments at the abscission site in mammalian cells [48].

There are significant differences in the cell division machinery that regulate cytokinesis in budding yeast and animal cells, reviewed in [1]. In budding yeast, components of the contractile ring are assembled in sequential manner with septins proteins arriving first, followed by actomyosin ring components and

components of the membrane remodeling machinery, including targeting of the transmembrane chitin-producing complex to the site of cell division [53]. Ingression of the yeast plasma membrane is driven by the septum, which forms as a result of the localized synthesis of chitin [54]. In addition, septum formation is directed by the contraction of the actomyosin ring [54]. Septins directly regulate septum formation and actomyosin ring assembly, explaining their essential role in budding yeast. Temperature-sensitive mutations in septins result in the formation of elongated buds that did not complete cytokinesis and therefore remained attached to the mother cells [55]. Abnormal elongated cellular morphology that arises in response to minor defects in the regulation of septin assembly directly trigger morphogenic checkpoint that delays the switch from polar bud growth [56]. Septins function as highly structured filamentous arrays, the assembly of which is regulated by a set of protein kinases, including Elm 1 [57].

Elm1 kinase was demonstrated to act through phosphorylation of other mitotic kinases, including Cla4 and Gin4 that help mediate proper localization of septins to the division site, as Elm1 localizes to the division site together with septins and deletion of *ELM1* results in mislocalization of the septins [55]. Indeed, *Δelm1* shows temperature-sensitive growth, elongated cellular phenotype and delay in cytokinesis, a phenotype similar to the temperature-sensitive mutations in septin genes [57]. Taking into account that Elm1 was recovered as a negative genetic interactor with ESCRT-machinery (Vps4 and Vps25) we used *Δelm1* as a cytokinesis-compromised background to uncover aggravation of the cytokinesis defect upon deletion of ESCRT-III gene *SNF7* and *VPS4.*

Elongated cellular phenotype is not aggravated in Δelm1Δvps4 and Δelm1Δsnf7 mutants. To test if *VPS4* and *SNF7* (ESCRT-III) contribute together with *ELM1* during cell division, we compared the morphology of *Δelm1* with *Δelm1Δvps4* and *Δelm1Δsnf7*. Wild-type cells, *Δelm1* and double mutant *Δelm1Δvps4* and *Δelm1Δsnf7* cells were grown at room temperature (21℃) in rich media conditions to OD_{600} ~0.6. Representative images of cells were taken using polarized light microscopy. Wild-type cells showed as round budded cells separated by the well-developed septum (Figure 3-6, panel A). *Δelm1* mutant showed more clustered growth with larger more elongated cells that contained multiple nuclei (on average 2-3 nuclei) that are not separated with a well-formed septum (Figure 3-6, panel B). *Δelm1Δvps4* and *Δelm1Δsnf7* mutant cells did not show a more sever elongated phenotype than ∆*elm1* (Figure 3-6, panel C and D). However, we noticed that *Δelm1Δvps4* and not *Δelm1Δsnf7* mutants had more pronounced plasma membrane appearance than observed in ∆*elm1*, which could be a consequence of higher chitin deposition in these double mutant strains. Indeed, a recent study demonstrated that chitin-synthases accumulate in *Δelm1Δvps4* mutant yeast cell [58]. Together, the morphology analysis suggested that Vps4 and ESCRT-III are not functioning with Elm1 during cytokinesis.

Functional Vps4 protein rescues temperature-sensitive growth defect of Δelm1Δvps4. Single deletion of *ELM1* was previously reported to result in a slower cell growth at 37℃ and normal growth at 30° C [59]. Therefore, to test for a synthetic growth defect of the double *Δelm1Δvps4* mutant, yeast cells were grown at permissive temperature (30℃). In brief, *Δvps4Δelm1* expressing either

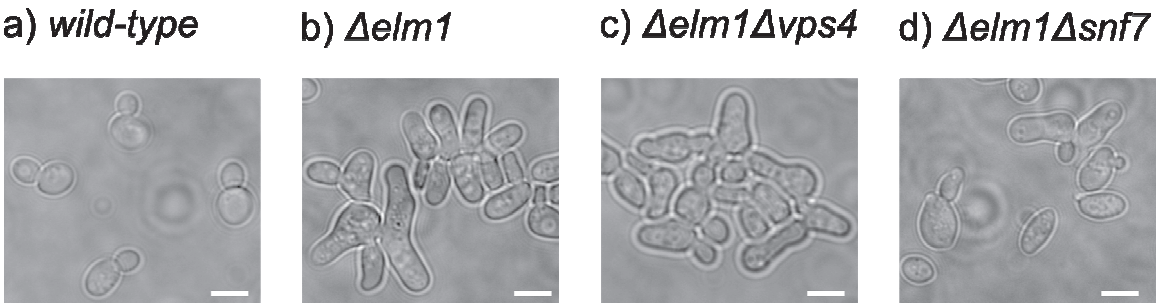

Figure 3-6. Abnormal elongated cellular morphology of *Δelm1* is not exacerbated in *Δelm1Δvps4* grown at permissive room temperature (~21℃). Yeas t cells were grown in rich YPD media at 21℃ to OD600 ~0.6. DIC images of yeast cells were taken using 60X objective. Bar = 10 μn.

wild-type Vps4, or functional linker mutations Vps4(Δ85-118+GT) and Vps4(long), or nonfunctional hydrolysis mutant Vps4(E233Q) and nonfunctional linker deletion Vps4(Δ85-120+GT) were grown at 30℃ for 30 hours. Final c ell densities (OD_{600} values) for each mutant were plotted on vertical axes and are depicted in (Figure 3-7). Indeed, cells depleted of both *VPS4* and *ELM1* genes had more severe growth defect than cells depleted of *ELM1* or *VPS4* (demonstrated by the Vps4(E233Q)). This result was in agreement with a recent publication from Dr. Thorner's group on interactions between ESCRTs and septin-modifying kinases in the cytokinesis of budding yeast [58]. Functional Vps4 linker mutants Vps4(long) and Vps4(Δ85-118) rescued cell growth of *Δvps4Δelm1* to the same extent as did wild-type Vps4. This result suggests that functional Vps4 rescues temperature-sensitive growth defect in *Δvps4Δelm1* independent of the Vps4 linker region.

Δvps4 mutant progresses slower through mitosis. We determined the

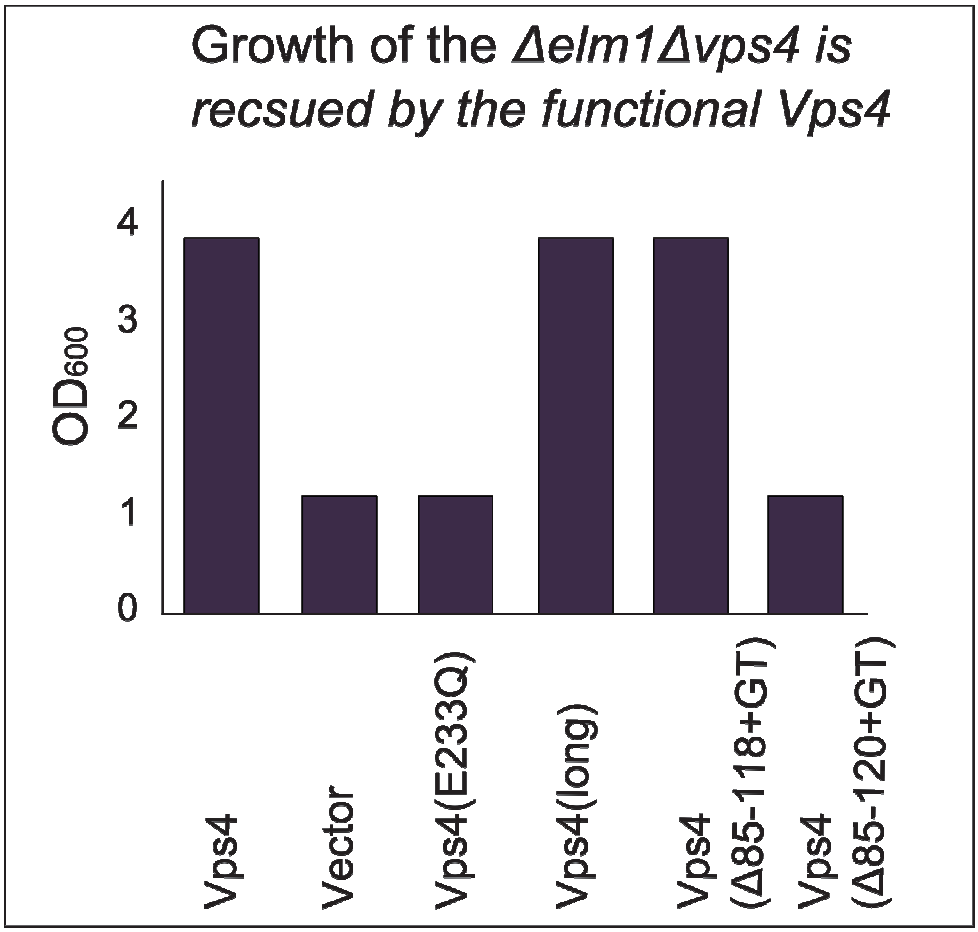

Figure 3-7. Functional Vps4 rescues temperature-sensitive growth defect of Δvps4Δelm1. Δvps4Δelm1 yeast strain expressing vps4 mutants was grown in liquid medium for 30 hours at nonpermissive temperature 30℃. Absorption at 600 nm was measured and plotted on vertical axes. Functional copy of VPS4 gene rescues temperature sensitive growth defect of Δvps4Δelm1. Wild-type Vps4 rescued growth similar to the functional Vps4 linker mutants (Vps4(long) and Vps4(Δ85-118+GT)).

timing of the different steps in the cell cycle progression of *Δvps4* mutant cells using an alpha(α)-factor/or α-pheromone-synchronization/release protocol [60]. The α-factor is secreted by haploid *S. cerevisiae* cells of the alpha mating type. Mature α- factor is a 13 amino acid peptide (WHWLQLKPGQPMT) that binds to Ste2 receptor expressed in a-cells, inducing mating-specific gene expression response and cellular arrest in G1. Bar1 is a protease that is secreted by a-cells and degrades α-factor and thus inhibits cell cycle arrest. Therefore, mutant *Δbar1* background is used to achieve more homogeneous cell cycle arrest with less amount of α-factor. Haploid a-type *Δbar1* cells that have been treated with α-factor can be synchronously released into a new cell cycle by resuspending in "preconditioned media" containing Bar1 protease as a result of the growth of *BAR1* a-cells.

Δbar1 (here referred to as *wild-type)* and *Δbar1Δvps4* strains were synchronized by incubating at 30℃ for 120 minutes in the presence of 5 μM (50 μg/ml) alpha-factor. DIC imaging demonstrated efficient arrest of cells in the G1 phase as judged by the pear-shaped "schmoo" morphology. Cells were released from the α-factor-mediated arrest by washing and culturing in fresh "preconditioned media" for 60 minutes. Cell cycle progression was monitored for the following 75 minutes by sampling yeast culture every 15 minutes. Cell cycle progression was judged by the DIC imaging of the septum formation and by fluorescence microscopy of the DAPI-stained nuclei.

Wild-type and *Δvps4* cells went through G1-to-S transition 60 minutes after removal of α-factor, as judged by the emergence of new bud (Table 3-5, 0

Table 3-5. Cell cycle progression of yeast cells synchronized with α-factor after release. Δvps4 shows delay in cell cycle progression.

New cycle, minutes	*wild-type*	*Δvps4*
0	Bud forming; Mononucleated G1/S	Bud forming; Mononucleated G1/S
75	Emerging septum; Nuclear migration G2/S	Emerging septum; Nuclear migration G2/S
90	Well-formed septum; Binucleated M	Well-formed septum; Binucleated M
105	New cell cycle. Small G1-phase cells; Mononucleated	Well-formed septum; Binucleated M
120	Bud forming; Mononucleated G1/S	New cell cycle. Small G1-phase cells Mononucleated,
135	Emerging septum; Nuclear migration G2/M	Bud forming; Mononucleated G1/S

minutes). G2-to-M transition was observed after 15 minutes in *wild-type* and *Δvps4* as judged by the developing septum and nuclear migration (Table 3-5, 15 minutes). After 30 minutes, *wild-type* and *Δvps4* cells appeared to undergo nuclear division, as a majority of cells were binucleated with well-developed septum (Table 3-5, 30 minutes, *wild-type* and *Δvps4* columns). Wild-type cells completed a cell cycle after 45 minutes as judged by the appearance of new small unbudded G1 cells (Table 3-5, 45 minutes, *wild-type* column). In contrast, *Δvps4* cells entered a new cell cycle at 60 minutes, which is 15 minutes later than wild-type cells, indicating delay in the progression through mitosis (Table 3-5, 45 and 60 minutes, *Δvps4* column).

In sum, abnormal elongated cellular phenotype of *Δelm1* cells was not aggravated by the deletion of *VPS4* and *SNF7*, suggesting that Elm1 and Vps4/Snf7 do not function in the same pathway that controls yeast cytokinesis. Double *Δelm1Δvps4* was had more sever temperature-sensitive growth defect than single mutants *Δelm1* and *Δvps4*, indicating that Vps4 and Elm1 contribute together to the cell growth. Rescue of the temperature-sensitive growth defect of *Δelm1Δvps4* depends on the functional copy of *VPS4* regardless of the linker region, as functional Vps4(Δ85-118+GT) linker deletion rescued *Δelm1Δvps4* temperature-sensitive growth phenotype. Indeed, *Δvps4* cells were identified to have a slower progression through mitosis than *wild-type* cells, indicating the role of the Vps4 in the progression through the cell cycle. Based on these findings, we concluded that Elm1 and Vps4 and Snf7 do not together regulate cytokinesis,

but rather contribute to the cell growth and viability possibly through independent pathways.

References

1. Balasubramanian, M.K., Bi, E. & Glotzer, M. Comparative Analysis of Cytokinesis in Budding Yeast, Fission Yeast and Animal Cells. *Current Biology* **14**, R806-R818 (2004).

2. Agromayor, M. *et al.* Essential role of hIST1 in cytokinesis. *Mol. Biol. Cell* **20**, 1374-1387 (2009).

3. Caballe, A. & Martin - Serrano, J. ESCRT Machinery and Cytokinesis: the Road to Daughter Cell Separation. *Traffic* doi:10.1111/j.1600-0854.2011.01244.x

4. Wollert, T., Wunder, C., Lippincott-Schwartz, J. & Hurley, J.H. Membrane scission by the ESCRT-III complex. *Nature* **458**, 172-177 (2009).

5. Lin, Y., Kimpler, L.A., Naismith, T.V., Lauer, J.M. & Hanson, P.I. Interaction of the mammalian endosomal sorting complex required for transport (ESCRT) III protein hSnf7-1 with itself, membranes, and the AAA+ ATPase SKD1. *J. Biol. Chem.* **280**, 12799-12809 (2005).

6. Erzberger, J.P. & Berger, J.M. Evolutionary relationships and structural mechanisms of AAA+ proteins. *Annu Rev Biophys Biomol Struct* **35**, 93-114 (2006).

7. Inoue, M. *et al.* Nucleotide-dependent conformational changes and assembly of the AAA ATPase SKD1/VPS4B. *Traffic* **9**, 2180-2189 (2008).

8. Yu, Z., Gonciarz, M.D., Sundquist, W.I., Hill, C.P. & Jensen, G.J. Cryo-EM structure of dodecameric Vps4p and its 2:1 complex with Vta1p. *J. Mol. Biol* **377**, 364-377 (2008).

9. Landsberg, M.J., Vajjhala, P.R., Rothnagel, R., Munn, A.L. & Hankamer, B. Three-dimensional structure of AAA ATPase Vps4: advancing structural insights into the mechanisms of endosomal sorting and enveloped virus budding. *Structure* **17**, 427-437 (2009).

10. Hartmann, C. *et al.* Vacuolar protein sorting: two different functional states of the AAA-ATPase Vps4p. *J. Mol. Biol* **377**, 352-363 (2008).

11. Shestakova, A. *et al.* Assembly of the AAA ATPase Vps4 on ESCRT-III. *Mol. Biol. Cell* **21**, 1059-1071 (2010).

12. Babst, M., Davies, B.A. & Katzmann, D.J. Regulation of Vps4 During MVB Sorting and Cytokinesis. *Traffic* (2011).doi:10.1111/j.1600-0854.2011.01230.x

13. Dimaano, C., Jones, C.B., Hanono, A., Curtiss, M. & Babst, M. Ist1 regulates Vps4 localization and assembly. *Mol. Biol. Cell* **19**, 465-474 (2008).

14. Azmi, I.F. *et al.* ESCRT-III family members stimulate Vps4 ATPase activity directly or via Vta1. *Dev. Cell* **14**, 50-61 (2008).

15. Azmi, I. *et al.* Recycling of ESCRTs by the AAA-ATPase Vps4 is regulated by a conserved VSL region in Vta1. *J. Cell Biol* **172**, 705-717 (2006).

16. Merrill, S.A. & Hanson, P.I. Activation of human VPS4A by ESCRT-III proteins reveals ability of substrates to relieve enzyme autoinhibition. *J. Biol. Chem* **285**, 35428-35438 (2010).

17. Hill, C.P. & Babst, M. Structure and function of the membrane deformation AAA ATPase Vps4. *Biochimica Et Biophysica Acta* (2011).doi:10.1016/j.bbamcr.2011.08.017

18. Tang, W.K. *et al.* A novel ATP-dependent conformation in p97 N-D1 fragment revealed by crystal structures of disease-related mutants. *EMBO J* **29**, 2217-2229 (2010).

19. Xiao, J. *et al.* Structural basis of Ist1 function and Ist1-Did2 interaction in the multivesicular body pathway and cytokinesis. *Mol. Biol. Cell* **20**, 3514-3524 (2009).

20. Xiao, J., Xia, H., Yoshino-Koh, K., Zhou, J. & Xu, Z. Structural characterization of the ATPase reaction cycle of endosomal AAA protein Vps4. *J. Mol. Biol* **374**, 655-670 (2007).

21. Maillard, R.A. *et al.* ClpX(P) generates mechanical force to unfold and translocate its protein substrates. *Cell* **145**, 459-469 (2011).

22. Thomsen, N.D. & Berger, J.M. Running in reverse: the structural basis for translocation polarity in hexameric helicases. *Cell* **139**, 523-534 (2009).

23. Gonciarz, M.D. *et al.* Biochemical and structural studies of yeast Vps4 oligomerization. *J. Mol. Biol* **384**, 878-895 (2008).

24. Babst, M., Sato, T.K., Banta, L.M. & Emr, S.D. Endosomal transport function in yeast requires a novel AAA-type ATPase, Vps4p. *EMBO J* **16**, 1820-1831 (1997).

25. Odorizzi, G., Babst, M. & Emr, S.D. Fab1p PtdIns(3)P 5-kinase function essential for protein sorting in the multivesicular body. *Cell* **95**, 847-858 (1998).

26. Babst, M., Wendland, B., Estepa, E.J. & Emr, S.D. The Vps4p AAA ATPase regulates membrane association of a Vps protein complex required for normal endosome function. *EMBO J* **17**, 2982-2993 (1998).

27. Odorizzi, G., Babst, M. & Emr, S.D. Phosphoinositide signaling and the regulation of membrane trafficking in yeast. *Trends Biochem. Sci* **25**, 229-235 (2000).

28. Davies, B.A., Azmi, I.F. & Katzmann, D.J. Regulation of Vps4 ATPase activity by ESCRT-III. *Biochem. Soc. Trans* **37**, 143-145 (2009).

29. Rue, S.M., Mattei, S., Saksena, S. & Emr, S.D. Novel Ist1-Did2 complex functions at a late step in multivesicular body sorting. *Mol. Biol. Cell* **19**, 475-484 (2008).

30. Teis, D., Saksena, S., Judson, B.L. & Emr, S.D. ESCRT-II coordinates the assembly of ESCRT-III filaments for cargo sorting and multivesicular body vesicle formation. *EMBO J* **29**, 871-883 (2010).

31. Babst, M., Katzmann, D.J., Estepa-Sabal, E.J., Meerloo, T. & Emr, S.D. Escrt-III: an endosome-associated heterooligomeric protein complex required for mvb sorting. *Dev. Cell* **3**, 271-282 (2002).

32. Nickerson, D.P., West, M., Henry, R. & Odorizzi, G. Regulators of Vps4 ATPase activity at endosomes differentially influence the size and rate of formation of intralumenal vesicles. *Mol. Biol. Cell* **21**, 1023-1032 (2010).

33. Nickerson, D.P., West, M. & Odorizzi, G. Did2 coordinates Vps4-mediated dissociation of ESCRT-III from endosomes. *The Journal of Cell Biology* **175**, 715 -720 (2006).

34. Morano, K.A. & Klionsky, D.J. Differential effects of compartment deacidification on the targeting of membrane and soluble proteins to the vacuole in yeast. *J. Cell. Sci* **107 (Pt 10)**, 2813-2824 (1994).

35. Horwich, A.L. Chaperoned protein disaggregation--the ClpB ring uses its central channel. *Cell* **119**, 579-581 (2004).

36. Weibezahn, J. *et al.* Thermotolerance Requires Refolding of Aggregated Proteins by Substrate Translocation through the Central Pore of ClpB. *Cell* **119**, 653-665 (2004).

37. Wang, L. & Xie, J. [Bacterial ClpX protease structure and function--a review]. *Wei Sheng Wu Xue Bao* **50**, 1281-1287 (2010).

38. Yamada-Inagawa, T., Okuno, T., Karata, K., Yamanaka, K. & Ogura, T. Conserved pore residues in the AAA protease FtsH are important for

proteolysis and its coupling to ATP hydrolysis. *J. Biol. Chem* **278**, 50182-50187 (2003).

39. Davies, B.A. *et al.* Coordination of substrate binding and ATP hydrolysis in Vps4-mediated ESCRT-III disassembly. *Mol. Biol. Cell* **21**, 3396-3408 (2010).

40. Scott, A. *et al.* Structural and mechanistic studies of VPS4 proteins. *EMBO J* **24**, 3658-3669 (2005).

41. Scott, A. *et al.* Structural and mechanistic studies of VPS4 proteins. *EMBO J* **24**, 3658-3669 (2005).

42. Caballe, A. & Martin-Serrano, J. ESCRT Machinery and Cytokinesis: the Road to Daughter Cell Separation. *Traffic* no-no (2011).doi:10.1111/j.1600-0854.2011.01244.x

43. Samson, R.Y., Obita, T., Freund, S.M., Williams, R.L. & Bell, S.D. A role for the ESCRT system in cell division in archaea. *Science* **322**, 1710-1713 (2008).

44. Costanzo, M. *et al.* The genetic landscape of a cell. *Science* **327**, 425-431 (2010).

45. Barr, F.A. & Gruneberg, U. Cytokinesis: Placing and Making the Final Cut. *Cell* **131**, 847-860 (2007).

46. Glotzer, M. The Molecular Requirements for Cytokinesis. *Science* **307**, 1735 - 1739 (2005).

47. Guizetti, J. & Gerlich, D.W. Cytokinetic abscission in animal cells. *Semin. Cell Dev. Biol.* **21**, 909-916 (2010).

48. Guizetti, J., Mäntler, J., Müller-Reichert, T. & Gerlich, D.W. Correlative time-lapse imaging and electron microscopy to study abscission in HeLa cells. *Methods Cell Biol.* **96**, 591-601 (2010).

49. Morita, E. *et al.* Human ESCRT and ALIX proteins interact with proteins of the midbody and function in cytokinesis. *EMBO J* **26**, 4215-4227 (2007).

50. Morita, E. *et al.* Human ESCRT-III and VPS4 proteins are required for centrosome and spindle maintenance. *Proc. Natl. Acad. Sci. U.S.A* **107**, 12889-12894 (2010).

51. Wollert, T. & Hurley, J.H. Molecular mechanism of multivesicular body biogenesis by ESCRT complexes. *Nature* **464**, 864-869 (2010).

52. Hanson, P.I., Roth, R., Lin, Y. & Heuser, J.E. Plasma membrane deformation by circular arrays of ESCRT-III protein filaments. *J. Cell Biol.* **180**, 389-402 (2008).

53. Wang, C.-W., Hamamoto, S., Orci, L. & Schekman, R. Exomer: a coat complex for transport of select membrane proteins from the trans-Golgi network to the plasma membrane in yeast. *The Journal of Cell Biology* **174**, 973 -983 (2006).

54. Nishihama, R. *et al.* Role of Inn1 and its interactions with Hof1 and Cyk3 in promoting cleavage furrow and septum formation in S. cerevisiae. *J Cell Biol* **185**, 995-1012 (2009).

55. Longtine, M.S. *et al.* The septins: roles in cytokinesis and other processes. *Current Opinion in Cell Biology* **8**, 106-119 (1996).

56. Barral, Y., Parra, M., Bidlingmaier, S. & Snyder, M. Nim1-related kinases coordinate cell cycle progression with the organization of the peripheral cytoskeleton in yeast. *Genes & Development* **13**, 176 -187 (1999).

57. Bouquin, N. *et al.* Regulation of cytokinesis by the Elm1 protein kinase in Saccharomyces cerevisiae. *J. Cell. Sci* **113 (Pt 8)**, 1435-1445 (2000).

58. McMurray, M.A. *et al.* Genetic interactions with mutations affecting septin assembly reveal ESCRT functions in budding yeast cytokinesis. *Biol. Chem* **392**, 699-712 (2011).

59. Bouquin, N. *et al.* Regulation of cytokinesis by the Elm1 protein kinase in Saccharomyces cerevisiae. *J. Cell. Sci* **113 (Pt 8)**, 1435-1445 (2000).

60. Abelson, J.N., Simon, M.I. & Dunphy, W.G. *Cell Cycle Control*. (Academic Press: 1997).

CHAPTER 4

CONCLUSIONS AND FUTURE DIRECTIONS

Summary for Chapter 2: Functional importance of the Vps4-ESCRT-III-mediated interactions *in vivo*

Vps4 ATPase is a key enzyme that participates in protein sorting at the late endosomal compartment termed MVB 1. Function of Vps4 is regulated through its recruitment to the endosome-associated ESCRT-III complex, where Vps4 assembles into a functional ATPase capable of ESCRT-III disassembly [2]. The recruitment step of Vps4 is regulated by a network of ESCRT-III core proteins (Vps20, Snf7, Vps2 and Vps24) and ESCRT-III-associated proteins (Did2, Ist1 and Vta1). The N-terminal MIT domain of Vps4 is a major recruitment determinant that interacts with C-terminal regions of Vps20, Snf7, Vps2, Vps24, Did2 and Ist1 [3], whereas Vta1 recruits Vps4 through interactions with its ATPase domain [4].

MIT-mediated interactions with ESCRT-III MIMs are redundant. To dissect details of the MIT-mediated interactions, we studied endosomal recruitment of the GFP-tagged MIT domain of Vps4 (GFP-MIT). MIT domain of Vps4 has a three alpha-helical structure that interacts with C-terminal regions of ESCRT-III proteins termed MIMs. The MIM1 motif is found at the C-terminus of Vps2, Vps24, Did2 and Ist1. MIM1 binds to the MIT domain parallel to helix three, in the groove formed by helixes one and three. MIM2 motif is found proximal to the C-terminus of Vps20, Snf7 and Ist1 and binds parallel to the helix three, in the groove formed by helixes two and three. This arrangement allows simultaneous binding of the MIT domain to the MIM1 and MIM2 motifs.

We found that single deletion of either the MIM1 or MIM2 motif decreased

endosomal localization of GFP-MIT, suggesting that remaining interactions are capable of mediating partial recruitment of the Vps4. MIM1 motifs were demonstrated to be more important for the recruitment of MIT-GFP than MIM2, as block in all MIM1-MIT interactions abolished endosomal recruitment of MIT-GFP, whereas block in all MIM2-MIT interactions resulted in a decrease of endosomal recruitment of MIT-GFP. In agreement with the recruitment data, we found that MIM1 interactions are more important for the function of Vps4 in the MVB sorting.

Vps4-Vps4 interactions are sufficient to recruit Vps4. Vps4-Vps4 interactions are mediated by the ATPase domain of Vps4. Therefore, ATPase-mediated interactions were addressed using the GFP-tagged ATPase domain of Vps4 (GFP-Vps4(ΔMIT,E233Q)). Our *in vivo* analysis demonstrated that GFP-Vps4(ΔMIT,E233Q) can be recruited to ESCRT-III either Vta1 or via interactions with ESCRT-III-associated Vps4.

Indication for the functionally distinct rings in the Vps4 oligomer. MIT domains were previously reported to be dispensable for the ATPase activity of Vps4 measured *in vitro* [5]. Therefore, Vps4 lacking its MIT domains Vps4(ΔMIT) that is recruited to ESCRT-III via interaction with Vta1 might assemble into oligomer capable of ATP hydrolysis. However, Vps4(ΔMIT) does not support MVB sorting, indicating that MIT-mediated interactions with ESCRT-III are essential in function of the Vps4 ATPase. Moreover, the hydrolysis mutant of Vps4(ΔMIT,E233Q) does not interfere with the function of wild-type Vps4, suggesting that Vps4(ΔMIT,E233Q) is either not incorporated into the Vps4

oligomer or, if incorporated, does not inhibit function of the wild-type Vps4. Class II AAA+ ATPase containing two ATPase domains homooligomerize into a ring composed of two separate tiers of the ATPase domains [6], a structure that resembles a double-stacked ring oligomer formed by Vps4. Moreover, one of the ATPase is dispensable for ATP hydrolysis and serves as a regulator [7]. Therefore, we speculate that two rings in the Vps4 oligomer serve different functions and preferential incorporation of Vps4(ΔMIT,E233Q) into one of them does not block function of Vps4.

Indications for the sequence of recruitment of Vps4 form cytosol. *In vitro* binding experiments (Figure 2-5, Chapter 2, experiment performed by Abraham Hanono) demonstrated that Ist1 is a preferred binding partner of Did2 that enhances interaction between Vps4 and Did2. Based on the previous study, Did2 was proposed to interact with Ist1 in cytoplasm [8]. Therefore, we speculated that in cytoplasm, Ist1 is bound to Did2 and Vps4 and this complex is recruited to ESCRT-III. Further on, Vta1 interactions with ESCRT-III and Vps4 induce rearrangements that promote assembly of the functional ATPase.

Summary for Chapter 3: Functional and biochemical studies of the linker region of Vps4

Three domains comprise Vps4 ATPase – the N-terminal ESCRT-III-interacting domain, the C-terminal ATPase domain and the linker region that connects those [9]. The linker region is an unstructured, quite long stretch of ~42 amino acids that comprises almost 10 percent of the Vps4 amino acid sequence.

Single particle analysis of the Vps4 oligomer showed that ATPase domains of Vps4 assemble into two rings that form central cavity or pore that is functionally important [10] [11]. MIT domains are found above the cavity in one ring and on the periphery in another ring, indicating that position of MIT domains vary. We set up to test if MIT domains function together with the pore in the processing of substrate. We reasoned that the linker region might mediate movement of MIT domains to allow the pore region to process substrate. Therefore, we performed functional and biochemical analysis of serial deletions within the linker region to find minimal length of the linker that supports function of Vps4.

Length of the Vps4 linker region is dispensable for the sorting of GFP-CPS into MVBs. We used GFP-CPS fluorescence microscopy assay to identify functionality of Vps4(linker deletions) in the MVB sorting. Our functional analysis of the linker region identified that a short linker of just two amino acids Vps4(Δ79-118+GT) supports partial function of the Vps4 in MVB sorting, indicating that linker length is largely dispensable for the sorting of GFP-CPS.

Deletion of the linker region affects interactions with Vps4-regulatory proteins. We tested if deletion of the linker region affects interaction with Vps4-regulatory regulatory proteins Did2, Ist1, Vta1 and Vps60. We found that Vps4(linker deletions) are defective in interacting with Vta1 and Vps60 in the absence of Did2.

Deletion of the linker region produces larger MVB vesicles as judged by the transmission electron microscopy (TEM). We measured the size of intralumenal MVB vesicles in cells expressing fully functional deletion of the linker region Vps4

(Δ85-115+GT). TEM identified that the size of the vesicles expressing mutant Vps4(Δ85-115+GT) is approximately thirty percent higher than those expressing wild-type Vps4, indicating that deletion of the linker region affects MVB biogenesis.

Deletion of the linker region results in the higher ATPase activity. We demonstrated that deletion of the linker region correlates with the increase in the Vps4 ATPase activity. Moreover, we found that deletion of the linker that produces nonfunctional Vps4 Vps4(Δ78-118) has increased ATPase activity. We speculated that increased ATPase might act too early to disassemble ESCRT-III and therefore cause MVB sorting defects.

Vps4 does not regulate cytokinesis in budding yeast. Since Vps4 regulates cytokinesis in mammalian cells [12], we tested the role of the Vps4 and its linker in the cytokinesis. We concluded that Vps4 does not directly regulate cytokinesis in budding yeast.

Future directions

One of the big questions is to understand mechanistic details of the substrate processing by the Vps4 ATPase. Does Vps4 apply pulling force and thread substrate through its pore region?

Major determinants that mediate recruitment of Vps4 to ESCRT-III are well understood [2]. We still need to map sites in Vps4 and ESCRT-III proteins that mediate substrate processing. What are the sites in the ESCRT-III proteins that directly interact with the pore region? Ultimately, one would like to have a crystal

structure of the fully assembled Vps4 bound to the substrate.

Results of the ESCRT-driven reconstitution of the MVB vesicles biogenesis *in vitro* imply that Vps4 functions in solubilization of ESCRT-III complex [13]. *In vivo*, Vps4 assembles into functional oligomer on ESCRT-III-enriched membranes. Therefore, one possibility is that Vps4 oligomerization regulates the polymerization rate of the ESCRT-III lattice and therefore regulates formation of MVB vesicles. Solubilization of ESCRT-III by Vps4 ATPase is the final step that releases vesicles and allows ESCRT-III proteins to be reused for further rounds of sorting. Furthermore, how many Vps4 oligomers are required to form one intralumenal MVB vesicle?

References

1. Babst, M., Wendland, B., Estepa, E.J. & Emr, S.D. The Vps4p AAA ATPase regulates membrane association of a Vps protein complex required for normal endosome function. *EMBO J* **17**, 2982-2993 (1998).

2. Shestakova, A. *et al.* Assembly of the AAA ATPase Vps4 on ESCRT-III. *Mol. Biol. Cell* **21**, 1059-1071 (2010).

3. Hurley, J.H. & Yang, D. MIT domainia. *Dev. Cell* **14**, 6-8 (2008).

4. Azmi, I. *et al.* Recycling of ESCRTs by the AAA-ATPase Vps4 is regulated by a conserved VSL region in Vta1. *J. Cell Biol* **172**, 705-717 (2006).

5. Babst, M., Sato, T.K., Banta, L.M. & Emr, S.D. Endosomal transport function in yeast requires a novel AAA-type ATPase, Vps4p. *EMBO J* **16**, 1820-1831 (1997).

6. Erzberger, J.P. & Berger, J.M. Evolutionary relationships and structural mechanisms of AAA+ proteins. *Annu Rev Biophys Biomol Struct* **35**, 93-114 (2006).

7. Esaki, M. & Ogura, T. ATP-bound form of the D1 AAA domain inhibits an essential function of Cdc48p/p97. *Biochem. Cell Biol.* **88**, 109-117 (2010).

8. Dimaano, C., Jones, C.B., Hanono, A., Curtiss, M. & Babst, M. Ist1 regulates Vps4 localization and assembly. *Mol. Biol. Cell* **19**, 465-474 (2008).

9. Hill, C.P. & Babst, M. Structure and function of the membrane deformation AAA ATPase Vps4. *Biochimica Et Biophysica Acta* (2011).doi:10.1016/j.bbamcr.2011.08.017

10. Yu, R.C., Hanson, P.I., Jahn, R. & Brünger, A.T. Structure of the ATP-dependent oligomerization domain of N-ethylmaleimide sensitive factor complexed with ATP. *Nat. Struct. Biol.* **5**, 803-811 (1998).

11. Landsberg, M.J., Vajjhala, P.R., Rothnagel, R., Munn, A.L. & Hankamer, B. Three-dimensional structure of AAA ATPase Vps4: advancing structural insights into the mechanisms of endosomal sorting and enveloped virus budding. *Structure* **17**, 427-437 (2009).

12. Caballe, A. & Martin-Serrano, J. ESCRT Machinery and Cytokinesis: the Road to Daughter Cell Separation. *Traffic* no-no (2011).doi:10.1111/j.1600-0854.2011.01244.x

13. Wollert, T. & Hurley, J.H. Molecular mechanism of multivesicular body biogenesis by ESCRT complexes. *Nature* **464**, 864-869 (2010).